НАЦІОНАЛЬНА АКАДЕМІЯ НАУК УКРАЇНИ
ІНСТИТУТ ЗАГАЛЬНОЇ ТА НЕОРГАНІЧНОЇ ХІМІЇ імені В. І. ВЕРНАДСЬКОГО
КИЇВСЬКИЙ НАЦІОНАЛЬНИЙ УНІВЕРСИТЕТ імені ТАРАСА ШЕВЧЕНКА

УКРАЇНСЬКИЙ ХІМІЧНИЙ ЖУРНАЛ

№ 11
Том 91 / Vol. 91
2025
https://ucj.org.ua

UKRAINIAN CHEMISTRY JOURNAL

Зміст

Contents

UDC 546.3+543.4+539.26 doi: 10.33609/2708-129X.91.11.2025.3-21

STRUCTURE AND SPECTRAL EVALUATION OF COVALENCY IN ND(III) TETRAKIS COMPLEXES WITH CARBACYLAMIDOPHOSPHATE LIGANDS.

Mariia B. Struhatska[a,*], Nataliia S. Kariaka[a], Viktor O. Trush[a], Viktoriya V. Dyakonenko[b], Svitlana V. Shishkina[c], Sergii S. Smola[d], Nataliia V. Rusakova[d], Volodymyr M. Amirkhanov[a]

[a] Faculty of Chemistry, Taras Shevchenko National University of Kyiv, 12 Hetman Pavlo Skoropadsky Str., 01033 Kyiv, Ukraine;
[b] SSI "Institute for Single Crystals", National Academy of Science of Ukraine, 60 Nauky ave., 61072 Kharkiv, Ukraine;
[c] Institute of Organic Chemistry of the National Academy of Sciences of Ukraine, 5 Akademika Kukharya Str., 02660 Kyiv, Ukraine;
[d] A.V. Bogatsky Physicochemical Institute of the National Academy of Sciences of Ukraine, 86 Lustdorfska doroga Str, 65080 Odessa, Ukraine
**e-mail: mariia.struhatska@knu.ua*

Two neodymium(III) tetrakis complexes with different carbacylamidophosphate ligands and a tetraethylammonium cation of the formulas $NEt_4[NdL^1_4]$ (**1Nd**) and $NEt_4[NdL^2_4]\cdot iPrOH$ (**2Nd**) were synthesized, where $[L^1]^-$ is dimethyl-N-trichloroacetylamidophosphate, $Cl_3CC(O)NP(O)(OCH_3)_2^-$, and $[L^2]^-$ is diphenyl-N-trichloroacetylamidophosphate, $Cl_3CC(O)NP(O)(OC_6H_5)_2^-$. The compounds were characterized by elemental analysis, infrared spectroscopy, diffuse reflectance electronic spectroscopy, and single-crystal X-ray diffraction analysis. Structural analysis confirmed the formation of anionic complexes featuring a NdO_8 coordination environment. Coordination polyhedra of central ions are best described as a triangular dodecahedron for **1Nd** and a square antiprism for **2Nd**. Diffuse reflectance spectra in the UV–vis–NIR region revealed characteristic f–f transitions of Nd^{III}, with ligand-dependent modulation of band shape and intensity of the "hypersensitive" transitions. The bonding between the metal and the ligands was found to have weak covalent character. Luminescence studies of the **2Nd** complex revealed weak emission sensitization by the ligands.

Keywords: Nd^{III}, carbacylamidophosphate, tetrakis complex, tetraethylammonium cation, electronic spectroscopy, crystal structure.

INTRODUCTION.

Lanthanide complexes with organic ligands have emerged as key materials in a wide range of high-tech applications, owing to the unique photophysical, magnetic, and catalytic properties imparted by their 4f electronic configuration [1, 2, 3]. Their sharp emission bands, large excitation–emission energy difference, and long excited-state lifetimes make these complexes promising candidates for luminescent devices such as organic light-emitting diodes (OLEDs) [4, 5]. In molecular sensing, lanthanide complexes act as selective probes for detecting molecules, ions, or environmental changes, due to their environment-sensitive emission[6, 7]. In the biomedical field, lanthanides are used in bioimaging and diagnostic agents, where deep tissue penetration and minimal autofluorescence are critical [8, 9]. Other applications of lanthanide(III) complexes with organic ligands include single-molecule magnets [10, 11, 12, 13], structural damage and pressure sensors [14, 15, 16, 17], polymeric optical waveguides and amplifiers [18, 19, 20], security inks [21, 22, 23], luminescent thermometers [24, 25, 26, 27], solar concentrators [28, 29], and catalysis [30, 31].

A structurally appealing subclass of coordination compounds is represented by tetrakis complexes, in which four acido-ligands surround the metal center, typically resulting in discrete anionic units balanced by organic or inorganic counterions [32]. In the case of lanthanides, such tetrakis complexes offer several advantages: high stability, predictable geometry, and elimination of lanthanide luminescence quenching due to saturation of the metal's coordination sites – particularly crucial for NIR-emitting lanthanide ions.

Among the various ligand systems employed for lanthanide complexation [33], carbacylamidophosphates (CAPhs) represent a versatile and promising class. Bidentate CAPh ligands offer phosphoryl and carbonyl oxygen donor atoms, capable of forming air-stable chelates with lanthanide ions. The modular nature of the CAPh framework allows fine-tuning of the photophysical properties of their metal complexes through substitution at the carbon or phosphorus atoms. Moreover, CAPh ligands tend to form rigid complexes with favorable solubility and crystallization behavior and, with suitable substituents and triplet-state energy, they may act as "antennas" and efficiently sensitize Ln^{III} luminescence [32, 34, 35].

Electronic spectroscopy is a valuable tool for characterizing lanthanide complexes, which, unlike transition metal complexes, often display sharp and well-defined electronic transitions due to the shielding of f-electrons within the inner orbitals of the lanthanide ions. Each lanthanide ion exhibits characteristic absorption bands that can provide insight into the coordination environment surrounding the metal ion. Changes in ligand field strength or coordination number may lead to shifts in some of the absorption bands or variations in their intensity [36]. The most commonly studied lanthanide ions in electronic spectroscopy include Pr^{III}, Nd^{III}, Ho^{III}, and Er^{III}, due to the relatively high intensity of their absorption bands [37].

The absorption bands of neodymium(III) in the visible and near-infrared regions arise from intra-4f transitions from the ground state $^4I_{9/2}$, which are Laporte-forbidden but become partially allowed due to mixing of the 4f and 5d orbitals via the ligand field [38]. In Nd^{III} complexes, these bands typically exhibit a ba-

thochromic shift compared to the aqua ion, known as the nephelauxetic shift [39, 40, 41, 42]. The nephelauxetic effect is related to the degree of covalency in the metal-ligand bond within the complex compared to the metal salt in aqueous solution; stronger covalency leads to a larger nephelauxetic shift. The degree of the nephelauxetic shift has been found to depend on the central ion's coordination number [43] and is therefore related to the metal–ligand distance [44]. The polarizability of the ligand also affects the nephelauxetic shift [42]. The multiplicity of the $^2P_{1/2} \leftarrow {}^4I_{9/2}$ transition band, observed around 430 nm, can be used to determine the number of optical centers in a complex and thereby infer the structural individuality of the compound. In the absence of a magnetic field, this transition is degenerate and unaffected by the symmetry field, making its splitting a valuable diagnostic parameter. The so-called "hypersensitive" transition $^4G_{5/2}$, $^2G_{7/2} \leftarrow {}^4I_{9/2}$ near 580–600 nm is responsive to ligand field effects and coordination geometry [45]. Complexation results in a pronounced increase in the intensities of the components of this transition band. The band profile has also been utilized as a diagnostic tool for determining the coordination number of the central metal ion [45, 46], including in complexes with CAPh ligands [47, 48, 53].

In this work, we report the synthesis and comprehensive characterization of two Nd^{III} tetrakis complexes with two types of CAPh ligands, with the formulas $NEt_4[NdL^1_4]$ (**1Nd**) and $NEt_4[NdL^2_4]\cdot iPrOH$ (**2Nd**), where $[L^1]^-$ is deprotonated dimethyl-N-trichloroacetylamidophosphate, $Cl_3CC(O)NP(O)(OCH_3)_2^-$, and $[L^2]^-$ is diphenyl-N-trichloroacetylamidophosphate-anion, $Cl_3CC(O)NP(O)(OC_6H_5)_2^-$. Graphical formulas of the ligands are shown in Figure 1. The compounds were characterized using elemental analysis, single-crystal X-ray diffraction, infrared, and diffuse reflectance electronic spectroscopy. The luminescence properties of the **2Nd** were also studied. The work aims to evaluate how variations in ligand structure influence the coordination geometry, Nd–O bonds covalency, and spectral properties of the Nd^{III} ion in the solid state.

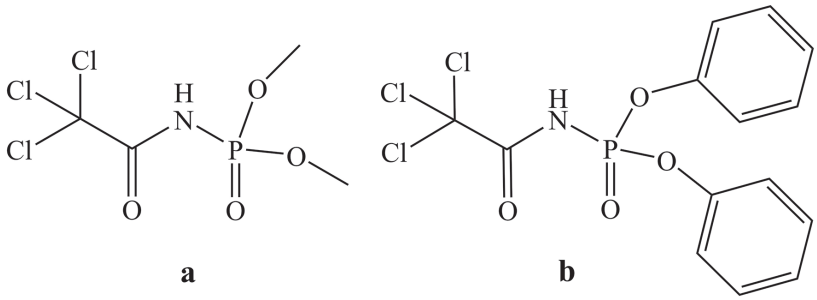

Fig. 1. Graphical formulas of HL^1 (a) and HL^2 (b).

EXPERIMENT AND DISCUSSION OF THE RESULTS.

Materials and methods.

All reagents were obtained from commercial sources and used without further purification. Solvents used in the syntheses were dried using standard literature procedures.

Elemental analysis was performed using a CHNS Vario EL Cube Elemental Analyzer. The lanthanide content in the complexes was

determined by standard titrimetric methods for lanthanide ions [49].

Single-crystal X-ray diffraction data for structure **1Nd** were collected at 294 K using an Xcalibur Sapphire3 diffractometer, and for structure **2Nd** at 296 K using a Bruker APEX-II CCD diffractometer, both equipped with graphite-monochromated MoKa radiation (λ = 0.71073 Å). Using Olex2 software [50], the structures were solved with the SHELXT [51] program using Intrinsic Phasing and refined with the SHELXL [52] refinement package. Full-matrix least-squares refinement against F^2 in anisotropic approximation was used for non-hydrogen atoms. Positions of the hydrogen atoms were located from electron density difference maps and refined by "riding" model with $U_{iso} = nU_{eq}$ of the carrier atom (n = 1.5 for methyl and hydroxyl groups and n = 1.2 for other hydrogen atoms). Crystal data and refinement parameters are summarized in Table 1.

Infrared (IR) spectra were recorded on a Perkin Elmer Spectrum BX spectrometer using KBr pellets in the range of 400–4000 cm^{-1}.

Diffuse reflectance electronic spectra of solid **1Nd** and **2Nd** were measured with a Shimadzu UV-2600i spectrometer.

Emission and excitation spectra of **2Nd** were measured on a "Fluorolog FL 3-22" spectrofluorometer at 298 K.

Synthesis.

The ligands HL^1 and HL^2, as well as their sodium salts, were synthesized according to previously described procedures [34, 53, 54].

The Ln^{III} complexes were obtained according to the following schemes:

$Nd(NO_3)_3 \cdot 6H_2O + 4NaL^1 + NEt_4Cl =$
$= NEt_4[NdL^1_4] + 3NaNO_3 + NaCl + 6H_2O,$

$Nd(NO_3)_3 \cdot 6H_2O + 4NaL^2 + NEt_4Cl + iPrOH =$
$= NEt_4[NdL^2_4] \cdot iPrOH + 3NaNO_3 + NaCl + 6H_2O.$

The hydrated neodymium(III) nitrate (1 mmol, 0.43835 g) was dissolved in acetone (10 mL) under heating for one minute. Next, the dehydrating reagent, triethyl orthoformate (6 mmol, 1 ml), was added, and the resulting solution was boiled for 1 min. Separately, NaL^1 (4 mmol, 1.1696 g) or NaL^2 (4 mmol, 1.6664 g) was dissolved in acetone (10 mL) under heating. Additionally, tetraethylammonium chloride (1 mmol) was dissolved in 2-propanol (5 mL) under heating. The three prepared solutions were combined and refluxed for 10 min. The resulting solution was cooled to room temperature for 10 min, and the precipitated $NaNO_3$ was filtered off. After 1 - 2 days, the target complexes began to crystallize from the filtrate. The compounds were separated from the mother liquor, washed with 2-propanol, and dried in air. The average yields of products **1Nd** and **2Nd** were 55 and 78 %, respectively. The obtained complexes were stable in air, well soluble in methanol, acetone, dimethylformamide (DMF), dimethyl sulfoxide (DMSO), acetonitrile, ethyl acetate, 1,4-dioxane, dichloromethane, chloroform, and in 2-propanol (upon heating). The compounds were insoluble in tetrachloromethane, benzene, hexane, and water.

$NEt_4[NdL^1_4]$ (**1Nd**) Yield: 55 %. M.p.: 157 °C. Anal. Calcd for $C_{24}H_{44}Cl_{12}N_5NdO_{16}P_4$ (M_r = 1352.20) (%): Nd, 10.67; C, 21.32; H, 3.28; N 5.18. Found, %: Nd, 11.3; C, 21.14; H, 3.25; N, 5.32. IR (KBr): ν_{max} = 2992 (w), 2952 (m), 2850 (w), 1620 (vs), 1484 (m), 1462 (w), 1456 (w), 1442 (w, sh), 1393 (w), 1366 (vs), 1186 (s), 1164 (vs), 1046 (vs), 1012 (s), 882 (vs), 845 (s), 836 (s), 820 (s), 780 (m), 726 (m), 674 (m), 548 (s), 498 (m), 460 (m) cm^{-1}.

$NEt_4[NdL^2_4]$·iPrOH (**2Nd**) Yield: 78 %. M.p.: 225 °C. Anal. Calcd for $C_{67}H_{68}Cl_{12}N_5NdO_{17}P_4$ (M_r = 1908.85) (%): Nd, 7.6; C, 42.16; H, 3.59; N 3.67. Found, %: Nd, 8.1; C, 41.67; H, 3.49; N, 3.81. IR (KBr): ν_{max} = 3070 (w), 2924 (m), 2854 (w), 1618 (vs), 1588 (vs), 1490 (vs), 1455 (m), 1440 (w), 1393 (m, sh), 1370 (vs), 1288 (w), 1218 (s), 1192 (vs), 1180 (vs, sh), 1166 (vs), 1072 (w), 1020 (s), 1005 (s, sh), 948 (vs, sh), 939 (vs), 908 (m), 876 (s), 820 (s), 776 (s), 761 (s), 718 (w), 690 (s), 677 (s), 615 (w), 590 (m), 574 (w), 526 (s), 504 (m), 462 (w, sh) cm^{-1}.

X-ray Crystal Structure.

The **1Nd** and **2Nd** complexes crystallize in the monoclinic crystal system in space groups $P2_1/c$ and $C2/c$, respectively. The crystallographic data for the compounds are listed in Table 1. The asymmetric unit cell of **1Nd** and eight of **2Nd** complexes contains one anion $[NdL^1/L^2_4]^-$ ($[L^1]^-$ is a deprotonated dimethyl-N-trichloroacetylamidophosphate, $Cl_3CC(O)NP(O)(OCH_3)_2^-$, and $[L^2]^-$ is diphenyl-N-trichloroacetylamidophosphate-anion, $Cl_3CC(O)NP(O)(OC_6H_5)_2^-$) and one cation NEt_4^+. The **2Nd** complex crystallizes as solvate with isopropanol. Deprotonated CAPh ligands coordinate to the lanthanide ions in a bidentate chelating mode via the oxygen atoms of phosphoryl and carbonyl groups, forming six-membered metallacycles (Figure 2). The coordination polyhedra of the lanthanide ions were determined using the SHAPE 2.1 software [55] as a triangular dodecahedron for **1Nd** and a square antiprism for **2Nd** (Table 2, Figure 3). Compared with the free ligand HL^1 and sodium salt NaL^2 [56], the average bond lengths of P—O and C—O in the **1Nd** and **2Nd** complexes are elongated, while the P—N and C—N bonds are shortened, which is consistent with coordination-induced π-delocalization. The average Ln—O(P) bond lengths are shorter than the Ln—O(C) ones, which is attributed to the stronger affinity of the phosphoryl group for lanthanide ions. However, replacement of substituents from OMe to OPh leads to an elongation of Ln—O(P) bonds and a shortening of Nd—O(C) bonds in **2Nd** compared with **1Nd**. The Nd—O(P) and Nd—O(C) distances vary within 2.374(7)–2.395(8) Å and 2.492(8)–2.499(9) Å, respectively, for complex **1Nd**, and 2.391(7)–2.425(7) Å and 2.432(6)–2.472(7) Å for complex **2Nd**. All the Nd—O bonds are shorter than the sum of the van der Waals radii of oxygen and the Nd^{3+} ionic radius (2.61 Å). The average length of Nd—O bonds in **2Nd** (2.43363 Å) is slightly smaller than in **1Nd** (2.43725 Å). The O—Nd—O bond angles vary from 72.0(3)° to 74.7(3)° for **1Nd** and from 71.6(3)° to 73.5(3)° for **2Nd** (Table 3). The values of the distances and angles are in good agreement with the data obtained for Nd^{III} complexes with CAPhs [57, 58].

As a result of the coordination of Nd atoms by organic ligands in structures **1Nd** and **2Nd**, the six-membered metallacycles are formed. The metallacycles in the **1Nd** and **2Nd** structures are either planar or adopt sofa- or boat-like conformations. The geometric characteristics of the conformations of the six-membered metallacycles are presented in Table 4.

In the crystal phase, the molecules of the anion and cation (in **1Nd**), as well as the anion, cation, and solvent molecules (in **2Nd**), are linked by numerous intermolecular interactions, forming a three-dimensional molecular packing network.

Table 1.

Crystal data and structure refinement parameters for 1Nd and 2Nd.

Parameter	**1Nd**	**2Nd**
formula	$C_{24}H_{44}Cl_{12}N_5NdO_{16}P_4$	$C_{67}H_{48}Cl_{12}N_5NdO_{17}P_4$
M	1352.16	1887.62
T [K]	294	296.15
crystal system	monoclinic	monoclinic
space group	$P2_1/c$	$C2/c$
a [Å]	20.5200(11)	25.610(3)
b [Å]	12.3252(6)	15.281(3)
c [Å]	21.4083(11)	42.846(6)
α [°]	90	90
β [°]	92.577(4)	97.330(13)
γ [°]	90	90
V [Å^3]	5409.0(5)	16631(4)
Z	4	8
Dc [mg cm^{-3}]	1.660	1.509
μ [mm^{-1}]	1.730	1.151
F(000)	2700	7560
crystal size [mm]	0.2 x 0.4 x 0.5	0.1 x 0.2 x 0.3
reflections collected	38576	71669
independent reflections (R_{int})	10616	14544
data/parameters	10616 / 624	14544 / 990
GOF	0.999	1.125
R_1 [I>2σ(I)]	0.098	0.1045
wR_2 [I>2σ(I)]	0.2422	0.1970
R_1 [all data]	0.1698	0.1572
wR_2 [all data]	0.2883	0.2140
CCDC	2486751	2486752

Table 2.

Continuous Shape Measures (CShMs) of the coordination geometry for 1Nd and 2Nd crystal structures.

Label	Symmetry	Shape	**1Nd**	**2Nd**
OP-8	D8h	Octagon	31.986	28.250
HPY-8	C7v	Heptagonal pyramid	23.995	23.297
HBPY-8	D6h	Hexagonal bipyramid	16.557	16.220
CU-8	Oh	Cube	10.324	8.961

Table 2.

Label	Symmetry	Shape	1Nd	2Nd
SAPR-8	**D4d**	**Square antiprism**	1.938	**0.221**
TDD-8	**D2d**	**Triangular dodecahedron**	**0.450**	2.206
JGBF-8	D2d	Johnson gyrobifastigium J26	13.036	16.327
JETBPY-8	D3h	Johnson elongated triangular bipyramid J14	28.648	28.275
JBTPR-8	C2v	Biaugmented trigonal prism J50	2.311	2.934
BTPR-8	C2v	Biaugmented trigonal prism	2.016	2.140
JSD-8	D2d	Snub diphenoid J84	2.205	5.191
TT-8	Td	Triakis tetrahedron	10.878	9.779
ETBPY-8	D3h	Elongated trigonal bipyramid	25.123	23.577

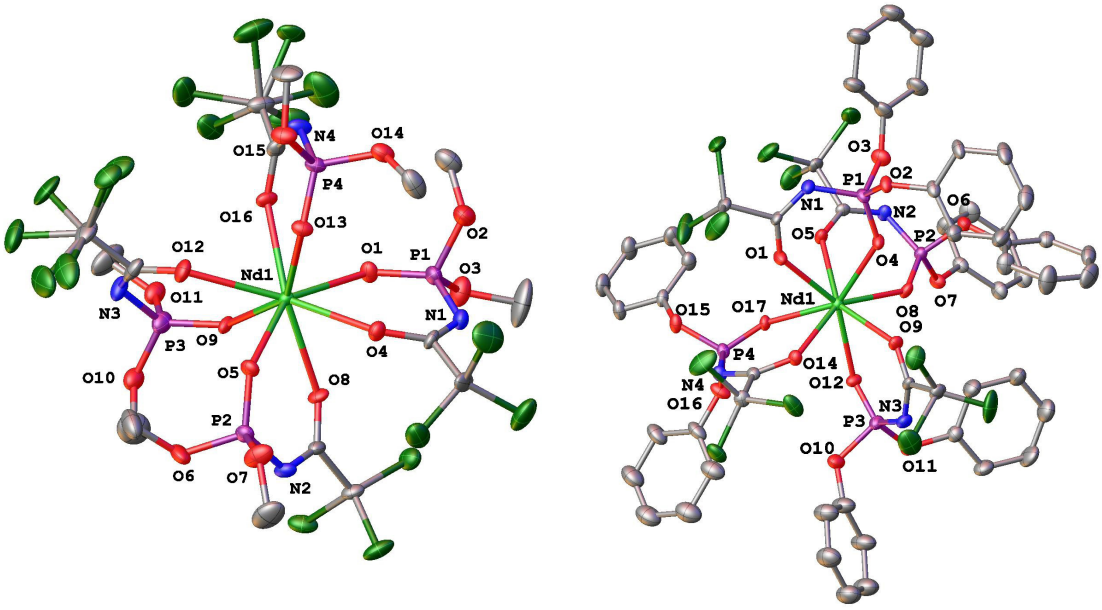

1Nd **2Nd**

Fig. 2. The molecular structures of the $[NdL^1/L^2_4]^-$ anions in 1Nd and 2Nd (H atoms are omitted for clarity). Thermal ellipsoids are shown at 50 % probability level.

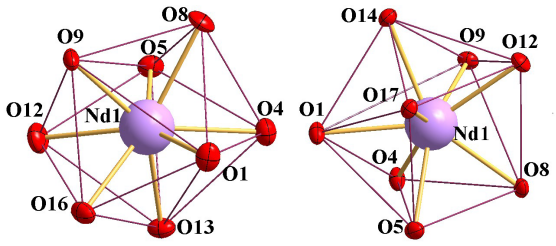

1Nd **2Nd**

Fig. 3. Coordination polyhedra of the Nd^{III} ions in 1Nd and 2Nd.

Table 3.

Selected bond lengths [Å] and angles [°] in 1Nd and 2Nd complexes.

1Nd		**2Nd**	
Nd1—O1	2.395 (8)	Nd1—O1	2.436 (7)
Nd1—O4	2.499 (9)	Nd1—O4	2.391 (7)
Nd1—O5	2.374 (7)	Nd1—O5	2.465 (7)
Nd1—O8	2.482 (7)	Nd1—O8	2.425 (7)
Nd1—O9	2.378 (7)	Nd1—O9	2.472 (7)
Nd1—O12	2.493 (9)	Nd1—O12	2.432 (7)
Nd1—O13	2.385 (7)	Nd1—O14	2.443 (7)
Nd1—O16	2.492 (8)	Nd1—O17	2.405 (6)
P1—O1	1.478 (9)	P1—O4	1.486 (7)
P1—N1	1.589 (13)	P1—N1	1.613 (9)
P2—O5	1.491 (8)	P2—O8	1.482 (7)
P2—N2	1.590 (11)	P2—N2	1.600 (9)
P3—O9	1.479 (8)	P3—O12	1.440 (7)
P3—N3	1.563 (13)	P3—N3	1.608 (10)
P4—O13	1.475 (8)	P4—O17	1.478 (7)
P4—N4	1.564 (11)	P4—N4	1.590 (8)
O4—C3	1.279 (14)	O1—C1	1.227 (11)
O8—C7	1.221 (13)	O5—C15	1.240 (12)
O12—C11	1.27 (2)	O9—C29	1.216 (12)
O16—C15	1.231 (16)	O14—C43	1.273 (12)
N1—C3	1.280 (17)	N1—C1	1.286 (13)
N2—C7	1.355 (16)	N2—C15	1.286 (13)
N3—C11	1.27 (2)	N3—C29	1.298 (14)
N4—C15	1.312 (17)	N4—C43	1.286 (13)
O1—Nd1—O4	72.6 (3)	O1—Nd1—O4	71.6 (2)
O5—Nd1—O8	74.7 (3)	O5—Nd1—O8	71.8 (2)
O9—Nd1—O12	72.7 (3)	O9—Nd1—O12	72.0 (2)
O13—Nd1—O16	73.3 (3)	O14—Nd1—O17	73.5 (2)

Table 4.

The conformational characteristics of six-membered metallocycles in 1Nd and 2Nd.

Cycle	Mean plane atoms, rmsd/Å	Deviation of atom, Å	Type of conformation
1Nd			
Nd1–O1–P1–N1–C3–O4	Nd1…O1…N1…C3 0.01	O4 -0.21(3) P1 -0.21(4)	boat
Nd1–O5–P2–N2–C7–O8	Nd1…O8…C7…N2…O5 0.02	P2 -0.27(4)	sofa
Nd1–O9–P3–N3–C11–O12	Nd1…O9…P3…N3…C11…O12 0.03	–	planar
Nd1–O13–P4–N4–C15–O16	O13…P4…N4…C15…O16 0.03	Nd1 0.45(4)	sofa
2Nd			
Nd1–O4–P1–N1–C1–O1	O4…P1…N1…C1…O1 0.01	Nd1 0.53(4)	sofa
Nd1–O8–P2–N2–C15–O5	Nd1…O8…P2…N2…C15…O5 0.03	–	planar
Nd1–O12–P3–N3–C29–O9	O12…P3…N3…C29…O9 0.02	Nd1 -0.46(5)	sofa
Nd1–O17–P4–N4–C4–O14	Nd1…O17…P4…N4…C4…O14 0.03	–	planar

Infrared spectroscopy

The IR spectra of the **1Nd** and **2Nd** complexes, recorded as KBr pellets in the range of 4000–400 cm^{-1} (Figure 4), confirm the successful coordination of the deprotonated CAPh ligands to the Nd^{III} ions and the presence of tetraethylammonium counterions. The absence of a broad band around 3080 cm^{-1}, which would correspond to the ν(H—N) stretching vibration, indicates that the ligands in the obtained complexes exist in their acidic form. In the high-frequency region, a weak-intensity band at 3070 cm^{-1} corresponds to the C—H stretching vibrations of the phenyl rings in the $(L^2)^-$ ligand of **2Nd**, while medium- and weak-intensity bands in the region 2992–2850 cm^{-1} are assigned to the asymmetric and symmetric C—H stretching vibrations of the methyl groups in $(L^1)^-$ (**1Nd)** and of the methyl and methylene groups in the counterions of both complexes. A strong band at 1620 - 1618 cm^{-1} is assigned to the ν(C=O) stretching vibration of the coordinated carbonyl group. Compared to the free ligands HL^1 [56] and HL^2 [53], this band is shifted to lower wavenumbers in the IR spectra of the complexes, indicating coordination of the C=O group to the Nd^{III} ions through the carbonyl oxygen atom. The aromatic ring skeletal vibrations, involving carbon–carbon stretching, in the spectrum of **2Nd** appear at 1588 and 1490 cm^{-1}. The asymmetric bending vibration $\delta_{as}(CH_3)$ from the NEt_4^+ counterion, as well as from the HL^1 framework, appears at 1455 cm^{-1}, while the symmetric bending vibration $\delta_s(CH_3)$ is observed at 1393 cm^{-1}. The bending vibration $\delta_s(CH_2)$ of the methylene groups is located at 1462 cm^{-1}. Strong bands at 1366 cm^{-1} for **1Nd** and at 1370 cm^{-1} for **2Nd** are attributed to a mixed vibration involving C—C and C—N stretching. The phosphoryl group exhibits several distinct bands: the strong band in the region 1192–1186 cm^{-1} is assigned to the characteristic P=O stretching vibration of the CAPh ligand, while the band at 1166–1164 cm^{-1} corresponds to a coupled P=O and P—N stretching mode. These bands are shifted to lower wavenumbers in the spectra of the synthesized complexes compared to the spectra of the free ligands. Additional band in the region 1046–1020 cm^{-1} represents coupled stretching vibrations ν(PN)*ν(CC) of the ligands. Another strong band at 1012 cm^{-1} in the **1Nd** and at 1020 cm^{-1} in the **2Nd** spectra reflects coupled P=O and P—N stretching vibration. An aromatic C—H in-plane bending band from the ligands in **2Nd** appears at 948 and 1072 cm^{-1}, while the out-of-plane bending is reflected in the bands at 761 and 690 cm^{-1}. The CCl_3 group can be identified by absorption bands of an asymmetric stretching vibration at 780–776 cm^{-1} and a symmetric stretch at 677–674 cm^{-1}. A band at 726–718 cm^{-1} is attributed to chelate ring breathing ν(ϕ). A medium-intensity absorption band that appears in the spectrum of **2Nd** at 590 cm^{-1} is attributed to out-of-plane ring bending. A strong-intensity band at 548 cm^{-1} (**1Nd**) and 526 cm^{-1} (**2Nd)** is assigned to a coupled deformation involving in-plane chelate ring bending and Nd—O stretching modes δ(ϕ)*ν(Nd—O). Medium and weak bands at 504–498 and 462–460 cm^{-1} are assigned to the deformation vibrations of the trichloromethyl group (δ(C-Cl_3)) and in-plane chelate ring bending (δ(ϕ)) of the ligands, respectively. The band assignments were made according to references [59, 60, 61].

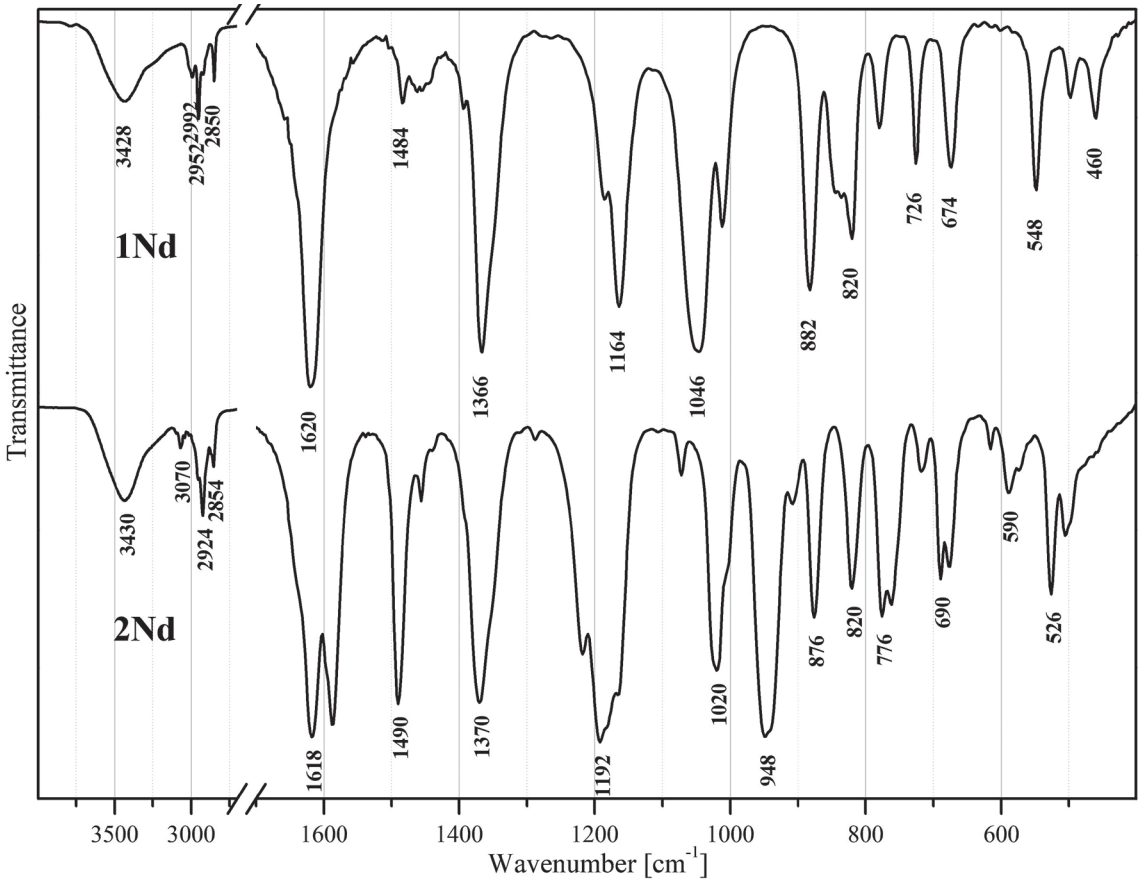

Fig. 4. Mid-FTIR spectra of 1Nd and 2Nd complexes in the form of KBr pellets.

Electronic spectroscopy.

The electronic diffuse reflectance spectra of powders of **1Nd** and **2Nd** complexes were recorded in the 400–900 nm range at room temperature and are shown in Figure 5. Both spectra exhibit characteristic f–f transitions of Nd^{III} ions from the $^4I_{9/2}$ ground state. The absorption bands were assigned according to reference [62]. The hypersensitive transition band in the region near 58–600 nm ($^4G_{5/2}$, $^2G_{7/2} \leftarrow {}^4I_{9/2}$) is similar to that observed in other previously reported CAPh-based lanthanide complexes with a coordination number of eight for the central atom[63, 64, 0]. The relative intensities of the components of this band vary slightly between **1Nd** and **2Nd** due to different coordination polyhedra of the central ions (Table 2). The band of the $^2P_{1/2} \leftarrow {}^4I_{9/2}$ transition, with maxima at 430.4 and 429.2 nm for **1Nd** and **2Nd,** respectively, shows no observable splitting in either spectrum, indicating single crystallographically equivalent Nd^{III} centers in both complexes, consistent with structural data from X-ray diffraction. Electronic transitions from thermally populated higher sublevels of the ground energy level result in the appearance of relatively intense absorption bands in the wavelength range of 432–436 nm.

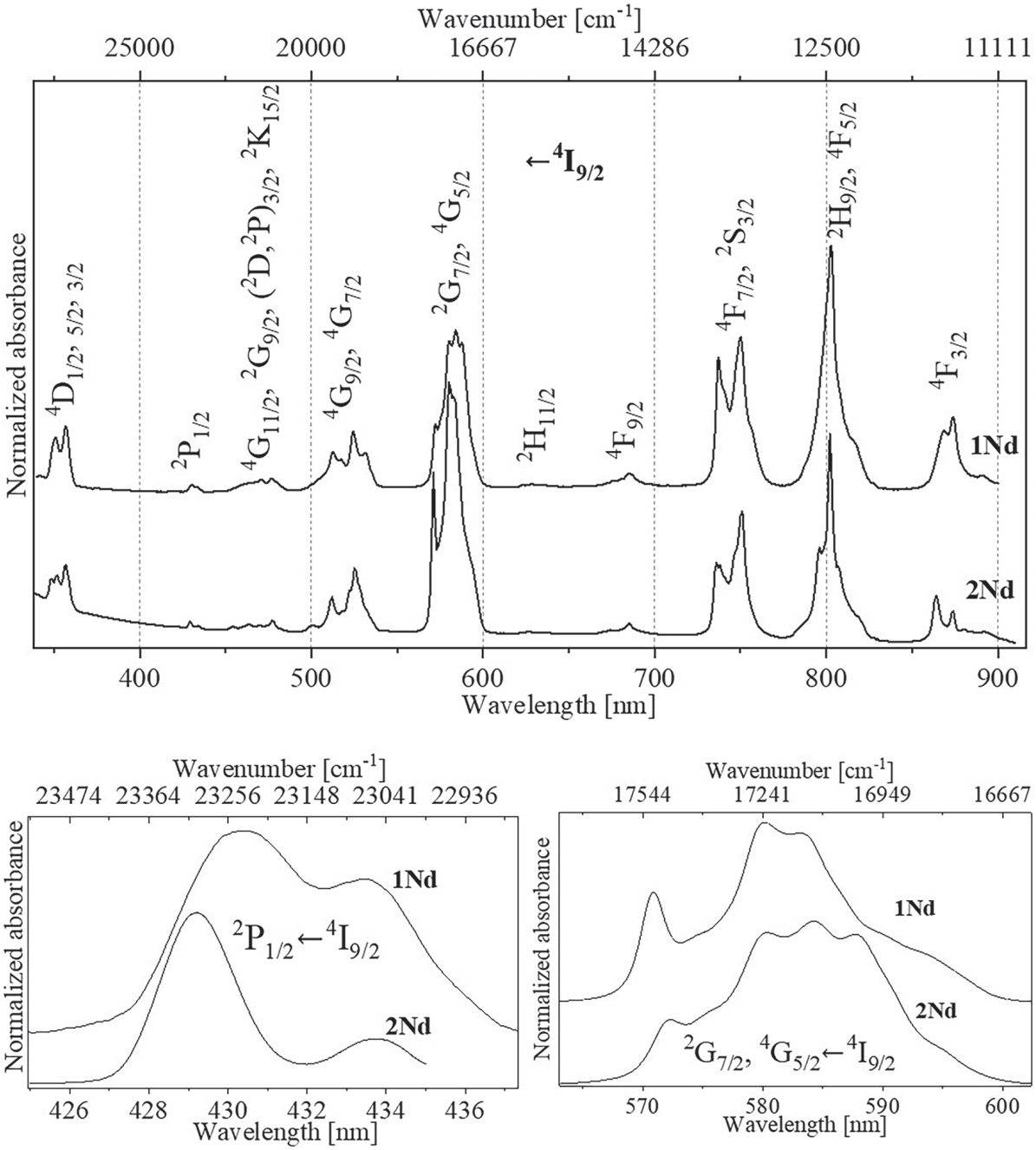

Fig. 5. Electronic diffuse reflection spectra (upper panel); $^2P_{1/2} \leftarrow {}^4I_{9/2}$ and $^2G_{7/2}$, $^4G_{5/2} \leftarrow {}^4I_{9/2}$ transition bands (lower panel) of 1Nd and 2Nd at 300 K.

To evaluate the extent of metal-ligand orbital mixing, the nephelauxetic parameter $\beta = \frac{1}{n}\sum^{n-1} \nu_c^i / \nu_{aq}^i$, the covalency parameter $\delta = \frac{1-\beta}{\beta}100\%$, the bonding parameter $b^{1/2} = \sqrt{\frac{1-\beta}{2}}$ and the angular overlap parameter $\eta = \frac{1-\sqrt{\beta}}{\sqrt{\beta}}$ were calculated by comparing the shifts of the transition bands in the diffuse reflectance spectra of the complexes (ν_c^i) with respect to the positions of the corresponding bands in the spectrum of the Nd^{III} aquo-ion (ν_{aq}^i) (Tables 5, 6) [40, 62, 65]. The obtained results are very similar for the **1Nd** and **2Nd** complexes and suggest weak covalent bonding between the Nd^{III} ions and the ligands, which is in agreement with data reported for other complexes with CAPhs [47]. A slightly larger value of δ for **2Nd** is consistent with the slightly shorter Nd—O bonds in this complex compared to **1Nd**.

Table 5.

Positions of electronic transition spectral band maxima in diffuse reflection spectra of an aquo-ion and 1Nd and 2Nd complexes [cm^{-1}].

J-level	Aquo-ion	**1Nd**	**2Nd**
$^4D_{1/2}$	28850	-	28694
$^4D_{5/2}$	28500	28498	28417
$^4D_{3/2}$	28300	28019	28019
$^2D_{5/2}$	23900	23759	-
$^2P_{1/2}$	23250	23234	23299
$^4G_{11/2}$	21650	21575	21575
$^2G_{9/2}$, $(^2D, ^2P)_{3/2}$	21300	21249	21281
$^2K_{15/2}$	21000	20964	20964
$^4G_{9/2}$	19550	19508	19535
$^4G_{7/2}$	19160	19073	19048
$^2G_{7/2}$	17460	17238	17232
$^4G_{5/2}$	17300	17150	17117
$^2H_{11/2}$	15870	15918	15949
$^4F_{9/2}$	14700	14596	14599
$^4F_{7/2}$, $^2S_{3/2}$	13500	13335	13317
$^2H_{9/2}$	12590	12458	12469
$^4F_{5/2}$	12480	-	12392
$^4F_{3/2}$	11460	11443	11443

Table 6.

The nephelauxetic parameter β, the covalency parameter δ, the bonding parameter $b^{1/2}$ and the angular overlap parameter η for 1Nd and 2Nd.

	β	δ [%]	$b^{1/2}$	η
1Nd	0.99498	0.50471	0.05011	0.00252
2Nd	0.99494	0.50863	0.05030	0.00254

Luminescence spectroscopy

Considering the presence of aromatic substituents in the HL^2, we undertook widespread investigations of **2Nd** for luminescence measurements. The HL^2 ligand possesses a triplet excited state T_1 located at 24270 cm^{-1} [54], which lies significantly above the emissive $^4F_{3/2}$ level of Nd^{3+} (11698 cm^{-1}). The energy gap between the ligand triplet state and the Nd^{III} emitting level is therefore sufficiently large to allow ligand-to-metal energy transfer to occur in **2Nd**. However, the relatively high value of ΔE also implies that additional non-radiative pathways may compete with the sensitization process. In particular, the excess energy gap can facilitate back energy transfer and multiphonon relaxation, which may partially quench the population of the Nd^{III} emissive state. Upon excitation of **2Nd** at 354 nm, the complex exhibits typical f-f emission of the Nd^{III} ion in the NIR region, with narrow bands observed near 900, 1060 and 1330 nm (Figure 6, right panel). The luminescence excitation spectrum of **2Nd**, recorded by monitoring Nd^{III} f-f emission at 1060 nm, exhibits a number of narrow bands, which were assigned to Nd^{III} f-f transitions from the ground $^4I_{9/2}$ level (Figure 6, left panel). The predominance of f-f transitions in the excitation spectrum indicates inefficient sensitization of Nd^{III} emission by the ligands, which is probably due to the large distance between the lanthanide ion and the aromatic substituents in HL^2 as well as due to the excess energy gap between the ligands' lowest triplet state and the emissive level of the neodymium ion, which can facilitate energy dissipation. Earlier, we have reported dimethyl-N-benzoylamidophosphate based complex NEt_4NdL_4 [66], in which, despite of the big energy gap between the ligand triplet state and the Nd^{III} emitting level an efficient sensitization of Nd^{III} emission was observed. This example underlines the importance of the distance between the ligands' chromophore and the lanthanide for efficiency of the antenna effect.

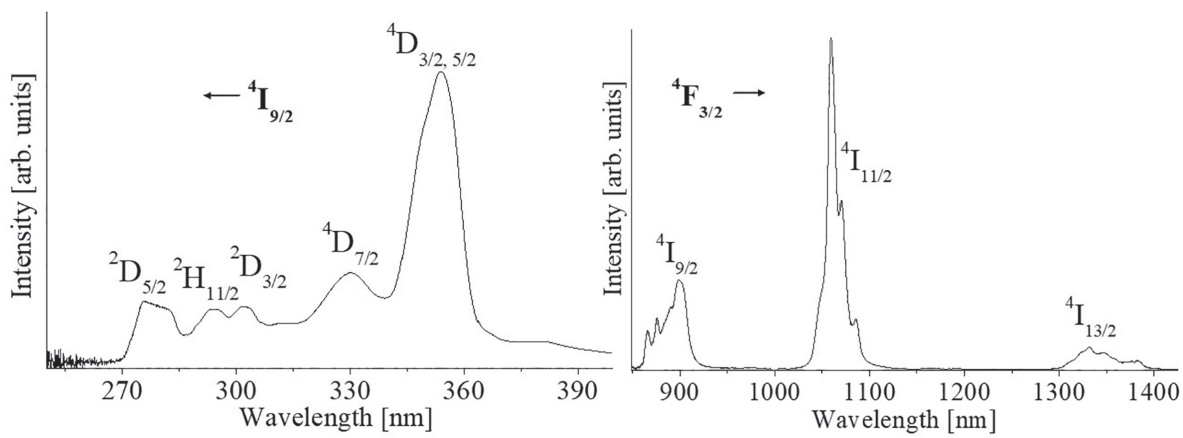

Fig. 6. Luminescence excitation (left panel) and luminescence (right panel) spectra of 2Nd at room temperature.

CONCLUSIONS.

Two new neodymium(III) tetrakis complexes with different carbacylamidophosphate ligands were synthesized and structurally and spectrally characterized.

Structural analysis revealed that variation in the organic substituents on the CAPh ligands results in distinct coordination polyhedra: a triangular dodecahedron in complex **1Nd** and a square antiprism in **2Nd**, both maintaining an eight-coordinate NdO_8 environment. The substitution of OCH_3 with OPh also causes minor differences in metal–ligand distances; however, confirmation of this conclusion requires the investigation of a broader series of related compounds.

Electronic diffuse reflectance spectra of the complexes display well-resolved f–f transitions of Nd^{III}, including hypersensitive bands whose shape depends on the ligand framework. The absence of splitting in the $^2P_{1/2} \leftarrow {}^4I_{9/2}$ transition indicates the presence of a single crystallographically unique Nd^{III} ion in each complex, corroborating the crystallographic data. Covalency parameters (δ, $b^{1/2}$, and η), calculated based on nephelauxetic shifts (β) relative to the Nd^{III} aquo ion, indicate weak covalency in the Nd–ligand bonding. The slightly higher δ value observed for **2Nd** compared to **1Nd** is consistent with shorter metal–ligand distances in the structure of **2Nd**.

Analysis of the excitation spectrum of **2Nd** showed that diphenyl-N-trichloroacetylamidophosphate in this complex insufficiently sensitizes neodymium(III) emission, despite the high enough energy of the ligand triplet state relative to the Nd^{III} emissive level, which highlights the need for future ligand designs that combine appropriate triplet-state alignment with enhanced absorption and improved suppression of nonradiative decay channels.

This study demonstrates that the structural variation in CAPh ligands enables fine-tuning of both coordination geometry and electronic spectral characteristics in lanthanide complexes. These findings support further exploration of CAPh ligands for designing Nd-based materials with tailored spectral properties for potential photonic and sensing applications.

ACKNOWLEDGEMENT. This work was supported by Ministry of Education and Science of Ukraine (grant 22BF037-04).

СТРУКТУРА ТА СПЕКТРАЛЬНА ОЦІНКА КОВАЛЕНТНОСТІ У ТЕТРАКІС-КОМПЛЕКСАХ ND(III) З КАРБАЦИЛАМІДОФОСФАТНИМИ ЛІГАНДАМИ

М. Б. Стругацька[а,*], Н. С. Каряка[а], В. О. Труш[а], В. В. Дьяконенко[б], С. В. Шишкіна[в], С. С. Смола[г], Н. В. Русакова[г], В. М. Амірханов[а]

[а] Хімічний факультет Київського національного університету ім. Тараса Шевченка, вул. Гетьмана Павла Скоропадського, 12, Київ 01033, Україна;

[б] Науково-технологічний комплекс "Інститут монокристалів" Національної академії наук України, просп. Науки, 60, Харків 61072, Україна;

[в] Інститут органічної хімії Національної академії наук України, вул. Академіка Кухаря, 5, Київ 02094, Україна;

[г] Фізико-хімічний інститут ім. О. В. Богатського Національної академії наук України, вул. Люстдорфська дорога, 86, Одеса 65080, Україна

**e-mail: mariia.struhatska@knu.ua*

Синтезовано два тетракіс-комплекси неодиму(III) $NEt_4[NdL^1_4]$ (**1Nd**) та $NEt_4[NdL^2_4]$·iPrOH (**2Nd**) із тетраетиламонієвим катіоном та різними карбациламідофосфатними лігандами: $[L^1]^-$ – диметил-N-трихлорацетиламідофосфат, $Cl_3CC(O)NP(O)(OCH_3)_2^-$, та $[L^2]^-$ – дифеніл-N-трихлорацетиламідофосфат, $Cl_3CC(O)NP(O)(OC_6H_5)_2^-$. Сполуки було охарактеризовано за допомогою елементного аналізу, інфрачервоної спектроскопії, електронної спектроскопії дифузного відбиття та рентгеноструктурного аналізу. Методом РСтА встановлено утворення аніонних комплексів із координаційним оточенням неодиму(III) NdO_8. Координаційні поліедри центральних йонів найкраще описують як трикутний додекаедр у випадку **1Nd** і квадратна антипризма для **2Nd**. Спектри дифузного відбиття в УФ, видимій і ближній ІЧ-області демонструють f–f переходи, характерні для Nd^{III}, при цьому форма та інтенсивність смуг надчутливих переходів залежить від природи лігандів. Було встановлено слабкий ковалентний характер зв'язку метал – ліганд. Дослідження люмінесценції комплексу **2Nd** виявили слабку сенсибілізацію емісії лігандом.

Ключові слова: Nd^{III}, карбациламідофосфат, тетракіс-комплекс, тетраетиламонієвий катіон, електронна спектроскопія, кристалічна структура.

REFERENCES

1. Alexander C., Guo Z., Glover P.B., Faulkner S., Pikramenou Z. Luminescent lanthanides in biorelated applications: from molecules to nanoparticles and diagnostic probes to therapeutics. *Chemical Reviews*. 2025. **125**(4): 2269–2370. https://doi.org/10.1021/acs.chemrev.4c00615
2. Binnemans K. Rare-earth beta-diketonates. *Handbook on the physics and chemistry of rare earths*. Elsevier. 2005. 35: 107–272. https://doi.org/10.1016/S0168-1273(05)35003-3
3. Singh A.K. Multifunctionality of lanthanide-based luminescent hybrid materials. *Coordination Chemistry Reviews*. 2022. **455**: 214365. https://doi.org/10.1016/j.ccr.2021.214365
4. Bünzli J.C.G. Rising stars in science and technology: luminescent lanthanide materials. *European Journal of Inorganic Chemistry*. 2017. **2017**(44): 5058–5063. https://doi.org/10.1002/ejic.201701201
5. de Bettencourt-Dias A. Lanthanide-based emitting materials in light-emitting diodes. *Dalton Transactions*. 2007. **22**: 2229–2241. https://doi.org/10.1039/B702341C
6. Sahoo J., Jaiswar S., Jena H.S., Subramanian P.S. Sensing of phosphate and ATP by lanthanide complexes in aqueous medium and its application on living cells. *Chemistry Select*. 2020. **5**(42): 12878–12884. https://doi.org/10.1002/slct.202002714
7. Bodman S.E., Butler S.J. Advances in anion binding and sensing using luminescent lanthanide complexes. *Chemical Science*. 2021. **12**(8): 2716–2734. https://doi.org/10.1039/D0SC05419D
8. Wang M., Kitagawa Y., Hasegawa Y. Current development of lanthanide complexes for biomedical applications. *Chemistry–An Asian Journal*. 2024. **19**(7): e202400038. https://doi.org/10.1002/asia.202400038
9. Lacerda S., Tóth É. Lanthanide complexes in molecular magnetic resonance imaging and theranostics. *ChemMedChem*. 2017. **12**(12): 883–894. https://doi.org/10.1002/cmdc.201700210
10. Bag P., Rastogi C.K., Biswas S., Sivakumar S., Mereacre V., Chandrasekhar V. Homodinuclear lanthanide {Ln2} (Ln = Gd, Tb, Dy, Eu) complexes prepared from an o-vanillin based

ligand: Luminescence and single-molecule magnetism behavior. *Dalton Transactions*. 2015. **44**(9): 4328–4340. https://doi.org/10.1039/c4dt03429e
11. Gil Y., Aravena D. Understanding Single-Molecule Magnet properties of lanthanide complexes from 4f orbital splitting. *Dalton Transactions*. 2024. **53**(5): 2207–2217. https://doi.org/10.1039/D3DT04179D
12. Wang J., Sun C.Y., Zheng Q., Wang D.Q., Chen Y.T., Ju J.F., Tang Y.F. Lanthanide Single-molecule Magnets: Synthetic strategy, structures, properties and recent advances. *Chemistry–An Asian Journal*. 2023. **18**(7): e202201297. https://doi.org/10.1002/asia.202201297
13. Long J., Guari Y., Ferreira R.A., Carlos L.D., Larionova J. Recent advances in luminescent lanthanide based Single-Molecule Magnets. *Coordination Chemistry Reviews*. 2018. **363**: 57–70. https://doi.org/10.1016/j.ccr.2018.02.019
14. Hirai Y. Triboluminescence of lanthanide coordination polymers. *Assembled lanthanide complexes with advanced photophysical properties*. Singapore: Springer Singapore. 2018. 81–100.
15. Bünzli J.C.G., Wong K.L. Lanthanide mechanoluminescence. *Journal of Rare Earths*. 2018. **36**(1): 1–41. https://doi.org/10.1016/j.jre.2017.09.005
16. Fontenot R.S., Hollerman W.A., Bhat K.N., Aggarwal M.D., Penn B.G. Incorporating strongly triboluminescent europium dibenzoylmethide triethylammonium into simple polymers. *Polymer journal*. 2014. **46**(2): 111–116. https://doi.org/10.1038/pj.2013.78
17. Olawale D.O., Dickens T., Sullivan W.G., Okoli O.I., Sobanjo J.O., Wang B. Progress in triboluminescence-based smart optical sensor system. *Journal of Luminescence*. 2011. **131**(7): 1407–1418. https://doi.org/10.1016/j.jlumin.2011.03.015
18. Moynihan S., Van Deun R., Binnemans K., Redmond G. Optical properties of planar polymer waveguides doped with organo-lanthanide complexes. *Optical Materials*. 2007. **29**(12): 1821–1830. https://doi.org/10.1016/j.optmat.2006.10.005
19. Yang J., Diemeer M.B., Geskus D., Sengo G., Pollnau M., Driessen A. Neodymium-complex-doped photodefined polymer channel waveguide amplifiers. *Optics letters*. 2009. **34**(4): 473–475. https://doi.org/10.1364/ol.34.000473
20. Moynihan S., Van Deun R., Binnemans K., Krueger J., von Papen G., Kewell A., Redmond G. Organo-lanthanide complexes as luminescent dopants in polymer waveguides fabricated by hot embossing. *Optical Materials*. 2007. **29**(12): 1798–1808. https://doi.org/10.1016/j.optmat.2006.10.010
21. Gao M., Li J., Xia D., Jiang L., Peng N., Zhao S., Li G. Lanthanides-based security inks with reversible luminescent switching and self-healing properties for advanced anti-counterfeiting. *Journal of Molecular Liquids*. 2022. **350**: 118559. https://doi.org/10.1016/j.molliq.2022.118559
22. Li J., Xia D., Gao M., Jiang L., Zhao S., Li G. Invisible luminescent inks and luminescent films based on lanthanides for anti-counterfeiting. *Inorganica Chimica Acta*. 2021. **526**: 120541. https://doi.org/10.1016/j.ica.2021.120541
23. Andres J., Hersch R.D., Moser J.E., Chauvin A.S. A new anti-counterfeiting feature relying on invisible luminescent full color images printed with lanthanide-based inks. *Advanced Functional Materials*. 2014. **24**(32): 5029–5036. https://doi.org/10.1002/adfm.201400298
24. Carlotto A., Babetto L., Carlotto S., Miozzi M., Seraglia R., Casarin M., Armelao L. Luminescent thermometers: from a library of europium (III) β-diketonates to a general model for predicting the thermometric behaviour of europium-based coordination systems. *ChemPhotoChem*. 2020. **4**(9): 674–684. https://doi.org/10.1002/cptc.202000116

25. Zhernakov M.A., Sedykh A.E., Denisenko Y.G., Molokeev M.S., Mirzayanov I.I., Becker J., Müller-Buschbaum K. Luminescent thermometer systems Dy3+/Eu3+ and Tb3+/Sm3+ based on coordination compounds: new pairs to the approved Tb3+/Eu3+?. *Chemistry of Materials.* 2024. **36**(19): 9704–9717. https://doi.org/10.1021/acs.chemmater.4c01851
26. Miyata K., Konno Y., Nakanishi T., Kobayashi A., Kato M., Fushimi K., Hasegawa Y. Chameleon luminophore for sensing temperatures: control of metal-to-metal and energy back transfer in lanthanide coordination polymers. *Angewandte Chemie*. 2013. **125**(25). https://doi.org/10.1002/anie.201301448
27. Wang X.D., Wolfbeis O.S., Meier R.J. Luminescent probes and sensors for temperature. *Chemical Society Reviews.* 2013. **42**(19): 7834–7869. https://doi.org/10.1039/c3cs60102a
28. Katsagounos G., Stathatos E., Arabatzis N.B., Keramidas A.D., Lianos P. Enhanced photon harvesting in silicon multicrystalline solar cells by new lanthanide complexes as light concentrators. *Journal of luminescence.* 2011. **131**(8): 1776–1781. https://doi.org/10.1016/j.jlumin.2011.04.023
29. Shahi P.K., Singh P., Rai S.B. Sunlight activated lanthanide complex for luminescent solar collector applications: effect of waveguide matrix. *Journal of Physics D: Applied Physics.* 2017. **50**(7): 075501. https://doi.org/10.1088/1361-6463/aa4ecd
30. Bennett S.D., Core B.A., Blake M.P., Pope S.J., Mountford P., Ward B.D. Chiral lanthanide complexes: coordination chemistry, spectroscopy, and catalysis. *Dalton Transactions* 2014. **43**(15): 5871–5885. https://doi.org/10.1039/C4DT00114A
31. Dicken R.D., Motta A., Marks T.J. Homoleptic lanthanide amide catalysts for organic synthesis: experiment and theory. *Acs Catalysis.* 2021. **11**(5): 2715–2734. https://doi.org/10.1021/acscatal.0c04882
32. Costa I.F., Blois L., Paolini T.B., Assunção I.P., Teotonio E.E., Felinto M.C.F., Brito H.F. Luminescence properties of lanthanide tetrakis complexes as molecular light emitters. *Coordination Chemistry Reviews*. 2024. **502**: 215590. https://doi.org/10.1016/j.ccr.2023.215590
33. Sastri V.R., Perumareddi J.R., Rao V.R., Rayudu G.V.S., Bünzli J.C. Modern aspects of rare earths and their complexes. Amsterdam: Elsevier. 2003. ISBN 0444510109
34. Amirkhanov V., Ovchynnikov V., Trush V., Gawryszewska P., Jerzykiewicz L.B. Powerful new ligand systems: carbacylamidophosphates (CAPh) and sulfonylamidophosphates (SAPh). *Ligands: Synthesis, Characterization and Role in Biotechnology*. New York: NOVA publishers. 2014. 199–248.
35. Kariaka N.S., Lipa A., Carneiro Neto A.N., Malta O.L., Gawryszewska P. and Amirkhanov V.M. Eu3+ and Tb3+ coordination compounds with phenyl-containing carbacylamidophosphates: comparison with selected Ln3+ β-diketonates. *Frontiers in Chemistry*. 2023. **11**: 1188314. https://doi.org/10.3389/fchem.2023.1188314
36. Sinha S.P. Spectroscopic investigations of some neodymium complexes. *Spectrochimica Acta*. 1966. **22**(1): 57–62. https://doi.org/10.1016/0371-1951(66)80008-5
37. Carnall W.T., Fields P.R., Rajnak K. Electronic energy levels in the trivalent lanthanide aquo ions. I. Pr3+, Nd3+, Pm3+, Sm3+, Dy3+, Ho3+, Er3+, and Tm3+. *The Journal of chemical physics*. 1968. **49**(10): 4424–4442. https://doi.org/10.1063/1.1669893
38. Wybourne B.G., Meggers W.F. Spectroscopic properties of rare earths. New York: John Wiley. 1965. 236.
39. Agarwal R.K., Prasad S., Garg R., Sidhu S.K. Synthesis and preliminary structural characterization of some lanthanide (III) semicarbazone complexes. *Bulletin of the Chemical Society of Ethiopia.* 2006. **20**(1): 167–172. http://dx.doi.org/10.4314/bcse.v20i1.21157

40. Sinha S.P. Ternary Lanthanide Complexes of the Type [M(HMPA)4(NO3)3]: A new method of synthesis and spectroscopic studies including a comparison of the electronic spectra of the [M(HMPA)x(ClO4)3] complexes. *Zeitschrift für anorganische und allgemeine Chemie*. 1977. **434**(1): 277–292. https://doi.org/10.1002/zaac.19774340134
41. Wyart J.F., Meftah A., Bachelier A., Sinzelle J., Tchang-Brillet W.Ü.L., Champion N., Sugar J. Energy levels of 4f3 in the Nd3+ free ion from emission spectra. *Journal of Physics B: Atomic, Molecular and Optical Physics*. 2006. **39**(5): L77. http://dx.doi.org/10.1088/0953-4075/39/5/L01
42. Gao F., Zhang S. Investigation of mechanism of nephelauxetic effect. *Journal of Physics and Chemistry of Solids*. 1997. **58**(12): 1991–1994. https://doi.org/10.1016/S0022-3697(96)00139-4
43. Ryan J.L., Jørgensen C.K. Absorption spectra of octahedral lanthanide hexahalides. *The Journal of Physical Chemistry*. 1966. **70**(9): 2845–2857. https://doi.org/10.1021/j100881a021
44. Davidenko N.K., Yatsimirskii K.B. Determination of metal-ligand distances from the position of the spectral bands in lanthanide complexes. *Dokl. Akad. Nauk SSSR*. 1970. **191**(2): 384-387. (in Russian).
45. Karraker D.G. Hypersensitive transitions of six-, seven-, and eight-coordinate neodymium, holmium, and erbium chelates. *Inorganic chemistry*. 1967. **6**(10): 1863–1868. http://dx.doi.org/10.1021/ic50061a018
46. Karraker D.G. Spectral studies on the Nd3+ and Er3+ chelates of heptafluorodimethyloctanedione. *Journal of Inorganic and Nuclear Chemistry*. 1971. **33**(11): 3713–3718. https://doi.org/10.1016/0022-1902(71)80278-6
47. Kariaka N.S., Kolotilov S.V., Gawryszewska P., Kasprzycka E., Weselski M., Dyakonenko V.V., Shishkina S.V., Trush V.A., Amirkhanov V.M. Structures and spectral and magnetic properties of a series of carbacylamidophosphate pentanuclear lanthanide(III) hydroxo complexes. *Inorganic Chemistry*. 2019. **58** (21): 14682–14692. https://doi.org/10.1021/acs.inorgchem.9b02354
48. Pham Y.H., Trush V.A., Korabik M., Amirkhanov V.M., Gawryszewska P. Nd3+ and Yb3+ complexes with N-(diphenylphosphoryl) pyrazine-2-carboxamide as UV-NIR radiation converters and single-ion magnets. *Dyes and Pigments*. 2021. **186**: 108986. http://dx.doi.org/10.1016/j.dyepig.2020.108986
49. Lyle S.J., Rahman M.M. Complexometric titration of yttrium and the lanthanons—I: A comparison of direct methods. *Talanta*. 1963. **10**(11): 1177–1182. https://doi.org/10.1016/0039-9140%2863%2980170-8
50. Dolomanov O.V., Bourhis L.J., Gildea R.J., Howard J.A., Puschmann H. OLEX2: a complete structure solution, refinement and analysis program. *Applied Crystallography*. 2009. **42**(2): 339–341. https://doi.org/10.1107/S0021889808042726
51. Sheldrick G.M. SHELXT – Integrated space-group and crystal-structure determination. *Foundations of Crystallography*. 2015. **71**(1): 3–8. https://doi.org/10.1107/S2053273314026370
52. Sheldrick G.M. Crystal structure refinement with SHELXL. *Crystal Structure Communications*. 2015. **71**(1): 3–8. https://doi.org/10.1107/S2053229614024218
53. Savchuk M.O., Litsis O.O., Sliva T.Yu., Trush V.A., Amirkhanov V.M. Synthesis of diphenyl-N-trichloroacetylamidophosphate and IR spectroscopic investigations of REE anionic coordination compounds on its base. *Voprosy khimii i khimicheskoi tekhnologii*. 2017. **6**: 44–49. ISSN 0321-4095
54. Savchuk M.O., Litsis O.O., Kariaka N.S., Trush V.O., Dyakonenko V.V., Smola S.S., Amirkhanov V.M. Polymeric sodium salts and monomeric lanthanide coordination compounds with diphenyl-N-trichloroacetylami-

dophosphate: synthesis and characterization. *Inorganica Chimica Acta.* 2024. **559**: 121783. https://doi.org/10.1016/j.ica.2023.121783
55. Llunell M., Casanova D., Cirera J., Alemany P., Alvarez S. SHAPE, Ver. 2.0. University of Barcelona: Barcelona, Spain. 2010.
56. Amirkhanov V.M., Trush V.A. Properties and structure of dimethyl ether of trichloroacetylamidophosphoric acid. *Russian Journal of General Chemistry.* 1995. **65**(7): 1120–1124. (in Russian).
57. Kariaka N.S., Dyakonenko V.V., Znovjyak K.O., Shishkina S.V., Amirkhanov V.M. Synthesis, crystal structure and Hirshfeld surface analysis of the tetrakis complex NaNdPyr4(i-PrOH)2·i-PrOH with a carbacylamidophosphate of the amide type. *Structure Reports*. 2023. **79**(12): 1218–1222. https://doi.org/10.1107/S2056989023010071
58. Litsis O.O., Ovchynnikov V.A., Scherbatskii V.P., Nedilko S.G., Sliva T.Y., Dyakonenko V.V., Amirkhanov V.M. Lanthanide mixed-ligand complexes of the [Ln(CAPh)3(Phen)] and [LaxEu1-x(CAPh)3(Phen)] (CAPh= carbacylamidophosphate) type. A comparative study of their spectral properties. *Dalton Transactions.* 2015. **44**(35): 15508–15522. https://doi.org/10.1039/C5DT02557E
59. Sokolnicki J., Legendziewicz J., Amirkhanov W., Ovchinnikov V., Macalik L., Hanuza J. Comparative optical studies of lanthanide complexes with three types of phosphoro-azo derivatives of β-diketones. *Spectrochimica Acta Part A: Molecular and Biomolecular Spectroscopy.* 1999. **55**(2): 349–367. https://doi.org/10.1016/S1386-1425(98)00193-0
60. Coates J. Interpretation of infrared spectra, a practical approach. *Encyclopedia of analytical chemistry.* 2000. **12**: 10815–10837. https://doi.org/10.1002/9780470027318.a5606
61. Silverstein R.M., Webster F.X., Kiemle D.J., Bryce D.L. Spectrometric identification of organic compounds. – 8th ed. Wiley. 2014. 464.
62. Yatsimirskii K.B., Davidenko N.K. Absorption spectra and structure of lanthanide coordination compounds in solution. *Coordination Chemistry Reviews.* 1979. **27**(3): 223–273. https://doi.org/10.1016/S0010-8545(00)82068-8
63. Kariaka N.S., Trush V.A., Medviediev V.V., Dyakonenko V.V., Shishkin O.V., Smola S.S., Amirkhanov V.M. Coordination compounds based on CAPh type ligand: synthesis, structural characteristics and luminescence properties of tetrakis-complexes CsLnL4 with dimethylbenzoylamidophosphate. *Journal of Coordination Chemistry.* 2016. **69**(1): 123–134. http://dx.doi.org/10.1080/00958972.2015.1115024
64. Znovjyak K.O., Moroz O.V., Ovchynnikov V.A., Sliva T.Y., Shishkina S.V., Amirkhanov V.M. Synthesis and investigations of mixed-ligand lanthanide complexes with N,N′-dipyrrolidine-N′′-trichloracetylphosphortriamide, dimethyl-N-trichloracetylamidophosphate, 1,10-phenanthroline and 2,2′-bipyrimidine. *Polyhedron*. 2009. **28**(17): 3731–3738. https://doi.org/10.1016/J.POLY.2009.08.017
65. Henrie D.E., Choppin G.R. Environmental effects on f–f transitions. II. "Hypersensitivity" in some complexes of trivalent neodymium. *The Journal of Chemical Physics.* 1968. **49**(2): 477–481. https://doi.org/10.1063/1.1670099
66. Kariaka N.S., Trush V.A., Dyakonenko V.V., Shishkina S.V., Smola S.S., Rusakova N.V., Sliva T.Y., Gawryszewska P., Carneiro Neto A.N., Malta O.L., Amirkhanov V.M. New luminescent lanthanide tetrakis-complexes NEt4[LnL4] based on dimethyl-N-benzoylamidophosphate. *ChemPhysChem.* 2022. **23**(14): e202200129. https://doi.org/10.1002/cphc.202200129

Стаття надійшла 17.09.2025.

UDC 546.3+543.4+543.572 doi: 10.33609/2708-129X.91.11.2025.22-34

CATION EFFECT ON THERMAL STABILITY AND LUMINESCENT PROPERTIES OF BINUCLEAR RARE EARTH ANIONIC COMPLEXES WITH BISCARBACYLAMIDOPHOSPHATE.

Nataliia Kariaka[1,*], Viktor Trush[1], Igor Fesych[1], Olena Gnatyuk[2], Ivan Gnatyuk[2], Galyna Dovbeshko[2], Volodymyr Amirkhanov[1]

[1]Taras Shevchenko National University of Kyiv, Department of Chemistry, 64 Volodymyrska str., 01601 Kyiv, Ukraine;
[2] Department of Physics of Biological Systems, Institute of Physics of the National Academy of Sciences of Ukraine, 46 Prospekt Nauki, 03028 Kyiv, Ukraine
e-mail: natka04@i.ua

A series of new binuclear anionic coordination compounds of yttrium (III) and europium (III) with bis-carbacylamidophosphate ligand tetramethyl N,N′-(2,2,3,3,4,4-hexafluoro-1,5-dioxopentane-1,5-diyl)bis(phosphoramidate) and six different cations has been obtained with an aim to study the cation influence on the thermal and spectral properties of the complexes. The synthesis of coordination compounds was carried out using standard techniques based on the exchange reaction between lanthanide nitrates and the sodium or triethylammonium salt of the ligand in non-aqueous solutions. The complexes' composition was established by means of elemental and thermal gravimetric analyses as well as ^{1}H NMR spectroscopy. The chelating type of metal binding with participation of both chelating cores of the bis-carbacylamidophosphate was confirmed by IR spectroscopy. It was shown that the cation nature greatly influences the properties of complexes, such as solubility, thermal stability, and luminescence characteristics, as well as determines the degree of the complexes' hydration. The europium (III) complexes exhibit f-f emission, which is sensitized by the ligands. The luminescence intensity, bands splitting, and bands intensity ratios, as well as luminescence decay time and intrinsic quantum yield, were found to be strongly dependent on the cation in the complexes under study. The red/orange ratio for the europium (III) complexes varies from 2.6 to 7.6, the luminescence decay time varies from 0.76 to 2.74 ms, and the intrinsic quantum yield varies from 24 to 90 %. The temperature of decomposition varies in the range near 155–190 °C, depending on the cation. The manuscript contributes to the studies of influence of outer sphere interactions on the luminescence of lanthanides' complexes, which is important for design of luminescent compounds with suitable for practical application properties.

Key words: rare earth element, bis-carbacylamidophosphate, coordination compounds, luminescence, thermal gravimetric analysis.

INTRODUCTION. Coordination compounds of lanthanides are objects of intensive research due to their specific spectral and magnetic properties, which are of interest for modern technologies [1–6]. Organic ligands in the coordination compounds of lanthanides play an important role, being used to enhance or modulate properties of Ln^{III} ions as well as to adjust other useful properties of compounds such as solubility, conductivity, biological activity, etc. An additional significant effect on luminescent and magnetic properties of lanthanides can result from outer-spherical ions and intermolecular interactions in the complex [7–13]. Such an influence occurs due to changes in the geometry and electronic properties of the ligand. As a result, the geometry of the coordination polyhedron of the lanthanide, the "rigidity" of the complex, or the energy of the triplet state of the ligand can vary. These affect the efficiency of energy transfer from the ligand to the metal as well as the efficiency of excited states deactivation. The influence of the second coordination domain on the photophysical properties of Ln^{III} coordination compounds is difficult to predict, and the relationships found are often not well understood. Therefore, research aimed at a deeper understanding of the mechanisms of influence of the second coordination sphere of lanthanide complexes on their properties is relevant. The knowledge gained will make it possible to design and improve the photophysical characteristics of electromagnetic radiation converters based on lanthanide complexes.

This study is devoted to the synthesis and investigation of new anionic binuclear rare earth complexes of general formula $(Cation)_2Ln_2L_4$ (where Ln = Y, Eu) with biscarbacylamidophosphate ligand H_2L (Figure 1) and different cations ($[Cation_2]^{2+}$ = $[Na_2]^{2+}$, $[Cs_2]^{2+}$, $[(NH_4)_2]^{2+}$, $[(NMe_4)_2]^{2+}$, $[NaNEt_4]^{2+}$, and $[(HNEt_3)_2]^{2+}$). Different radii and different nature of the cations cause different polarizability and affect the possibility of hydrogen bond formation and their strength, thus can significantly affect the geometry of the complex, spectral properties, and ability to crystallize.

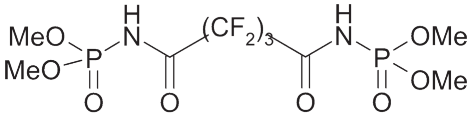

Fig. 1. The structural formula of H_2L

EXPERIMENT AND DISCUSSION OF THE RESULTS.

Synthesis of the complexes.

The H_2L and its sodium salt were synthesized and identified as described earlier [14, 15]. The complexes were obtained according to the following schemes:

$$2Ln(NO_3)_3{\times}6H_2O + 4Na_2L = Na_2[Ln_2L_4]{\cdot}3H_2O + 6NaNO_3 + 6H_2O$$
$$2Ln(NO_3)_3{\times}6H_2O + 4Cs_2L = Cs_2[Ln_2L_4]{\cdot}H_2O + 6CsNO_3 + 6H_2O$$
$$2Ln(NO_3)_3{\times}6H_2O + 4Na_2L + 2NH_4NO_3 = (NH_4)_2[Ln_2L_4]{\cdot}4H_2O + 8NaNO_3 + 6H_2O$$
$$2Ln(NO_3)_3{\times}6H_2O + 4Na_2L + 2NMe_4Cl = (NMe_4)_2[Ln_2L_4]{\cdot}H_2O + 6NaNO_3 + 2NaCl + 6H_2O$$
$$2Ln(NO_3)_3{\times}6H_2O + 4Na_2L + NEt_4Cl = NEt_4[NaLn_2L_4]{\cdot}H_2O + 6NaNO_3 + NaCl + 6H_2O$$
$$2Ln(NO_3)_3{\times}6H_2O + 4H_2L + 8NEt_3 = (HNEt_3)_2[Ln_2L_4]{\cdot}3H_2O + 6HNEt_3NO_3 + 6H_2O$$
$$Ln = Eu, Y.$$

To obtain $Na_2[Ln_2L_4]\cdot 3H_2O$ and $Cs_2[Ln_2L_4]\cdot H_2O$ the mixture of hydrated rare earth nitrates (0.2 mmol) and triethyl orthoformate (1.2 mmol) were dissolved in acetone (4 mL) upon refluxing and heating to acetone boiling temperature. Separately, Na_2L or Cs_2L (0.4 mmol) were dissolved in a mixture of acetone and 2-propanol (1:1, 10 mL) upon heating. The obtained solutions were mixed, refluxed upon heating for a minute and left to cool down to the room temperature. Then, the precipitation of $NaNO_3$ or $CsNO_3$ was filtered off and the clear solution was left at room conditions for slow evaporation of the solvents. In few days, when the majority of the solvent was evaporated, the precipitation of the target complexes appeared. It was, filtered off, washed with 2-propanol and left on air to dry for a day and then for 8 hours in drying closet at 40 °C. The yield of the complexes was 70–76 %.

The complexes $(NH_4)_2[Ln_2L_4]\cdot 4H_2O$, $(NMe_4)_2[Ln_2L_4]\cdot H_2O$, and $NEt_4[NaLn_2L_4]\cdot H_2O$ were obtained in a similar way as described above by combining three solutions at the initial stage. The NH_4NO_3 was dissolved in ethanol, while NMe_4Cl and NEt_4Cl were dissolved in 2-propanol. The yield of the complexes was 57–75 %.

To obtain $(HNEt_3)_2[Ln_2L_4]\cdot 3H_2O$ the solution of mixture of hydrated rare earth nitrates (0.2 mmol) and triethyl orthoformate (1.2 mmol) in acetone was combined with the solution of mixture of H_2L (0.4 mmol, 0.18166 g) and NEt_3 (0.8 mmol, 0.111 ml) in 2-propanol. The obtained final solution was refluxed upon heating for a minute, then, cooled down to the room temperature and left to stand in air for slow evaporation of the solvents. The polycrystalline precipitate of the target complexes appeared in two days. It was filtered off, washed with 2-propanol and dried as described above. The yield of the complexes was near 80 %.

The obtained compounds are polycrystalline or amorphous powders, which are stable in air and have different solubility depending on the outer-sphere cations. All the complexes are soluble in methanol and insoluble in 2-propanol. The compounds $Cs_2[Ln_2L_4]\cdot H_2O$, $(NH_4)_2[Ln_2L_4]\cdot 4H_2O$ and $(NMe_4)_2[Ln_2L_4]\cdot H_2O$ are soluble in water, while the rest of the obtained complexes ($Na_2[Ln_2L_4]\cdot 3H_2O$, $NEt_4[NaLn_2L_4]\cdot H_2O$, and $(HNEt_3)_2[Ln_2L_4]\cdot 3H_2O$) do not dissolve in water. All the obtained complexes, except of $(NMe_4)_2[Ln_2L_4]\cdot H_2O$ are slightly soluble in acetone. The complexes $(HNEt_3)_2[Ln_2L_4]\cdot 3H_2O$ are soluble in dichloromethane as well.

Compound $Na_2[Y_2L_4]\cdot 3H_2O$ ($Na_2Y_2C_{36}H_{54}N_8P_8O_{35}F_{24}$). Elemental anal. Calcd (%): H 2.61%, C 20.72%, N 5.37%; found H 2.46%, C 21.54%, N 5.47%. NMR - ^{1}H (DMSO-d6): $[L]^-$ 3.56 (d) 48H; ^{31}P (DMSO-d6): 10.74 (s)

Compound $Na_2[Eu_2L_4]\cdot 3H_2O$ ($Na_2Eu_2C_{36}H_{54}N_8P_8O_{35}F_{24}$). Elemental anal. Calcd (%): H 2.46%, C 19.54%, N 5.06%; found H 2.26%, C 19.50%, N 5.31%.

Compound $Cs_2[Y_2L_4]\cdot H_2O$ ($Cs_2Y_2C_{36}H_{50}N_8P_8O_{33}F_{24}$). Elemental anal. Calcd (%): H 2.22%, C 19.05%, N 4.94%; found H 2.12%, C 18.88%, N 5.04%. NMR - ^{1}H (DMSO-d6): $[L]^-$ 3.56 (d) 48H; ^{31}P (DMSO-d6): 10.57 (s).

Compound $Cs_2[Eu_2L_4]\cdot H_2O$ ($Cs_2Eu_2C_{36}H_{50}N_8P_8O_{33}F_{24}$). Elemental anal. Calcd (%): H 2.10%, C 18.04%, N 4.68%; found H 2.06%, C 17.81%, N 4.80%.

Compound $(NH_4)_2[Y_2L_4]\cdot 4H_2O$ ($Y_2C_{36}H_{64}N_{10}P_8O_{36}F_{24}$). Elemental anal. Calcd (%): H 3.08%, C 20.64%, N 6.69%; found

H 2.99%, C 21.46%, N 6.85%. NMR - ^{1}H (DMSO-d6): $[L]^-$ 3.55 (d) 48H, $[NH_4]^+$ 7.12 (m) 8H; ^{31}P (DMSO-d6): 10.57 (s)

Compound $(NH_4)_2[Eu_2L_4]\cdot 4H_2O$ ($Eu_2C_{36}H_{64}N_{10}P_8O_{36}F_{24}$). Elemental anal. Calcd (%): H 2.91%, C 19.47%, N 6.31%; found H 2.68%, C 19.74%, N 6.46%.

Compound $(NMe_4)_2[Y_2L_4]\cdot H_2O$ ($Y_2C_{44}H_{74}N_{10}P_8O_{33}F_{24}$). Elemental anal. Calcd(%): H 3.46%, C 24.55%, N 6.51%; found H 3.37%, C 24.28%, N 6.62%. NMR - ^{1}H (DMSO-d6): $[L]^-$ 3.54 (d) 48H, $[NMe_4]^+$ 3.08 (s) 24H; ^{31}P (DMSO-d6): 10.99 (s).

Compound $(NMe_4)_2[Eu_2L_4]\cdot H_2O$ ($Eu_2C_{44}H_{74}N_{10}P_8O_{33}F_{24}$). Elemental anal. Calcd (%): H 3.27%, C 23.19%, N 6.15%; found H 3.22%, C 22.90%, N 6.24%.

Compound $NEt_4[NaY_2L_4]\cdot H_2O$ ($NaY_2C_{44}H_{70}N_9P_8O_{33}F_{24}$). Elemental anal. Calcd (%): H 3.27%, C 24.49%, N 5.84%; found H 3.24%, C 24.18%, N 5.97%. NMR - ^{1}H (DMSO-d6): $[L]^-$ 3.56 (d) 48H, $[NEt_4]^+$ 1.14 (m) 12H, 3.18 (m) 8H; ^{31}P (DMSO-d6): 10.74 (s).

Compound $NEt_4[NaEu_2L_4]\cdot H_2O$ ($NaEu_2C_{44}H_{70}N_9P_8O_{33}F_{24}$). Elemental anal. Calcd (%): H 3.09%, C 23.14%, N 5.52%; found H 3.08%, C 22.90%, N 5.60%.

Compound $(HNEt_3)_2[Y_2L_4]\cdot 3H_2O$ ($Y_2C_{48}H_{86}N_{10}P_8O_{35}F_{24}$). Elemental anal. Calcd (%): H 3.86%, C 25.68%, N 6.24%; found H 3.76%, C 25.96%, N 6.41%. NMR - ^{1}H (DMSO-d6): $[L]^-$ 3.57 (d) 48H, $[HNEt_3]^+$ 1.15 (m) 18H, 3.13 (m) 12H; ^{31}P (DMSO-d6): 10.96 (s).

Compound $(HNEt_3)_2[Eu_2L_4]\cdot 3H_2O$ ($Eu_2C_{48}H_{86}N_{10}P_8O_{35}F_{24}$). Elemental anal. Calcd (%): H 3.66%, C 24.31%, N 5.91%; found H 3.55%, C 24.36%, N 6.09%.

Methods

Elemental analysis was performed on a Perkin-Elmer 2400 CHN elemental analyzer.

The thermal stabilities of the complexes have been studied on a derivatograph Mettler-Toledo TGA/DSC 3+ STARe System and on a synchronous TG / DTA analyzer Shimadzu DTG-60H in the temperature range up to 600 °C in argon atmosphere with a heating rate equal to 5 °C/min.

^{1}H and ^{31}P NMR spectra for solutions in dimethyl sulfoxide were obtained on an AVANCE 400 Bruker NMR spectrometer at room temperature.

Infrared spectra were recorded using a TENSOR 27 (Bruker) infrared spectrometer with an ATR attachment, which was developed specifically for the study of solid and powdery samples. All spectra were recorded in the wide spectral region from 4000 to 400 cm^{-1}. For spectra processing, the Opus 8.0 program was used. All spectra were baselined and normalized by the intensity of a band near 1600 cm^{-1}.

Diffuse reflection spectra were recorded on a Shimadzu UV-2600i spectrometer.

The luminescence spectra and luminescence decay time were measured using a spectrofluorometer FS5 (Edinburgh Instruments). It is a high-tech, all-in-one solution that allows the measurement of fluorescence spectra, UV and visible absorption spectra, and fluorescence decay times. This system has a guaranteed signal-to-noise ratio of > 6000:1 at 350 nm excitation and 397 nm emission, with an integration time of 1 s. A special vertically inclined and linearly positioned solid sample holder was used to record the spectra to maximize the signal from the sample. The fluorescence decay times were measured using the Time-Correlated Single-Photon Counting Technique, which

is a quantum-based, highly sensitive method that is less sensitive to noise. This allows the measurement of decay times of less than 30 ps. The resolution of the TCSPC matrix is 305 ps. The continuous light source was a 150W xenon arc lamp. For fluorescence decay time, the EPL laser at 375 nm was used. The spectra were measured using identical conditions for each sample.

Spectroscopic studies of the complexes

IR and NMR spectroscopy

The ^{1}H NMR spectroscopy of the diamagnetic Y^{III} complexes allowed establishing the ratio between the organic cations and the ligand's protons. The ^{1}H NMR spectra of the complexes contain the doublet signal of methylate groups of $[L]^{2-}$ at 3.54–3.57 ppm. This signal is shifted compared to the spectrum of H_2L (3.74 ppm [15]) towards the high field. The signal of the amide proton is absent in the spectra of the complexes, confirming the ligands' deprotonated form in the complex compositions. The residual solvent 2-propanol can be observed in the ^{1}H NMR spectra of $Na_2[Y_2L_4]\cdot 3H_2O$ and $(NH_4)_2[Y_2L_4]\cdot 4H_2O$. The ^{31}P NMR spectrum of each Y^{III} complex contains a singlet band with the maximum in the range 10.57–10.99 ppm. This testifies the equivalence of the phosphorus atoms in the composition of the complexes, and also confirms their individuality.

IR spectra of all the complexes are very similar to each other (Figure 2). In the high wavelength part of the spectra, one can observe a series of narrow ν(CH) bands in the region 3060–2830 cm^{-1} and broad bands ν(OH) in the region 3600–3200 cm^{-1}. The latter has different intensity depending on the complex and appears due to the presence of the small amount of moisture and residual 2-propanol solvent in the samples. A band ν(NH) at near 3250 cm^{-1} is also observed for the complexes $(NH_4)_2[Ln_2L_4]\cdot 4H_2O$ and $(HNEt_3)_2[Ln_2L_4]\cdot 3H_2O$ due to respective cations' vibrations. The ν(NH) band of the ligand is not observed in the IR spectra of the coordination compounds, confirming the double deprotonated form of the ligands in the complexes' composition. There are numerous narrow bands in the region 1800–400 cm^{-1} of the IR spectra of the complexes. The most intense are bands of C=O valence vibrations (at near 1600 cm^{-1}), P=O valence vibrations (at near 1250 cm^{-1}), and POC deformational vibrations (at near 1030 cm^{-1}). The bands of C=O and P=O valence vibrations are shifted significantly towards lower frequencies compared to the spectrum of H_2L (Table 1), indicating coordination of both carbonyl and phosphoryl oxygen atoms to the metals. The blue shift of ν(PN) band results from distribution of electron density in the ligands' chelating cores OCNPO.

Table 1.

Positions of the main characteristic bands in the IR spectra of the complexes.

Compound/ Assignment of bands	ν(C=O)	ν(P=O)	ν(P-N)
H_2L [15]	1746	1212	877
$Na_2[Y_2L_4]\cdot 3H_2O$	1603	1149	964
$Na_2[Eu_2L_4]\cdot 3H_2O$	1606	1147	962
$Cs_2[Y_2L_4]\cdot H_2O$	1598	1154	961
$Cs_2[Eu_2L_4]\cdot H_2O$	1597	1154	960
$(NH_4)_2[Y_2L_4]\cdot 4H_2O$	1605	1155	959
$(NH_4)_2[Eu_2L_4]\cdot 4H_2O$	1602	1158	959
$(NMe_4)_2[Y_2L_4]\cdot H_2O$	1615	1160	965
$(NMe_4)_2[Eu_2L_4]\cdot H_2O$	1612	1158	963
$NEt_4[NaY_2L_4]\cdot H_2O$	1604	1152	963
$NEt_4[NaEu_2L_4]\cdot H_2O$	1611	1159	963
$(HNEt_3)_2[Y_2L_4]\cdot 3H_2O$	1607	1149	963
$(HNEt_3)_2[Eu_2L_4]\cdot 3H_2O$	1607	1148	963

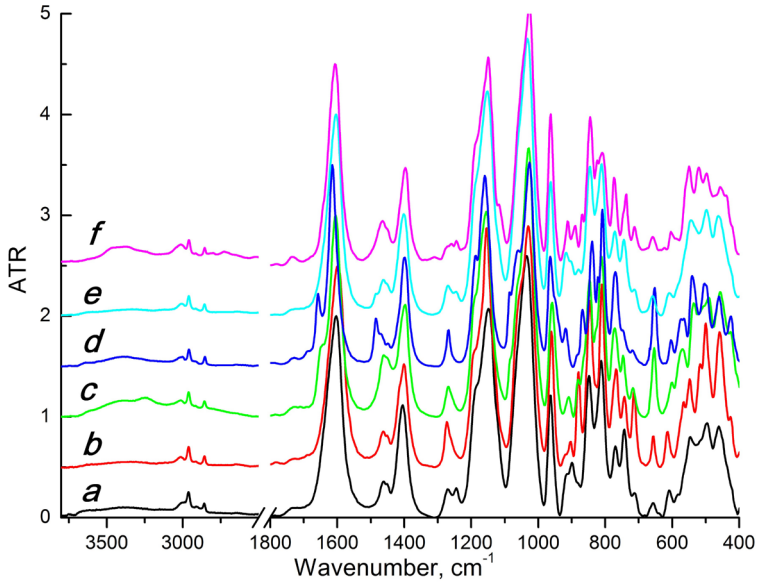

Fig. 2. IR spectra of $Na_2[Eu_2L_4]\cdot 3H_2O$ (a), $Cs_2[Eu_2L_4]\cdot H_2O$ (b), $(NH_4)_2[Eu_2L_4]\cdot 4H_2O$ (c), $(NMe_4)_2[Eu_2L_4]\cdot H_2O$ (d), $NEt_4[NaEu_2L_4]\cdot H_2O$ (e), and $(HNEt_3)_2[Eu_2L_4]\cdot 3H_2O$ (f).

The diffuse reflectance spectra of the complexes.

The diffuse reflectance spectra of the synthesized compounds were measured in the UV region and are presented in Figure 3. The broad band of the ligands' absorption is observed in the 220–340 nm region with a maximum near 250 nm. The Eu^{III} f-f transitions are also observed in the long-wavelength part of the spectra.

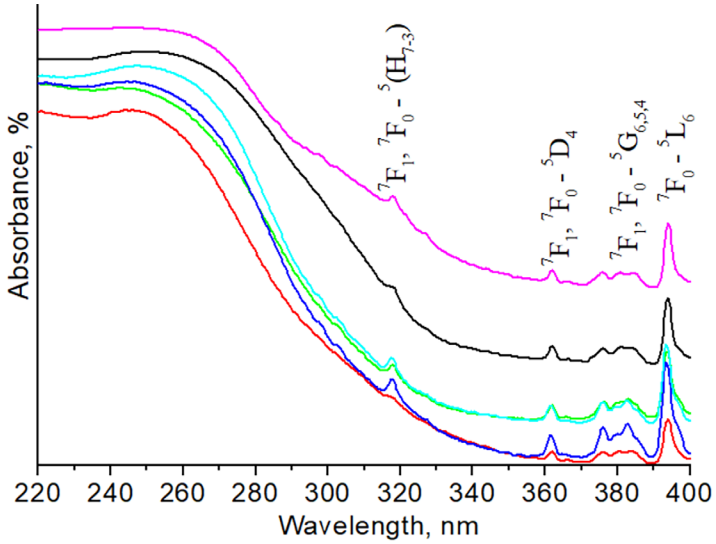

Fig. 3. Diffuse reflectance spectra of $Na_2[Eu_2L_4]\cdot 3H_2O$ (black line), $Cs_2[Eu_2L_4]\cdot H_2O$ (red line), $(NH_4)_2[Eu_2L_4]\cdot 4H_2O$ (green line), $(NMe_4)_2[Eu_2L_4]\cdot H_2O$ (blue line), $NEt_4[NaEu_2L_4]\cdot H_2O$ (light blue line), and $(HNEt_3)_2[Eu_2L_4]\cdot 3H_2O$) (pink line).

Luminescence spectroscopy.

All the obtained europium complexes exhibit red emission under UV lamp irradiation. The luminescence excitation spectra (Figure 4) were recorded by monitoring the emission of $^5D_0 \rightarrow ^7F_2$ transition. The spectra consist of a broad band of the ligands' absorption in the region 230–280 nm and numerous f-f transitions of the Eu^{III} ion. The identical conditions of measurements of the compounds' excitation spectra allow us to roughly compare the intensity of Eu^{III} emission. The intensity of bands is the highest in the spectrum of $(NMe_4)_2[Eu_2L_4]\cdot H_2O$ and the lowest in the spectrum of $(HNEt_3)_2[Eu_2L_4]\cdot 3H_2O$. The band of transition $^7F_0 \rightarrow ^5L_6$ dominates in the excitation spectra of all the obtained europium complexes. From the intensity ratio between ligand absorption band and the band of $^7F_0 \rightarrow ^5L_6$ transition one can conclude that the most efficient sensitization of Eu^{III} emission by the ligands takes place in the $Cs_2[Eu_2L_4]\cdot H_2O$ and the lowest sensitization efficiency is observed for $Na_2[Eu_2L_4]\cdot 3H_2O$.

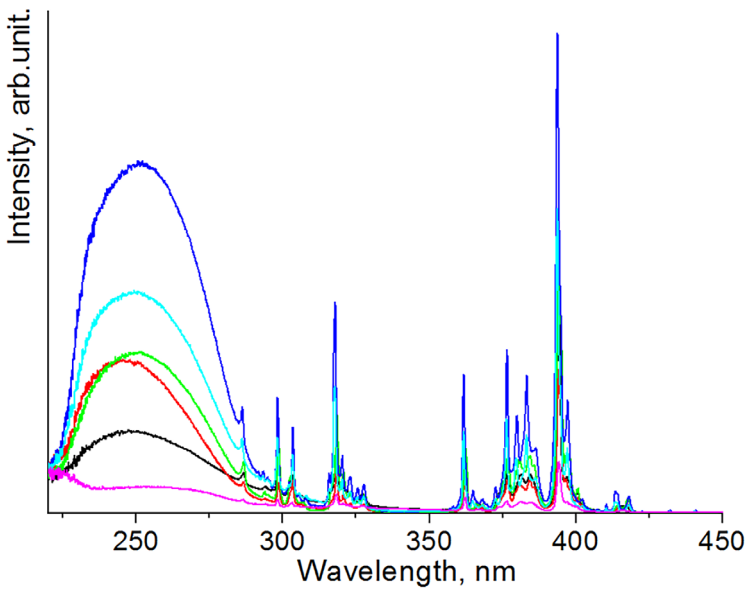

Fig. 4. Luminescence excitation spectra (emission at 611,4-612 nm) of $Na_2[Eu_2L_4]\cdot 3H_2O$ (black line), $Cs_2[Eu_2L_4]\cdot H_2O$ (red line), $(NH_4)_2[Eu_2L_4]\cdot 4H_2O$ (green line), $(NMe_4)_2[Eu_2L_4]\cdot H_2O$ (blue line), $NEt_4[NaEu_2L_4]\cdot H_2O$ (light blue line), and $(HNEt_3)_2[Eu_2L_4]\cdot 3H_2O$) (pink line).

Upon excitation by UV light, the complexes exhibit typical Eu^{III} ion f-f emission with narrow bands assigned to transitions $^5D_0 \rightarrow ^7F_j$ (j=0-4) (Figure 5). The emission spectra recorded upon excitation of the complexes into Eu^{III} f-f transition and the ligands' absorption bands are identical. It was found that the cations' nature significantly affects the splitting of f-f transition bands in luminescence spectra, their positions, and the ratio of their intensities. The weak band of transition $^5D_0 \rightarrow ^7F_0$ is observed for all the obtained europium complexes. The observation of this transition is an indication that the Eu^{III} ion occupies a site with C_{nv}, $C_{n,}$ or C_s symmetry [16]. The maximum of the band of $^5D_0 \rightarrow ^7F_0$ transition va-

ries depending on the cation from 577.9 nm (for $(NMe_4)_2[Eu_2L_4]\cdot H_2O$) to 578.9 nm (for $Na_2[Eu_2L_4]\cdot 3H_2O$ and $(NH_4)_2[Eu_2L_4]\cdot 4H_2O$). The transition $^5D_0\rightarrow{}^7F_1$ appears in the complexes' emission spectra as a band with different splitting. There are two separated bands in the region of $^5D_0\rightarrow{}^7F_1$ transition observed for $Cs_2[Eu_2L_4]\cdot H_2O$, $(NMe_4)_2[Eu_2L_4]\cdot H_2O$ and $NEt_4[NaEu_2L_4]\cdot H_2O$. The spectrum of $(NH_4)_2[Eu_2L_4]\cdot 4H_2O$ exhibits three components in this region, pointing to the lower Eu^{III} site symmetry in this complex compared to the previously mentioned three compounds. For $Na_2[Eu_2L_4]\cdot 3H_2O$ and $(HNEt_3)_2[Eu_2L_4]\cdot 3H_2O$ the band of $^5D_0\rightarrow{}^7F_1$ transition is broadened. The band of hypersensitive transition $^5D_0\rightarrow{}^7F_2$ is the most intensive in all the recorded emission spectra; however differs by splitting depending on the cation. The biggest number of components of the $^5D_0\rightarrow{}^7F_2$ band is observed for $Cs_2[Eu_2L_4]\cdot H_2O$ and $(NH_4)_2[Eu_2L_4]\cdot 4H_2O$. The relative integral intensities ratio $I(^5D_0\rightarrow{}^7F_2)/I(^5D_0\rightarrow{}^7F_1)$, so-called ratio, varies much (from 2.6 to 7.6) depending on the cation (Table 2). The highest values of red/orange ratio are observed for the complexes $Cs_2[Eu_2L_4]\cdot H_2O$ and $(NH_4)_2[Eu_2L_4]\cdot 4H_2O$. Thus, the lowest symmetry of the Eu^{III} ion coordination environment can be concluded for these two compounds. A known feature of many mononuclear tetrakis-complexes with CAPh ligands is the high intensity of transition $^5D_0\rightarrow{}^7F_4$ [9, 17]. The nature of this phenomenon was explained by the presence of the P=O group in the ligand structure, which is more polarizable compared to the C=O one. However, the dependence of this band's intensity on the cation nature of the tetrakis-complexes has not been explained yet and requires further studies. Among obtained in this work binuclear Eu^{III} tetrakis-complexes only two – $(NMe_4)_2[Eu_2L_4]\cdot H_2O$ and $NEt_4[NaEu_2L_4]\cdot H_2O$ – exhibit a high intensity of transition $^5D_0\rightarrow{}^7F_4$. The contribution of this band to the total integral intensity of the spectra of the two mentioned complexes is more than 30%. While for the rest of the obtained compounds, the contribution of $^5D_0\rightarrow{}^7F_4$ band equals only 17–23%.

Table 2.

Some photoluminescence characteristics of the complexes $(Cation)_2[Eu_2L_4]$.

$(Cation)_2$ =		Na_2	Cs_2	$(NH_4)_2$	$(NMe_4)_2$	NEt_4Na	$(HNEt_3)_2$
Photoluminescence intensity distribution (%)	$^5D_0\rightarrow{}^7F_0$	0.19	0.15	0.15	0.08	0.10	0.24
	$^5D_0\rightarrow{}^7F_1$	12.25	9.26	10.06	16.35	16.59	15.63
	$^5D_0\rightarrow{}^7F_2$	66.20	70.37	67.56	42.64	43.66	59.23
	$^5D_0\rightarrow{}^7F_3$	1.79	2.76	2.77	3.51	3.41	1.48
	$^5D_0\rightarrow{}^7F_4$	19.57	17.46	19.46	37.42	36.24	23.42
$I(^5D_0\rightarrow{}^7F_2)/I(^5D_0\rightarrow{}^7F_1)$		5.4	7.6	6.7	2.6	2.6	3.8
τ_{RAD} (ms)		2.48	1.87	2.03	3.31	3.36	3.16
τ_{obs} (ms)		1.33	1.69	1.57	2.74	1.91	0.76
Q^{Ln}_{Ln} (%)		54	90	77	83	57	24

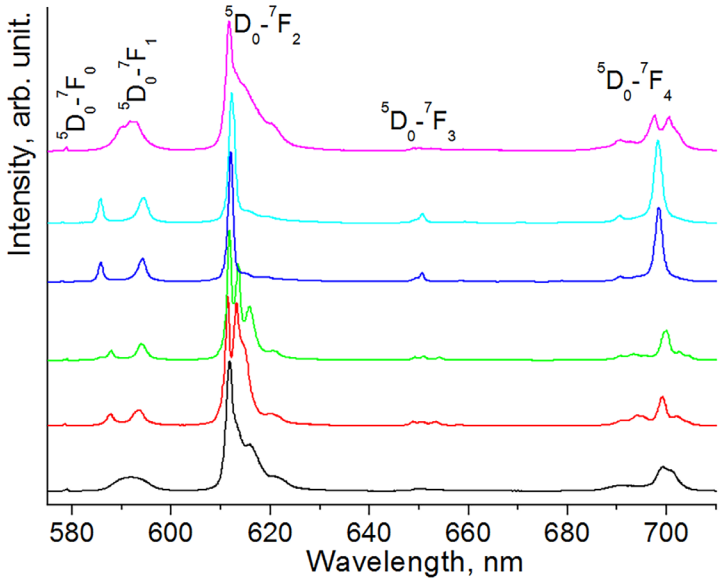

Fig. 5. Normalized luminescence spectra of $Na_2[Eu_2L_4]\cdot 3H_2O$ (black line), $Cs_2[Eu_2L_4]\cdot H_2O$ (red line), $(NH_4)_2[Eu_2L_4]\cdot 4H_2O$ (green line), $(NMe_4)_2[Eu_2L_4]\cdot H_2O$ (blue line), $NEt_4[NaEu_2L_4]\cdot H_2O$ (light blue line), and $(HNEt_3)_2[Eu_2L_4]\cdot 3H_2O$) (pink line) measured at 300 K and λ_{exc} = 394 nm.

The luminescence decay times were measured for the europium complexes by monitoring the emission of $^5D_0 \rightarrow {}^7F_2$ transition and excitation at a wavelength of 372 nm, which corresponds to the f-f transition of the Eu^{III} ion. The obtained decay curves were fitted by a monoexponential function and yielded values of τ_{obs} equal to 0.76–2.74 ms, depending on the cation (Table 3). The radiative lifetime of $^5D_0$ state τ_{RAD} was estimated from emission data using the following equation: $\tau_{RAD} = 1/(A_{MD,0}\cdot n^3\cdot(I_{tot}/I_{MD}))$ [18, 19], with $A_{MD,0}$ being equal to 14.65 s^{-1}, n considered to be 1.5 and (I_{tot}/I_{MD}) the ratio of the total integrated emission from the Eu($^5D_0$) level to the integrated intensity of MD transition $^5D_0 \rightarrow {}^7F_1$ [20, 21]. The $^5D_0$ intrinsic quantum yield (Q^{Ln}_{Ln}) for the europium complexes was estimated from the emission spectrum and measured $^5D_0$ lifetime: $Q^{Ln}_{Ln} = \tau_{obs} / \tau_{RAD}$. The obtained values of τ_{RAD} agree with the values of red/orange ratios, being changed in the opposite way. The values of τ_{obs} are not directly proportional to τ_{RAD}, which results in very different Q^{Ln}_{Ln} for the studied complexes. The lowest intrinsic quantum yield was found for $(HNEt_3)_2[Eu_2L_4]\cdot 3H_2O$. This can be evidence of efficient quenching of Eu^{III} f-f emission due to the non-rigid structure of the complex and high-energy vibrations of the cations. The complexes $Cs_2[Eu_2L_4]\cdot H_2O$ and $(NMe_4)_2[Eu_2L_4]\cdot H_2O$ demonstrated the highest intrinsic quantum yield.

Thermal gravimetric studies of the complexes.

The thermal gravimetric studies of the Y^{III} complexes (Figure 6) have shown that the main weight loss of the samples takes place at a temperature close to 200 °C. However, some minor weight losses preceded the compounds' decomposition for the majority of the samples studied. One can observe for $Na_2[Y_2L_4]\cdot 3H_2O$ and $(NH_4)_2[Y_2L_4]\cdot 4H_2O$ two small weight losses. The first one takes place at a temperature below 100 °C and is connected with the evaporation of

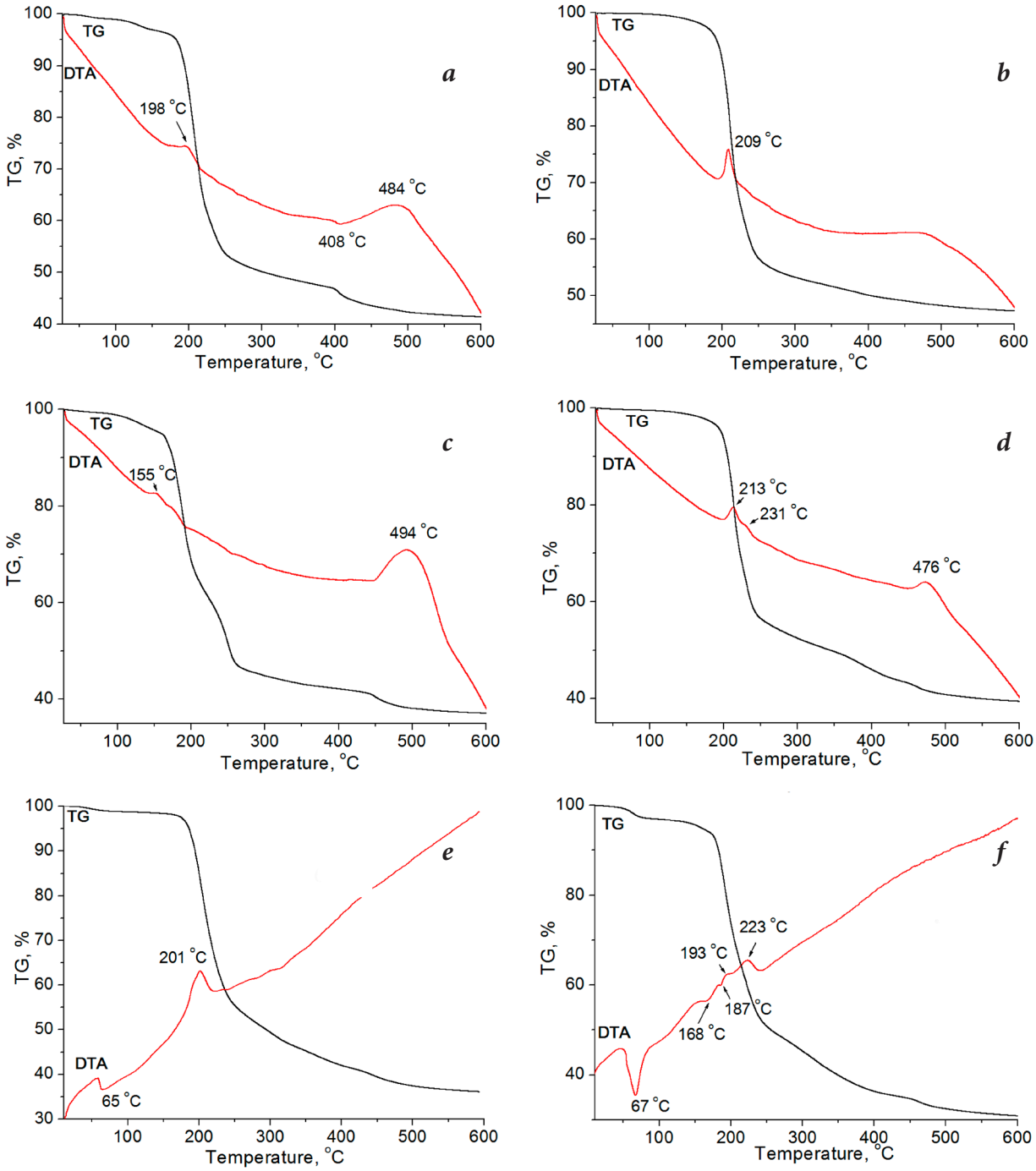

Fig. 6. Thermal gravimetric analysis of of $Na_2[Eu_2L_4]\cdot 3H_2O$ (a), $Cs_2[Eu_2L_4]\cdot H_2O$ (b), $(NH_4)_2[Eu_2L_4]\cdot 4H_2O$ (c), $(NMe_4)_2[Eu_2L_4]\cdot H_2O$ (d), $NEt_4[NaEu_2L_4]\cdot H_2O$ (e), and $(HNEt_3)_2[Eu_2L_4]\cdot 3H_2O$ (f).

residues of 2-propanol solvent, which was used for the synthesis of complexes. This conclusion correlates with the NMR spectra of these complexes. The second weight loss at a temperature higher than 100 °C can be due to evaporation of water molecules. Earlier, it was shown that a molecule of water can be encapsulated into the negatively charged environment of the ligand fluorine and carbonyl oxygen atoms of the helicate structure of lanthanide binuclear *tetrakis*-complexes with $[L]^{2-}$ [14]. Also, water molecules tend to bind the outersphere sodium cation in $Na[NaNd_2L_4(H_2O)]\cdot 2H_2O$ [14]. For the compounds $NEt_4[NaY_2L_4]\cdot H_2O$ and $(HNEt_3)_2[Y_2L_4]\cdot 3H_2O$, one can observe a small weight loss, which is accompanied by an endothermic effect at 65 and 67 °C, respectively. As there is no organic solvent in the complexes, which was confirmed by ^{1}H NMR analysis, the observed weight loss was assigned to the water molecules evaporation. Evaporation of solvents is followed by decomposition of organic part of the complexes, which takes place at 200 °C for the $Cs_2[Eu_2L_4]\cdot H_2O$, $(NMe_4)_2[Eu_2L_4]\cdot H_2O$, and $NEt_4[NaEu_2L_4]\cdot H_2O$ and at slightly lower temperature for $Na_2[Eu_2L_4]\cdot 3H_2O$ (198 °C), $(NH_4)_2[Eu_2L_4]\cdot 4H_2O$ (184 °C) and $(HNEt_3)_2[Eu_2L_4]\cdot 3H_2O$ (192 °C). The total weight loss upon heating of the samples till 600 °C equals 52–65 %.

CONCLUSIONS. The new binuclear tetrakis-complexes of Y^{III} and Eu^{III} with tetramethyl N,N′-(2,2,3,3,4,4-hexafluoro-1,5-dioxopentane-1,5-diyl)bis(phosphoramidate) and different cations have been successfully obtained and characterized. The variation of the cations has allowed obtaining compounds with different solubility, i.e., soluble in water or in organic solvents. It was found that complexes contain different amounts of moisture depending on the cation and the temperature of decomposition varies in the range near 155–190 °C. The highest thermal stability among Y^{III} compounds was observed for the complexes $Cs_2[Y_2L_4]\cdot H_2O$ and $(NMe_4)_2[Y_2L_4]\cdot H_2O$. The luminescence studies of the obtained compounds allowed us to conclude the lowest symmetry of Eu^{III} ion coordination environment for $Cs_2[Eu_2L_4]\cdot H_2O$ and $(NH_4)_2[Eu_2L_4]\cdot 4H_2O$, which results in the highest values of red/orange ratio and lowest values of radiative luminesce decay time. The highest Eu^{III} intrinsic quantum yield (90 and 83%, respectively) has been observed for $Cs_2[Eu_2L_4]\cdot H_2O$ and $(NMe_4)_2[Eu_2L_4]\cdot H_2O$, which can be partially explained by the absence of moisture in these complexes. The rather high intensity of transition $^5D_0 \rightarrow {}^7F_4$ observed for $(NMe_4)_2[Eu_2L_4]\cdot H_2O$ and $NEt_4[NaEu_2L_4]\cdot H_2O$ is an interesting feature, which needs further investigations.

ACKNOWLEDGMENTS. This work was supported by the Ministry of Education and Science of Ukraine (grants no. 22BF037-04, and B/218 (0123U100990)).

ВПЛИВ КАТІОНІВ НА ТЕРМІЧНУ СТІЙКІСТЬ ТА ЛЮМІНЕСЦЕНТНІ ВЛАСТИВОСТІ БІЯДЕРНИХ КОМПЛЕКСІВ РІДКОЗЕМЕЛЬНИХ ЕЛЕМЕНТІВ ІЗ БІС-КАРБАЦИЛАМІДОФОСФАТАМИ

Наталія Каряка[1,*], Віктор Труш[1], Ігор Фесич[1], Олена Гнатюк[2], Іван Гнатюк[2], Галина Довбешко[2], Володимир Амірханов[1]

[1]Хімічний факультет Київського національного університету ім. Тараса Шевченка, вул. Гетьмана Павла Скоропадського, 12, Київ 01033, Україна;
[2] Відділ фізики біологічних систем, Інститут фізики Національної академії наук України, проспект Науки, 46, Київ, Україна
e-mail: natka04@i.ua

Було одержано серію комплексних сполук ітрію (III) та європію (III) з біс-карбациламідофосфатом тетраметил-N,N′-(2,2,3,3,4,4-гексафлуоро-1,5-діоксопентан-1,5-диіл)біс(фосфорамідатом) та різними катіонами з метою вивчення впливу природи катіона на термічні та спектральні властивості комплексних сполук. Було показано, що природа катіона значно впливає на такі властивості комплексів, як розчинність, термічна стійкість та люмінесцентні характеристики. Комплекси європію (III) демонструють сенсибілізовану лігандами f-f люмінесценцію. Інтенсивність люмінесценції, розщеплення та співвідношення інтенсивностей смуг у спектрах, а також час життя люмінесценції і власний квантовий вихід для досліджених сполук суттєво залежали від природи катіона. Червоно/помаранчеве співвідношення для синтезованих комплексів європію (III) варіюється від 2.6 до 7.6, час життя люмінесценції – від 0.76 до 2.74 мс, а власний квантовий вихід – від 24 до 90 %. Температура розкладання комплексів залежно від природи катіона варіюється в діапазоні 155–190 °C.

Ключові слова: рідкоземельні елементи, біс-карбациламідофосфат, координаційні сполуки, люмінесценція, термогравіметричний аналіз.

REFERENCES

[1] Long J., Guari Y., Ferreira R.A., Carlos L.D., & Larionova J. Recent advances in luminescent lanthanide based Single-Molecule Magnets. *Coord Chem Rev.* 2018. **363**: 57–70. https://doi.org/10.1016/j.ccr.2018.02.019

[2] Jia J.H., Li Q.W., Chen Y.C., Liu J.L., & Tong M.L. Luminescent single-moleculemagnets based on lanthanides: Design strategies, recent advances and magneto-luminescent studies. *Coord Chem Rev.* 2019. 378: 365-381. https://doi.org/10.1016/j.ccr.2017.11.012

[3] Bünzli J-C.G., Rising Stars in Science and Technology: Luminescent Lanthanide Materials. *Eur J Inorg Chem.* 2017. 44: 5058-5063. https://doi.org/10.1002/ejic.201701201

[4] Kaczmarek M.T., Zabiszak M., Nowak M., & Jastrzab R. Lanthanides: Schiff base complexes, applications in cancer diagnosis, therapy, and antibacterial activity. *Coord Chem Rev.* 2018. 370: 42-54. https://doi.org/10.1016/j.ccr.2018.05.012

[5] Teo R.D., Termini J & Gray H.B. Lanthanides: applications in cancer diagnosis and therapy: miniperspective. *J Med Chem.* 2016. 59: 6012-6024. https://doi.org/10.1021/acs.jmedchem.5b01975

[6] Parker D., Fradgley J.D., Wong K.L. The design of responsive luminescent lanthanide probes and sensors. *Chem Soc Rev.* 2021. **50**: 8193–8213. https://doi.org/10.1039/D1CS00310K

[7] Costa I.F., Blois L., Paolini T.B., Assunção I.P., Teotonio E.E.S., Felinto M.C.F.C., Moura R.T. Jr., Longo R.L., Faustino W.M., Carlos L.D., Malta O.L., Carneiro Neto A.N., & Brito H. F. Luminescence properties of lanthanide tetrakis complexes as molecular light emitters. *Coord Chem*

Rev. 2024. **502**: 215590. https://doi.org/10.1016/j.ccr.2023.215590

[8] Kofod N., Thomsen M.S., Nawrocki P. & Sørensen T.J. Revisiting the assignment of innocent and non-innocent counterions in lanthanide (III) solution chemistry. *Dalton Trans.* 2022. 51: 7936-7949. https://doi.org/10.1039/D2DT00565D

[9] Struhatska M.B., Kariaka N.S., Dyakonenko V.V., Shishkina S.V., Smola S.S. , Rusakova N.V., Gawryszewska P., Malta O.L., Carneiro Neto A.N., Trush V.O. and Amirkhanov V.M. The influence of different cations on the structure and spectral properties of Ln^{3+} tetrakis-complexes with the CAPh-type ligand dimethyl- N-trichloroacetylamidophosphate, *New J Chem.* 2024. 48: 11886–11898. https://doi.org/10.1039/D4NJ01700E

[10] Paolini T.B., Assunção I.P., Costa I.F., Blois L., Felinto M.C.F., Moura R.T. Jr, Teotonio E.E.S., Malta O.L., Carneiro Neto A.N., & Brito H.F. The influence of imidazolium counterions on the luminescence properties of Cnmim[$Eu(tta)_4$] tetrakis complexes in solid-state and ionic liquid solutions. *J Lumin.* 2023. 263 120158. https://doi.org/10.1016/j.jlumin.2023.120158

[11] Lunkley J.L, Shirotani D., Yamanari K., Kaizaki S., & Muller G. Chiroptical spectra of a series of tetrakis ((+)-3-heptafluorobutylyrylcamphorato) lanthanide (III) with an encapsulated alkali metal ion: circularly polarized luminescence and absolute chiral structures for the Eu(III) and Sm(III) complexes. *Inorg Chem.* 2011. 50: 12724-12732. https://doi.org/10.1021/ic201851r

[12] Basal L.A., Kajjam A.B., Bailey M.D., & Allen M.J. Systematic tuning of the optical properties of discrete complexes of EuII in solution using counterions and solvents. *Inorg Chem.* 2020. 59: 9476-9480. https://doi.org/10.1021/acs.inorgchem.0c01516

[13] Liu C.M., Sun R., Wang B.W., Hao X., & Li X.L. Effects of counterions, coordination anions, and coordination solvent molecules on single-molecule magnetic behaviors and nonlinear optical properties of chiral Zn_2Dy Schiff base complexes. *Inorg Chem.* 2022. **61**: 18510–18523. https://doi.org/10.1021/acs.inorgchem.2c02743

[14] Horniichuk O.Y., Trush V.A., Kariaka N.S., Shishkina S.V., Dyakonenko V.V., Severinovskaya O.V., Gawryszewska P., Domasevitch K.V., Wattras A., Amirkhanov V.M. Novel quadruple-stranded heterometallic Ln2Na complexes hosting sodium ions inside the cryptand-like cavity, *New J Chem.* 2021. **45**: 22361–22368. https://doi.org/10.1039/D1NJ04353F

[15] Horniichuk O.Y., Kariaka N.S., Trush V.O., Smola S.S., Sliva T.Y., Rusakova N.V., Amirkhanov V.M. Synthesis and investigation of binuclear rare earth complexes based on bis-chelating carbacylamidophosphate (in Ukr.), *Issues of Chemistry and Chemical Technology.* 2019. **5**: 27–33. http://dx.doi.org/10.32434/0321-4095-2019126-5-27-33

[16] Binnemans K. Interpretation of europium(III) spectra. *Coord Chem Rev.* 2015. **295**: 1–45. https://doi.org/10.1016/j.ccr.2015.02.015

[17] Kariaka N.S., Lipa A., Carneiro Neto A.N., Malta O.L., Gawryszewska P. and Amirkhanov V.M. Eu^{3+} and Tb^{3+} coordination compounds with phenyl-containing carbacylamidophosphates: comparison with selected Ln^{3+} β-diketonates, *Front. Chem.* 2023. **11**: 1188314. https://doi.org/10.3389/fchem.2023.1188314

[18] van der Tol E.B., van Ramesdonk H.J., Verhoeven J.W., Steemers F.J., Kerver E.G., Verboom W., Reinhoudt D.N. Tetraazatriphenylenes as Extremely Efficient Antenna Chromophores for Luminescent Lanthanide Ions. *Chem Eur J.* 1998. **4**: 2315–2323. https://doi.org/10.1002/(SICI)1521-3765(19981102)4:11<2315::AID-CHEM2315>3.0.CO;2-E

[19] Werts M.H.V., Jukes R.T.F., Verhoeven J.W. The emission spectrum and the radiative lifetime of Eu^{3+} in luminescent lanthanide complexes, *Phys. Chem Chem Phys.* 2002. **4**: 1542–1548. https://doi.org/10.1039/B107770H

[20] Bünzli J.C.G., Eliseeva S.V. Basics of Lanthanide Photophysics. In: Hänninen, P., Härmä, H. (eds) Lanthanide Luminescence. Springer Series on Fluorescence, Springer. *Berlin, Heidelberg*. 2010. **7**: 1–46. https://doi.org/10.1007/4243_2010_3

[21] de Sa G.F., Malta O.L., de Mello Donega C., Simas A.M., Longo R.L., Santa-Cruz P.A., da Silva E.F. Spectroscopic properties and design of highly luminescent lanthanide coordination complexes, *Coord Chem Rev.* 2000. **196**: 165–195. https://doi.org/10.1016/S0010-8545(99)00054-5

Стаття надійшла 25.08.2025.

UDC 546.26-162: 541.13:549.21 doi: 10.33609/2708-129X.91.11.2025.35-62

ELECTROCHEMICAL SYNTHESIS OF FLUORINATED HETEROCYCLIC COMPOUNDS (review).

Alicja Wzorek[1], Taizo Ono[2], Daniel Baecker[3], Wei Zhang[4], Vadim A. Soloshonok[5*]

[1] Institute of Chemistry, Jan Kochanowski University in Kielce, Uniwersytecka 7, 25–406 Kielce, Poland;
[2] National Institute of Advanced Industrial Science and Technology (AIST), 2266–98, Anagahora, Shimoshidami, Moriyama-ku, Nagoya, 463–8560, Japan;
[5] Department of Pharmaceutical and Medicinal Chemistry, Institute of Pharmacy, Freie Universität Berlin, Königin-Luise-Straße 2+4, 14195 Berlin, Germany;
[4] Department of Chemistry, University of Massachusetts Boston, Boston MA 02125, Unites States of America;
[5] IKERBASQUE, Basque Foundation for Science, María Díaz de Haro 3, Plaza Bizkaia, 48013 Bilbao, Spain
e-mail: vadimsoloshonok@gmail.com

Fluorine-containing heterocycles play a crucial role in the pharmaceutical, agrochemical, and materials industries. The pursuit of effective and sustainable synthesis methods has driven the development of electrochemistry as a compelling alternative to conventional chemical transformations. Among these approaches, electrochemistry has emerged as a particularly promising technique for orchestrating multibond-forming processes under mild, environmentally benign conditions. This review highlights key advances over the past decade in the electrochemical synthesis of fluorinated heterocyclic compounds, encompassing bimolecular, trimolecular, and tetramolecular reactions. Emphasis is placed on multicomponent cascade strategies, radical-mediated couplings, and oxidant-free cyclizations that afford broad functional group tolerance and fluorine incorporation flexibility. Collectively, this work serves as a resource for researchers developing next-generation sustainable synthetic platforms tailored to fluorinated heterocycles with diverse structural and biological profiles.

Keywords: Electrochemistry, Heterocyclic Compounds, Fluorine, Fluorinated Pharmaceuticals, Green Chemistry, Sustainable Synthesis.

INTRODUCTION. Electrochemistry is a fascinating interdisciplinary branch of chemistry that studies the relationship between electrical energy and chemical reactions. At its core, it investigates processes where chemical energy is converted into electrical energy or where electrical energy is used to drive non-spontaneous chemical reactions. These transformations occur through redox reactions where electrons are transferred, typically at the interface between an electrode (an electrical conductor) and an electrolyte (an ion-conducting medium). The principles of electrochemistry underpin a vast array of modern technologies, from power sources like batteries and supercapacitors, to industrial processes such as the production of aluminum and chlorine, and analytical techniques like pH measurement and biosensors. [1–6].

Electrochemistry offers a powerful and increasingly vital approach to organic synthesis, enabling chemists to drive a wide range of transformations through the controlled transfer of electrons rather than relying solely on traditional chemical reagents. This method, often termed electrosynthesis, leverages the precise control of electrical potential to effect selective oxidations and reductions, allowing for the formation of C-C bonds, functional group interconversions, and the synthesis of complex molecules under remarkably mild conditions. Key advantages include enhanced selectivity (chemo-, regio-, and stereoselectivity), the elimination of hazardous or stoichiometric redox reagents, and the generation of cleaner reaction profiles with fewer byproducts. From sustainable anodic oxidations and cathodic reductions to electro-initiated radical reactions and the precise functionalization of sensitive substrates, electrosynthesis is revolutionizing synthetic routes, making complex organic transformations more efficient, environmentally friendly, and scalable. [7–16].

Electrochemistry offers compelling advantages over conventional organic synthesis methods, particularly in its alignment with green chemistry principles [17]. Foremost among these benefits is the replacement of stoichiometric chemical oxidants and reductants with electricity, which serves as a clean, tunable, and inexpensive reagent. This eliminates the need for often hazardous and costly reagents, significantly reducing waste generation and simplifying downstream purification processes. Furthermore, electrochemical reactions frequently proceed under milder conditions, such as ambient temperature and pressure, minimizing energy consumption and enabling the synthesis of sensitive compounds that might degrade under harsher thermal or chemical routes. The precise control over electron transfer at the electrode surface allows for unparalleled selectivity (chemo-, regio-, and stereoselectivity), leading to higher yields of desired products and fewer unwanted byproducts, thus contributing to greater efficiency and sustainability in modern organic synthesis. [18–21].

As part of our ongoing commitment to the design of modern pharmaceuticals [22–28]—particularly those incorporating residues of tailor-made amino acids [29–36] and fluorinated motifs [37–45]—we are strongly focused on developing innovative synthetic methodologies for their preparation [46–56]. Given that heterocyclic compounds and amino acids constitute the structural backbone of over 85% and 35% of contemporary drugs, respectively, these domains remain central to pharmaceutical research [57–65]. Notably, heterocyclic scaf-

folds serve as indispensable building blocks in medicinal chemistry, owing to their broad spectrum of biological activity and remarkable structural versatility, making them essential for rational drug design [66–71].

Recently, we presented a comprehensive overview of advancements in the synthesis of fluorinated heterocyclic compounds, highlighting innovative directions such as the use of carbon nanotubes as catalysts [72] and the application of mechanochemical principles [73]. In the present work, we extend this exploration by providing a detailed treatment of electrochemical methodologies for the synthesis of fluorinated heterocyclic compounds.

Electrochemistry is an emerging field with significant synthetic potential, offering sustainable and efficient alternatives to traditional chemical processes. Here, we summarize data published over the past decade on the electrochemical synthesis of fluorine-containing heterocycles. The material is organized according to the number of reacting species, focusing on reaction dynamics rather than mechanistic principles such as the molecularity of the rate-determining step. Accordingly, reactions involving three structural components—two of which are identical—are classified based on effective molecularity and treated as bimolecular in terms of structural diversity.

We believe this compilation will serve as a valuable resource for researchers and practitioners in synthetic and medicinal chemistry, as well as for those pursuing advances in green and sustainable methodologies.

Bimolecular reactions.

In 2020, Yang *et al.* [74] introduced an efficient electrochemical strategy for synthesizing 1,2,4-trisubstituted (*1H*)-imidazoles **3** (Scheme 1), .utilizing readily available starting materials and carbon rod electrodes in an undivided cell under metal- and oxidant-free conditions The approach involves the electrooxidative tandem cyclization of acetophenones **1** and substituted benzylamines **2**, proceeding via in situ generation of 2-iodoacetophenone through anodic oxidation of molecular iodine, which subsequently engages with the ketone **1**. This protocol stands out for its broad functional group tolerance and consistent delivery of moderate to excellent yields. Notably, both starting materials—highly electrophilic ketones **1** [75, 76] and benzylamines **2**—can incorporate fluorinated substituents, enabling a high degree of fluorination and structural versatility in the resulting products **3**. Furthermore, this electrochemical protocol eliminates the need for external metal catalysts or chemical oxidants, making it a simple, cost-effective, and environmentally sustainable alternative. While the primary focus is on nitrogen-containing heterocycles, the methodology also holds promise for the synthesis of related scaffolds across diverse heterocyclic systems.

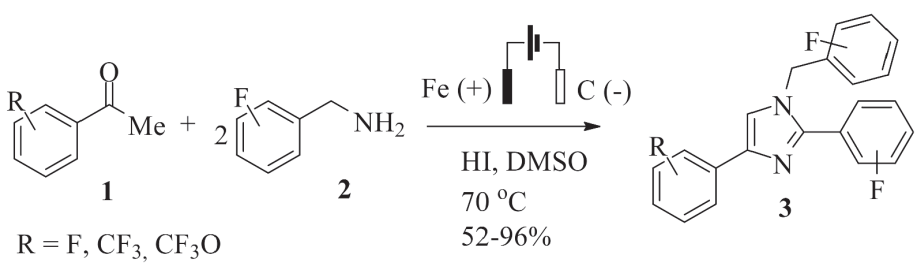

Scheme 1. Electrochemical strategy for synthesizing 1,2,4-trisubstituted (1*H*)-imidazoles.

Elinson and co-workers developed highly stereoselective electrocatalytic approach for synthesizing substituted (*R**,*R**)-*bis*-(spiro-2,4-dihydro-3*H*-pyrazol-3-one)cyclopropanes **6** (Scheme 2) [77] via an electrochemical multi-step cyclization reaction. This one-pot strategy employs fluoro-aldehydes **4** and pyrazolin-5-ones **5** as starting materials, proceeding through a direct electrochemical transformation to access functionally rich cyclopropane scaffolds. The process utilizes sodium iodide or bromide as a redox mediator in an undivided cell, with methanol as the solvent, and is conducted at ambient temperature. By circumventing conventional halogenation reagents and leveraging mild electrolysis conditions, the method delivers good yields (65–80%) with high current efficiency and virtually complete diastereoselectivity of relative (*R**,*R**) configuration. The underlying mechanism follows a typical mediator system: iodine is generated anodically, while methanol is deprotonated cathodically to produce methoxide anions and evolve hydrogen gas.

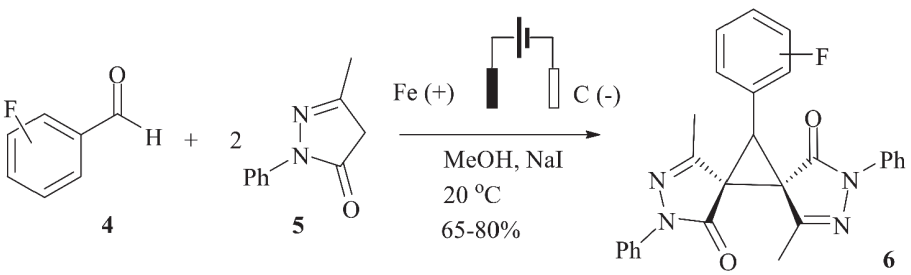

Scheme 2. Synthesis of (*R**,*R**)-*bis*-(spiro-2,4-dihydro-3*H*-pyrazol-3-one)cyclopropanes.

Qian *et al*. have recently introduced a novel electrochemical cascade cyclization strategy for the synthesis of *bis*-pyrazolo[3,4-*b*:4',3'-*e*] pyridines **9** (Scheme 3) [78]. Leveraging the enhanced electrophilicity of fluorinated aldehydes **7** [74, 79, 80], this method exploits their high reactivity in nucleophilic addition reactions. The transformation between fluoroaldehydes **7** and pyrazol-5-amines **8** proceeds smoothly under metal- and oxidant-free conditions. This electrochemical approach affords a diverse array of mono- and trifluoromethyl-substituted *bis*-pyrazolo[3,4-*b*:4',3'-*e*]pyridines **9** in moderate yields (50–70%). Key advantages of the protocol include its operational simplicity, broad substrate scope, and environmentally benign character, making it a promising alternative to conventional multistep syntheses.

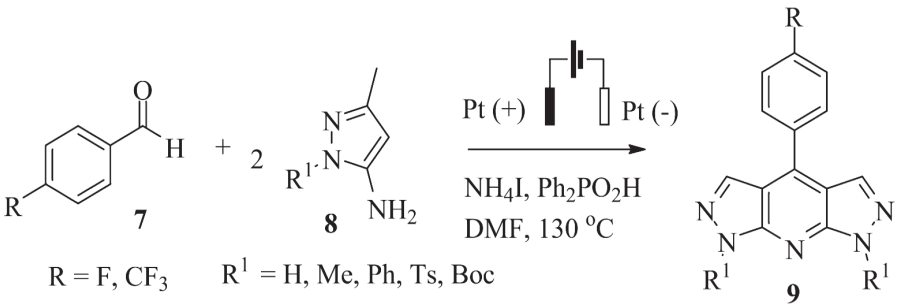

Scheme 3. Electrochemical approach for preparation of *bis*-pyrazolo[3,4-b:4',3'-e]pyridines.

A highly effective and operationally convenient electrochemical method has been developed for the synthesis of fluoro-spirocyclopropanes **11** (Scheme 4) [81], achieved by reacting indan-1,3-dione **10** with aromatic fluoro-aldehydes **4**. The reaction is conducted at 50 °C in a mixture of propanol and sodium bromide under constant current electrolysis. This method offers several significant advantages, including mild halogen production, the use of low-concentration currents, a neutral reaction solution pH, no need for by-product isolation, synthetically attractive yields (>75%), inexpensive reagents, environmental sustainability, and easy product isolation.

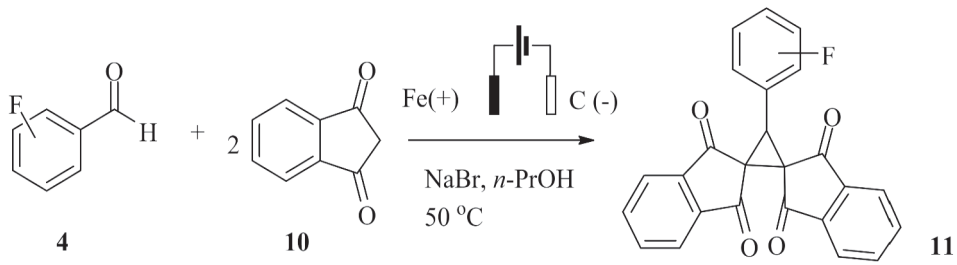

Scheme 4. Electrochemically aided synthesis of fluoro-spirocyclopropanes.

A straightforward and green electrochemical method for synthesizing CF_3-containing benzazepines has been developed by Zhang et al. via the radical cascade cyclization of alkynes. Starting compounds **12** (Scheme 5) [82], bearing an acetylenic residue properly positioned relative to the aromatic ring, were subjected to electrochemical conditions in an undivided cell with sodium trifluoromethanesulfinate **13** in acetonitrile at ambient temperature, yielding cyclized products **14** with a trifluoromethyl group bonded to the olefinic moiety. This transformation provides a novel approach to synthesizing seven-membered heterocycles without requiring any external catalyst or oxidant, operating under mild reaction conditions. A gram-scale experiment further demonstrated the practicality of this method. Benzazepines are an important class of seven-membered nitrogen-containing heterocyclic compounds, widely present in natural products and pharmaceuticals. They exhibit diverse biological activities, making them valuable in medicinal chemistry [83].

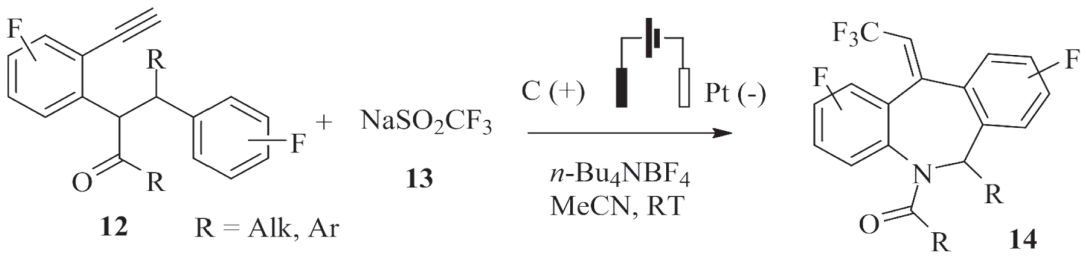

Scheme 5. Electrochemical synthesis of fluorinated benzazepines.

Lei *et al*. described a one-pot electrochemical oxidation-induced intermolecular annulation reaction for the synthesis of tetrasubstituted pyrroles **16** (Scheme 6) [84]. The reaction was conducted in an undivided cell at a constant current of 10 mA, using simple and readily available fluorinated ketones **15** and tert-butyl amine in the presence of tetrabutylammonium tetrafluoroborate (n-Bu_4NBF_4) as an electrolyte. Tetrasubstituted pyrroles **16** were obtained with yields ranging from 42% to 79%. Substituting *tert*-butyl amine with other amines led to complications due to the instability of intermediate imines, thereby limiting the synthetic utility of this method.

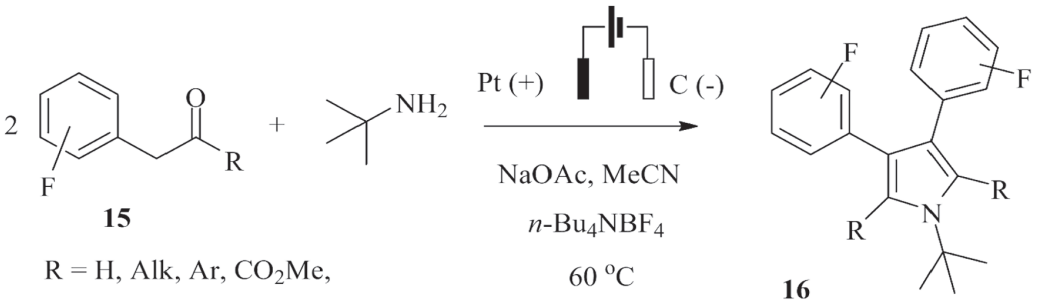

Scheme 6. Electrochemical preparation of tetrasubstituted pyrroles.

Ackermann *et al*. describe a rhodium-catalyzed cascade C–H activation and alkyne annulation for the novel synthesis of nitrogen-doped polycyclic aromatic hydrocarbons (aza- nanographenes) **19** (Scheme 7) [85], demonstrating high chemo- and regioselectivity. The method employs a specially designed multifunctional O-methylamidoxime directing group, using amidoxime **17** and various disubstituted **18** for the envisioned rhoda-electrocatalyzed cascade C–H annulation. The reaction is conducted with KOAc as the base, $[Cp^*RhCl_2]_2$ ($Cp^* = C_5Me_5$) as the catalyst precursor, MeOH as the solvent, and a constant current of 4.0 mA, yielding the desired products **19** in 42–94% yield. Through the identification of two key rhodacyclic intermediates, the authors determined the precise sequence in which the three steps of C–H activation occur. The metalla-electrocatalyzed multiple C–H transformations exhibit a unique functional group tolerance, accommodating even highly reactive iodo and azido groups. This innovative approach holds promising applications in materials science.

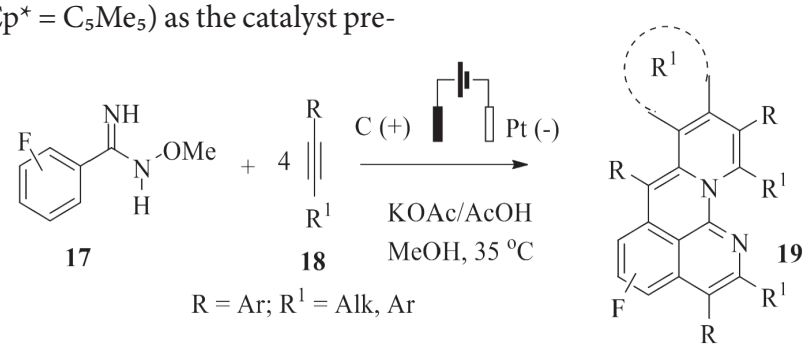

Scheme 7. Electrochemical synthesis of fluorine-containing aza-nanographene derivatives.

Trimolecular reactions.

Yao *et al.* demonstrated the synthesis of fluorine-containing 4-thiocyanato-1*H*-pyrazoles **23** (Scheme 8) [86] under mild, metal- and oxidant-free conditions, using fluorinated arylhydrazines **20**, 1,3-diketones **21**, and ammonium thiocyanate **22** in an undivided electrochemical cell. The reaction was performed at room temperature for 4 hours in an undivided cell equipped with graphite felt (GF) as the anode, a platinum plate (Pt) as the cathode, and $LiBF_4$ as the electrolyte, maintaining a constant current of 10 mA. This process afforded fluorinated phenyl-4-thiocyanato-1*H*-pyrazole **23** in moderate to excellent yields (41–94%).

Mechanistic studies revealed that anodic oxidation generates SCN• radicals, which subsequently undergo electrophilic substitution with the pyrazole intermediate adduct. The practicality and scalability of this thiocyanation protocol make it both cost-effective and environmentally friendly. Given its simplicity, mild reaction conditions, and neutral medium, this electrochemical multicomponent tandem approach is highly appealing for applications in the pharmaceutical and fine chemical industries, offering high scalability and functional group tolerance. Notably, fluorination in products **23** can manifest as a single fluorine atom, two fluorine atoms, or trifluoromethyl and trifluoromethoxy groups on the aromatic ring.

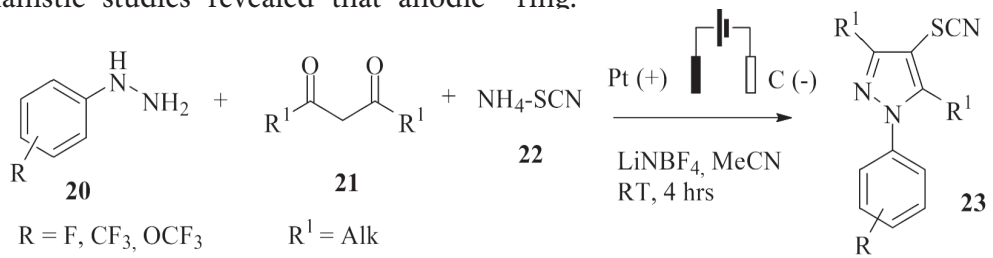

Scheme 8. Electrochemical approach to fluorinated 1-phenyl-4-thiocyanato-1*H*-pyrazoles.

Elinson *et al.* reported the synthesis of spiro-indole-3,4'-pyrano-pyranones **27** via electrochemical cascade trimolecular cyclization, using fluoro-isatins **24**, pyran-4-one **25**, and malonic acid derivatives **26** (Scheme 9) [87]. The reaction is conducted under reflux conditions in undivided cells, with potassium iodide as the electrolyte and *n*-propanol as the solvent, achieving high yields (~80%) of the spiro-heterocyclic system **27**. This catalytically efficient procedure requires no complex equipment, is easily executable, and allows straightforward product isolation. As a result, this novel approach provides significant advantages for large-scale processes, supporting environmentally friendly synthesis while enabling high molecular diversity.

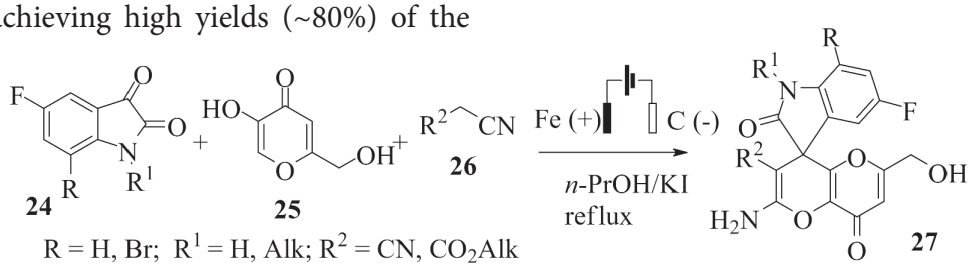

Scheme 9. Electrochemical approach to fluorinated spiro-indole-3,4'-pyrano- pyranones.

Fluorinated derivatives of 4*H*-pyran-2yl-(aryl)methyl-isoxazol-5(2*H*)-one **30** (Scheme 10) [88] can be synthesized electrochemically in propanol, heating at 97 °C, via a one-pot, three-component reaction involving aromatic aldehydes **28**, fluorinated 3-aryl-substituted isoxazol-5(4*H*)-one **29**, and pyran-4-one **25**. This method represents a significant achievement, performed in an undivided electrochemical cell using graphite as the anode and iron as the cathode.

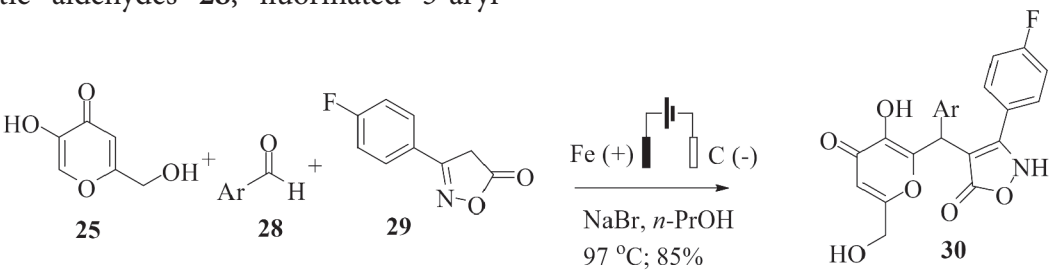

Scheme 10. Electrocatalytic trimolecular reaction affording fluorinated isoxazol-5(2*H*)-ones.

Fluorine-containing carbonyl compounds are highly effective reagents in various addition reactions performed under conventional conditions [89, 90]. A similar reactivity is observed for aldehydes **4** (Scheme 11) [91] in an electrochemical assembly with 6-methyl-3*H*-pyran-2,4-dione **30** and barbituric acid **31**. The reaction is carried out in an undivided electrochemical cell using sodium iodide as a mediator in methanol. The process yields fluorine-containing spiro[furo[3,2-*b*]-pyran-2,5'-pyrimidines **32** with high efficiency, achieving 73–82% yields.

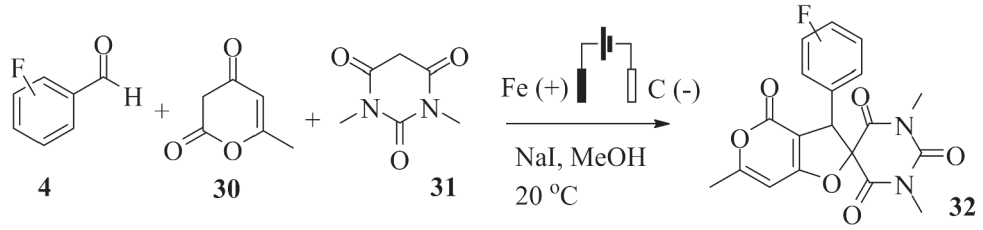

Scheme 11. Electrochemical synthesis of fluorine-containing spiro[furo[3,2-*b*]-pyran-2,5'-pyrimidines.

Indoles serve as a fundamental scaffold in drug design, valued for their versatile biological activity and capacity to interact with diverse molecular targets. They are widely present in both natural and synthetic pharmaceuticals, playing critical roles in anticancer, antimicrobial, anti-inflammatory, and neuroprotective therapies. Their structural adaptability enables medicinal chemists to optimize potency, selectivity, and bioavailability, making them indispensable in modern drug discovery [92–95]. Various strategies have been developed for synthesizing indole derivatives [96–99], including fluorine-containing variants [100–103].

Singh *et al.* developed an electrocatalytic tandem condensation method for synthesizing tri-substituted indoles **35** (Scheme 12) [104]. The process involves an electrocatalytic

conversion of fluorinated aldehydes **4**, indole **33**, and malononitrile **34**, conducted in EtOH at a current density of 10–15 mA/cm², using $LiClO_4$ as the electrolyte. Fluorinated benzaldehydes exhibit high reactivity and distinct reactivity patterns, which vary depending on the number and position of fluorine atoms on the aromatic ring [105, 106].

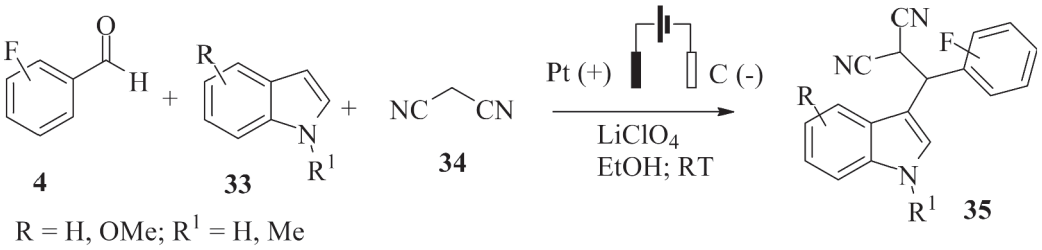

4 **33** **34** **35**

R = H, OMe; R^1 = H, Me

Scheme 12. Electrochemical synthesis of fluorine-containing indoles.

Triazoles and their derivatives exhibit a wide range of biological activities, making them valuable in medicinal chemistry. They are known for their antimicrobial, antiviral, antitubercular, anticancer, anticonvulsant, analgesic, antioxidant, anti-inflammatory, and antidepressant properties [107, 108].

Zhao *et al.* developed an electrochemical multicomponent [3+1+1] annulation reaction for the synthesis of fluoro-substituted 1,2,4-triazoles **37** (Scheme 13) [109], without the use of transition metals, acids, bases, or external oxidants. The electrolysis was conducted in an undivided cell, equipped with a graphite carbon anode, a platinum cathode, and 20 mol% $LiClO_4$ as the electrolyte, under constant current conditions. Substituted 1,2,4-triazoles **37** were obtained through the reaction of 1-benzylidene-2-phenylhydrazine **36** (derived from fluorinated benzaldehydes), aromatic aldehydes, and ammonium acetate. Given the ready availability of raw materials, reasonable yields (~75%), feasible scalability, and experimental convenience, this protocol offers a practical and efficient approach to triazole synthesis.

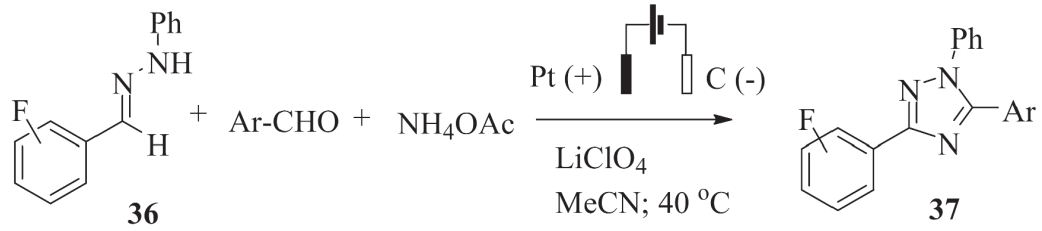

36 **37**

Scheme 13. Electrochemical preparation of fluorinated 1,2,4-triazole derivatives.

Imidazolines and oxazolidines exhibit diverse biological activities, making them valuable in medicinal chemistry [110–113]. Claraz *et al.* reported a one-pot, eco-friendly electrochemical method for synthesizing oxazolidine **39** (Scheme 13) [114] and imidazoline derivatives **40**, incorporating trifluoromethyl groups and aromatic fluorine substitutions under mild, environmentally benign conditions. The method involves electrochemical tandem

radical trifluoromethylation of allylamines **38**, followed by a formal (3+2)-cycloaddition with Alk-CN or aliphatic ketones. The starting allylamines are typically tosyl-protected, facilitating the reaction. The electrochemical reaction of tosyl-amines **38** with Langlois reagent (CF_3SO_2Na) is carried out in acetonitrile and dichloromethane using $LiClO_4$ as the supporting electrolyte, enabling the one-pot electrosynthesis of fluorinated 1,3-oxazolidines **39** and 2-imidazolines **40**.

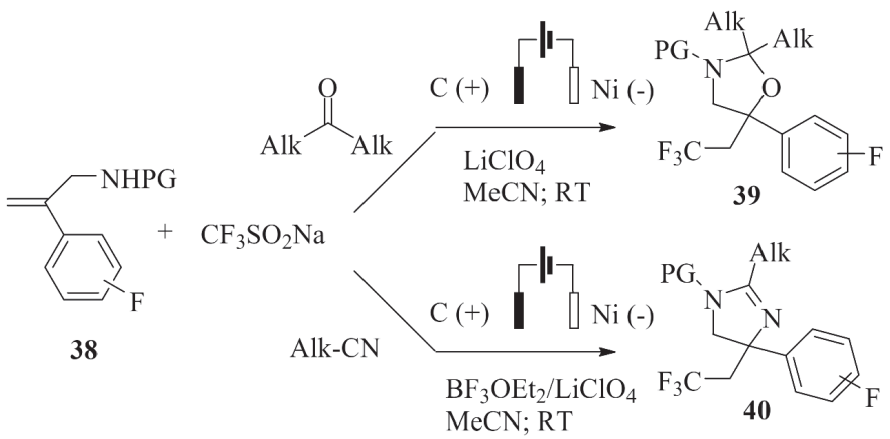

Scheme 14. Three-component synthesis of fluorinated imidazolines and oxazolidines.

Selenium-containing heterocyclic compounds exhibit a range of biological activities, making them valuable in medicinal chemistry and materials science [115, 116]. The reaction reported by He *et al*. involves the electrochemical transformation of fluoro-phenylhydrazine **41** (Scheme 15) [117], diketone **42**, and diphenyl diselenide **43**. Using readily available starting materials, the approach outlined in Scheme 15 provides a versatile method for synthesizing a broad range of fluorinated 4-selanylpyrazole derivatives **44**, achieving high yields (71–96%). Notably, fluorine atoms are both on the phenyl ring of the starting hydrazine **41** and on the selenide **43**. The reaction is conducted in an undivided electrochemical cell with reticulated vitreous carbon (RVC) as the anode, a platinum plate as the cathode, and $LiBF_4$ (20 mol%) as the electrolyte. Under mild conditions, at ambient temperature for 9 hours with a constant current of 6 mA, the desired fluorinated 4-phenylselanyl-pyrazoles **44** are obtained in MeCN, without the need for catalysts or chemical oxidants.

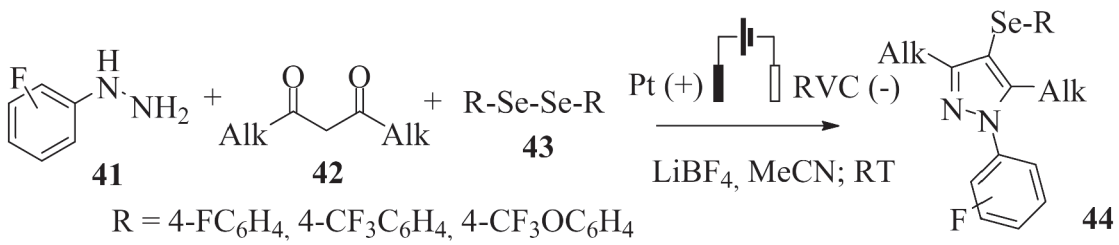

Scheme 15. Electrochemical approach to fluorinated 4-selanylpyrazoles.

Weimin *et al.* reported a mechanistically similar method to Scheme 15 for the synthesis of various 4-bromopyrazoles **46** (Scheme 16) [118], employing a three-component reaction involving fluorinated aryl-hydrazine **41**, diketone **42**, and bromomalonate **45** in an environmentally friendly approach. The reaction was conducted in an undivided electrochemical cell for 10 hours, using *n*-Bu_4NBF_4 (20 mol%) as the electrolyte in MeCN at ambient temperature. Mechanistically, hydrazine **41** undergoes condensation with diketone **42**, forming the pyrazole ring, which is subsequently brominated to yield 4-bromopyrazole **46**. This method can be generalized for the bromination of heterocyclic compounds, offering a sustainable and efficient synthetic strategy.

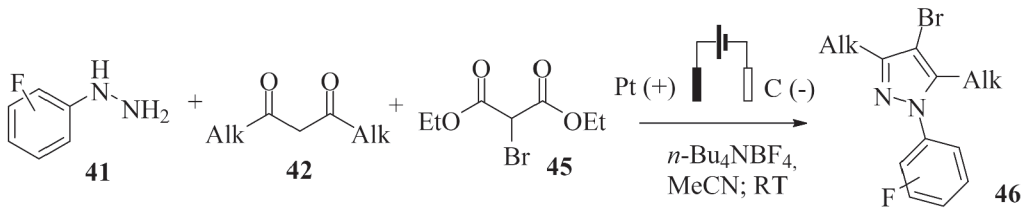

Scheme 16. Electrochemical approach to fluorinated 4-bromopyrazoles.

As emphasized throughout this review, fluorine-containing carbonyl compounds are highly valuable synthetic building blocks exhibiting significantly enhanced reactivity compared to their non-fluorinated counterparts [119–122]. Mohammadi *et al.* employed an electrochemical approach for the successful synthesis of fluorinated phthalazine derivatives **48** (Scheme 17) [123]. The reaction was conducted in an undivided electrochemical cell at a current density of 12 mA/cm^2, using NaBr as the electrolyte. This one-pot, three-component reaction involved fluorinated benzaldehydes 4, phthalhydrazide **47**, and malononitrile, carried out in propanol. The method efficiently yielded fluorine-containing pyrazolo[1,2-*b*]phthalazines **48** in good to excellent yields (75–92%).

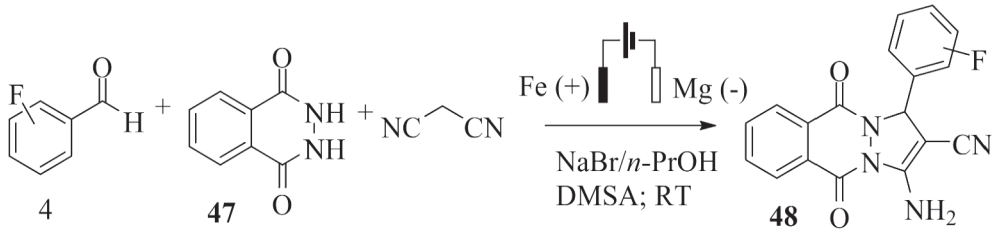

Scheme 17. Electrochemical synthesis of fluorinated pyrazolo[1,2-*b*]phthalazines.

Mechanistically and strategically similar to the electrochemical transformations described in Schemes 15 and 16, the method reported by He *et al.* enables the synthesis of 4-thiocyanato-1*H*-pyrazoles **49** (Scheme 18) [124]. Under mild, metal- and oxidant-free conditions, fluorinated arylhydrazines **41**, 1,3-diketones **42**, and ammonium thiocyanate undergo electrochemical coupling in an undivided cell, affording fluorine-containing products

49 in moderate to excellent yields (41–94%). Optimal results were obtained using graphite felt (GF) as the anode, a platinum plate as the cathode, and $LiBF_4$ as the electrolyte, at room temperature for 4 hours under a constant current of 10 mA. This setup efficiently produced fluorinated phenyl-4-thiocyanato-1*H*-pyrazole scaffolds **49**. Mechanistic investigations suggest that anodic oxidation generates an SCN• radical, which subsequently reacts with a pyrazole intermediate via electrophilic substitution. Owing to its cost-effectiveness, practicality, and scalability, this electrochemical thiocyanation protocol is not only environmentally benign but also highly appealing for applications in the pharmaceutical and fine chemical industries, thanks to its operational simplicity, mild reaction conditions, and broad functional group tolerance.

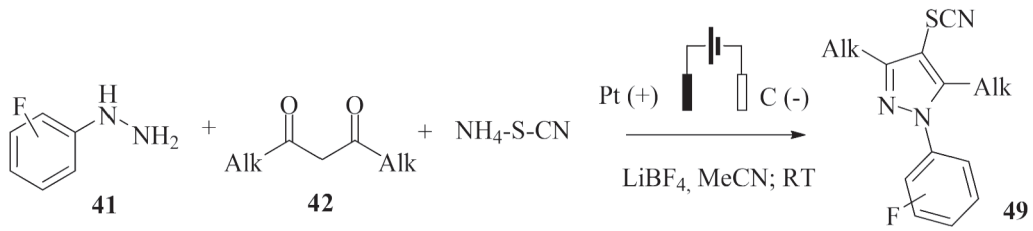

Scheme 18. Electrochemical synthesis of fluorinated phenyl-4-thiocyanato-1*H*-pyrazoles.

Benzylamines and their derivatives, such as pyridoxamine, play a significant role in biological enzymatic transamination, facilitating the interconversion of α-keto and α-amino acids [125–127]. Inspired by this natural process, biomimetic synthetic approaches have largely focused on the reductive amination of carbonyl compounds, employing benzylamines both as a nitrogen source and as a self-oxidizing agent through oxidative deamination [128–133]. Remarkably, both α-hydrogens of the CH_2–NH_2 moiety in benzylamine can participate in the reductive amination of carboxylic acids, yielding the corresponding amine products, while the benzylamine itself is oxidized to the corresponding carboxylic acid (Scheme 19) [134].

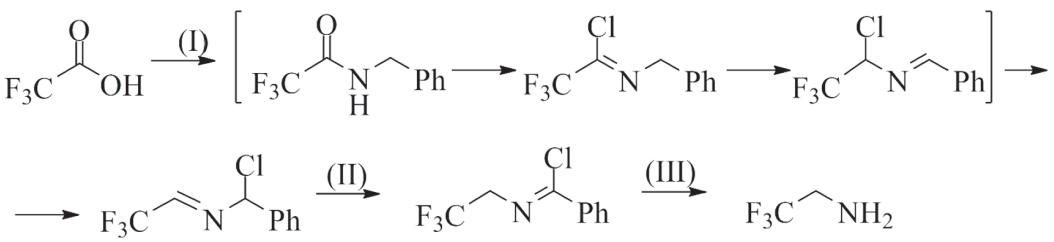

Key: (I) $BnNH_2$ (1 eq), Ph_3P (4 eq)/CCl_4 (4 eq), TEA (1.5 eq), $CHCl_3$ reflux, 40 min.; (II) TEA (3 eq)/H_2O; (III) MeOH/HCl (conc), reflux, 24 hr

Scheme 19. Reductive amination of trifluoroacetic acid to 2,2,2-trifluoroethylamine via 'double' biomimetic transamination.

A comparable transformation—oxidation of benzylamine to a formal benzoic acid residue—was reported by Wang *et al*. via an electrochemical three-component reaction involving quinoline derivatives **50**, benzylamines, and trimethylsilyl cyanide, yielding imidazo-fused *N*-heterocycles **51** with good to excellent efficiency (Scheme 20) [135]. Fluorine substituents, either as a single fluorine atom or a trifluoromethyl group, can be introduced on both the quinoline derivatives **50** and the benzylamine substrates, expanding the scope of this methodology. This anodic oxidation–driven cyclization proceeds under metal- and chemical oxidant-free conditions in an undivided cell, employing readily available starting materials. The method is notable for its substrate generality, environmental friendliness, mild reaction conditions, and excellent scalability, making it particularly appealing for applications in complex heterocycle synthesis.

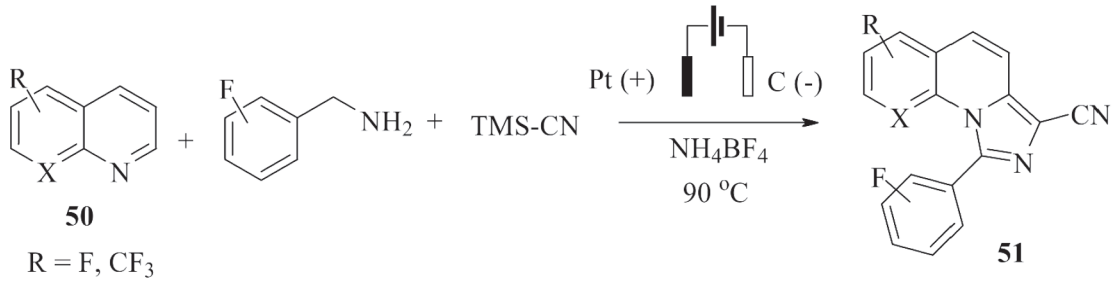

Scheme 20. Electrochemical synthesis of fluorinated imidazo-fused *N*-heterocycles.

Analogous to biomimetic transamination involving reduction of carbonyl compounds and the oxidation of benzylamine [136–138], the electrochemical reaction reported by Yang *et al*. describes the synthesis of 1,2,4-trisubstituted imidazoles **53** via a three-component coupling of fluorine-containing ketones **52**, benzylamine, and alkyl amines (Scheme 21) [139]. The reaction employs readily available starting materials in an undivided electrochemical cell equipped with carbon rod electrodes, proceeding under metal- and oxidant-free conditions. This electrochemical strategy offers a practical and scalable approach to the synthesis of fluorinated heterocycles **53**, with moderate to excellent yields across a broad substrate scope. Owing to its functional group tolerance, simplicity, and environmental compatibility, the method holds significant promise for large-scale applications in heterocyclic and medicinal chemistry.

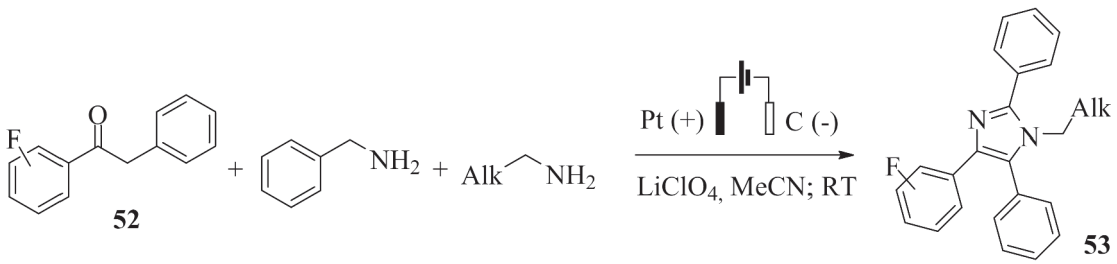

Scheme 21. Electrochemical synthesis of fluorinated 1,2,4-trisubstituted-(1*H*)imidazoles.

Another compelling example of electrochemical oxidation of benzylamine derivatives, analogous to biomimetic transamination processes [140–142], was developed by Chen *et al.* (Scheme 22) [143]. Their strategy enables the efficient synthesis of imidazole derivatives **54** under undivided electrolytic conditions, demonstrating the effectiveness of electrochemical-oxidation-induced three-component condensation. The methodology is notably metal- and peroxide-free, rendering it environmentally benign and sustainable. It also exhibits broad substrate compatibility, allowing for the introduction of fluorine substituents into the imidazole ring with consistently high yields. A particularly noteworthy application involves the reaction of di-trifluoromethylacetylene (perfluorobut-2-yne) with fluorinated benzylamine and trimethylsilyl azide (TMS-N_3), affording imidazole products **54** bearing two trifluoromethyl groups and a fluorinated phenyl ring—a valuable structural motif for pharmaceutical and agrochemical development.

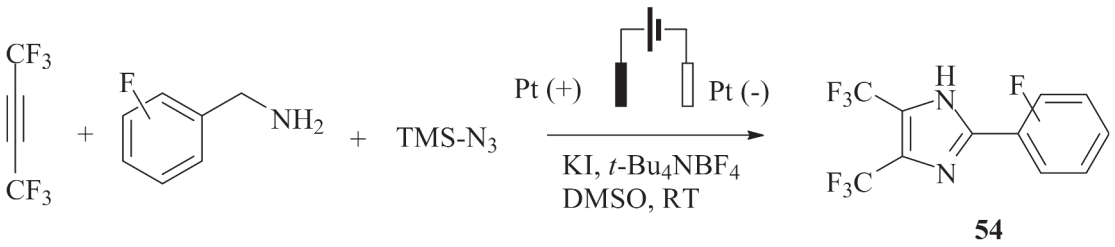

Scheme 22. Electrochemical synthesis of fluorinated imidazoles.

Mohammedi *et al.* reported the synthesis of a novel tetrahydroimidazo[1,2-*a*]pyridine-5(1*H*)-one derivative **56** (Scheme 23) [144] via a one-pot electrochemical strategy, combining fluoro-aldehydes **4**, Meldrum's acid **54**, and 2-(nitromethylene)imidazolidine **55**. The reaction proceeds in propanol using sodium bromide as the electrolyte within an undivided cell, maintained under a constant current of 50 mA, yielding the target heterocyclic compounds in good to excellent yields (70–96%). This green protocol demonstrates significant potential for the construction of fused polycyclic frameworks relevant to bioactive heterocycles. It offers several advantages, including high product yields, simple experimental setup, and environmentally benign conditions, making it an attractive approach for sustainable synthetic chemistry.

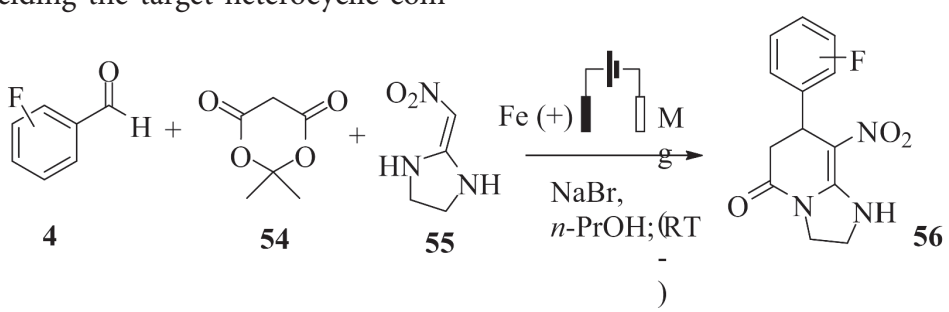

Scheme 23. Electrochemical preparation of fluorine-containing imidazo-pyridines.

Gao *et al*. demonstrated that an electrochemical strategy can be effectively employed to construct complex biologically relevant molecules bearing trifluoromethyl-substituted quinoline scaffolds **60** (Scheme 24) [145]. The method relies on a paired electrolysis–driven cascade annulation, designed to achieve two key objectives simultaneously: the direct synthesis of quinolines and their convergent incorporation into bioactive molecular frameworks. The transformation involves the electro-reduction–induced reaction of fluoro-substituted isatin **57**, methyl 4,4,4-trifluorobut-2-ynoate **58**, and alcohol-containing substrates **59**. Conducted in CH_3CN within an undivided cell equipped with a graphite rod anode and platinum cathode, and using KI (20 mol%) as the electrolyte, the reaction proceeds under a constant current of 5 mA, affording the desired quinoline derivatives **60** in moderate to excellent yields (40–99%). The reaction exhibits broad substrate tolerance—the R group in alcohol **59** can encompass virtually any organic residue: from simple aliphatic alcohols to heterocycles, fluorinated side chains, natural and tailor-made amino acids [146–148], as well as peptides, peptidomimetics, steroids, and small-molecule drugs. Of over sixty examples explored, only a few representative cases are shown in Scheme 24.

Importantly, the stereochemical integrity of chiral centers is preserved under the mild electrochemical conditions. Fluorine incorporation is also highly tunable, occurring as monofluoroaryl, aryl–CF_3, or aliphatic–CF_3 functionalities, providing access to a structurally diverse library of fluorinated quinolines with pharmaceutical potential.

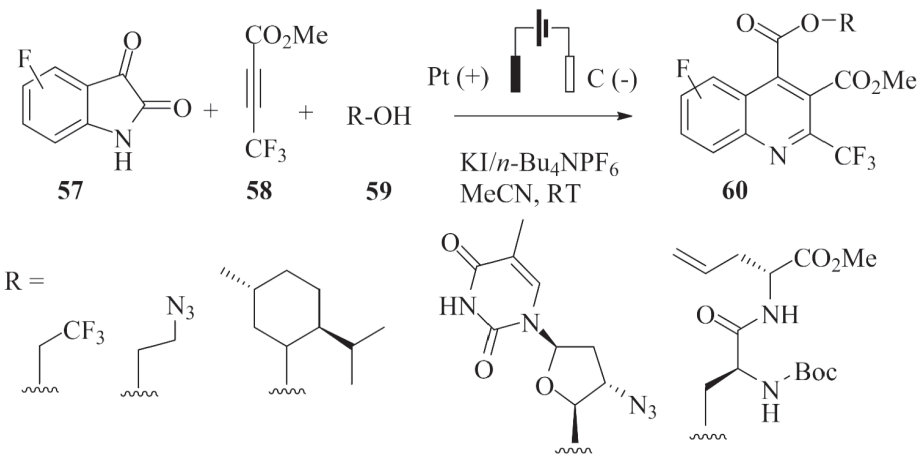

Scheme 24. Application of electrochemical approach for preparation of various quinoline-substituted bioactive molecules.

Sharma *et al*. developed a novel electrochemically induced oxidative cascade cyclization for the synthesis of fluorinated quinazolinone- and quinoline-decorated indolizine derivatives **64** (Scheme 25) [149]. This transformation proceeds in an undivided cell under metal- and oxidant-free conditions, showcasing an environmentally friendly approach. The reaction involves a three-component coupling of substituted pyridines **61**, fluorobenzyl-containing quinazolinone **62**, and fluoro-chalcones **63**. Conducted at 90 °C using two platinum plate electrodes,

with $NH_4I/n\text{-}Bu_4NPF_6$ as the electrolyte and dimethylacetamide (DMA) as the solvent, the method enables efficient construction of heterocycle-rich molecular frameworks.

A gram-scale synthesis was performed to demonstrate the scalability and practical applicability of the protocol. The study highlights the potential to expand this strategy toward the synthesis of more complex polycyclic architectures, offering broad utility in medicinal chemistry and materials science.

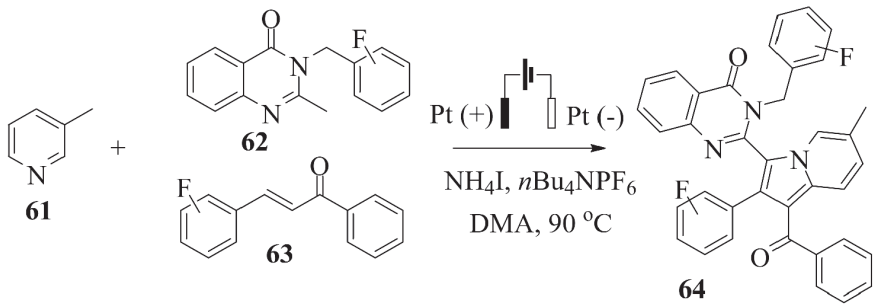

Scheme 25. Electrochemical synthesis of complex fluorinated quinazolin-indolizines.

Tetramolecular reactions.

Yang *et al.* developed a tetramolecular electrochemical strategy for the synthesis of fluorine-substituted 1,2,4-triazoles **66** (Scheme 26) [150]. The reaction combines fluorinated aryl hydrazines **41**, benzyl alcohols **65**, paraformaldehyde $(HCHO)_n$, and ammonium acetate (NH_4OAc) in a single pot. Electrolysis was performed under constant current conditions in an undivided cell equipped with a graphite rod anode and a nickel plate cathode. Notably, benzyl alcohol serves both as solvent and reactant, while $n\text{-}Bu_4NI$ (TBNI) acts as a redox mediator and *t*-BuOK as the base. The reaction proceeds under mild, metal- and oxidant-free conditions at room temperature, reflecting its practicality and environmental appeal. In the resulting triazole derivatives **66**, fluorine atoms are introduced on both aromatic rings, allowing for structural diversification and the potential to fine-tune biological properties of the synthesized compounds.

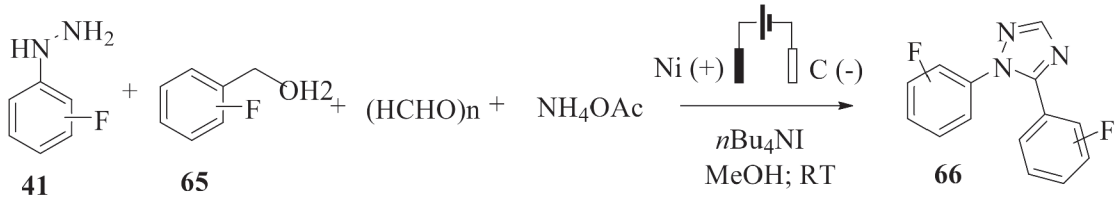

Scheme 26. Electrochemical synthesis of fluoro-substituted substituted 1,2,4-triazoles.

CONCLUSIONS. This review has showcased the breadth and sophistication of electrochemical strategies for synthesizing fluorine-containing heterocycles, highlighting their relevance to modern pharmaceutical, agrochemical, and materials-oriented research. Across a wide array of reaction classes, the recurring theme is the ability of electrochemical methods to drive

complex, multibond-forming transformations under sustainable, operationally simple, and transition-metal-free conditions.

Electrooxidative multicomponent reactions—including two-, three-, and four-component assemblies—have proven highly effective for constructing structurally rich heterocycles such as pyrazoles, imidazoles, triazoles, quinolines, and fused polycyclic systems. Many of these transformations rely on fluorinated building blocks (e.g., fluorinated aryl hydrazines, benzylamines, or fluoroalkynes) to deliver final products that possess both high synthetic value and tunable biological properties.

These methodologies also provide remarkable flexibility in fluorine incorporation, enabling the installation of fluorine in diverse chemical environments. Substituents may include single or multiple fluoroaromatic rings, aromatic CF_3 groups, aliphatic trifluoromethyl moieties, or combinations thereof, offering wide-ranging opportunities for structural design and biological fine-tuning. This versatility significantly enhances the utility of electrochemical platforms in the discovery and development of functional fluorinated heterocycles.

Several reactions capitalize on the oxidative transformations of benzylamine moieties, drawing biomimetic parallels to enzymatic transamination processes. These processes enable carbon–nitrogen bond construction via *in situ* formation of reactive imine intermediates, thus opening pathways to reductive amination and tandem heterocycle formation from simple precursors such as carboxylic acids, aldehydes, and ketones.

Noteworthy contributions include anodic SCN• radical generation for thiocyanation of fluorinated pyrazoles under mild, scalable conditions; electrosynthesis of imidazoles and triazoles from benzyl alcohols, fluorinated ketones, and amines in metal- and oxidant-free systems; cascade annulations involving complex bio-derived alcohols and trifluoromethyl alkynes, preserving stereochemical integrity during quinoline ring construction; and electrochemically induced ring-forming condensation of fluoroaryl fragments with isatins, azides, and heteroaromatic substrates, giving rise to heterocycle-rich molecular frameworks with structural and functional diversity.

The methodologies described herein employ commonly available electrodes (e.g., graphite felt, platinum, nickel), green solvents, and electrochemical mediators (such as tetrabutylammonium iodide), supporting both environmental and synthetic economy. Mild temperatures, functional group tolerance, and gram-scale validations further underscore the practical potential of these approaches.

In conclusion, the reviewed strategies demonstrate that electrochemistry is not merely a replacement for traditional oxidants and catalysts, but a powerful platform capable of orchestrating molecular complexity with precision—particularly in the realm of fluorinated heterocyclic synthesis. Future research is expected to further integrate paired redox processes, flow electrolysis, and computationally guided design, expanding the boundaries of what is synthetically and environmentally possible in this field.

ACKNOWLEDGMENTS: We gratefully acknowledge the financial support from IKERBASQUE, Basque Foundation for Science, (for Soloshonok). The authors acknowledge the assistance of Microsoft Copilot and Google Gemini for their support in translating to Ukrainian.

ЕЛЕКТРОХІМІЧНИЙ СИНТЕЗ ФТОРОВАНИХ ГЕТЕРОЦИКЛІЧНИХ СПОЛУК (огляд)

Аліція Взорек,[1] Таїзо Оно,[2] Даніель Беккер[3], Вей Чжан[4], Вадим А. Солошонок[5]*

[1] Хімічний інститут, Університет Яна Кохановського в Кельці, вул. Університетська 7, Кельце25–406, Польща;
[2] Національний інститут передової науки та технологій (AIST), 2266–98, Анагахора, Шімошідамі, район Моріяма, Нагоя 463–8560, Японія;
[3] Відділ фармацевтичної та лікарської хімії, Фармацевтичний інститут, Вільний університет Берліна, Кьонігін-Луїзе-Штрасе 2+4, Берлін 14195, Німеччина;
[4] Хімічний факультет, Університет Массачусетса в Бостоні, Бостон, Массачусетс 02125, Сполучені Штати Америки;
[5] ІКЕРБАСКЕ, Баскська наукова фундація, вул. Марія Діас де Харо 3, площа Бізкая, Більбао 48013, Іспанія
e-mail: vadimsoloshonok@gmail.com

Фторвмісні гетероцикли відіграють ключову роль у фармацевтичній, агрохімічній та матеріалознавчій промисловості. Прагнення до ефективних та сталих методів синтезу сприяло розвитку електрохімії як привабливої альтернативи традиційним хімічним перетворенням. Серед цих підходів електрохімія виявилася особливо перспективною технікою для здійснення багатозв'язкових процесів у м'яких, екологічно чистих умовах.

Цей огляд висвітлює ключові досягнення за останнє десятиліття в електрохімічному синтезі фторованих гетероциклічних сполук, що охоплюють бімолекулярні, тримолекулярні та чотиримолекулярні реакції. Особливу увагу приділено багатокомпонентним каскадним стратегіям, радикально-опосередкованим сполученням та безокиснювальним циклізаціям, які забезпечують широку толерантність до функціональних груп та гнучкість введення фтору. Сукупно ця робота слугує ресурсом для дослідників, які розробляють стійкі синтетичні платформи нового покоління, адаптовані до фторованих гетероциклів із різноманітними структурними та біологічними профілями.

Ключові слова: електрохімія, гетероциклічні сполуки, фтор, фторовані фармацевтичні препарати, зелена хімія, сталий синтез.

REFERENCES

[1] Glasstone S. *An introduction to electrochemistry*. Read Books Ltd; 2011.
[2] Bagotsky V.S., editor. *Fundamentals of electrochemistry*. John Wiley & Sons; 2005.
[3] Rieger P.H. *Electrochemistry*. Springer Science & Business Media; 2012.
[4] Rajeshwar K.I., Ibanez J.G., Swain G.M. Electrochemistry and the environment. *J. Appl. Electrochem*. 1994. **24**(11): 1077–1091. doi.org/10.1007/BF00241305.
[5] Heinze J. Ultramicroelectrodes in electrochemistry. *Angew. Chem. Int. Edi. Eng*. 1993. **32**(9): 1268–1288. doi.org/10.1002/anie.199312681.
[6] Ryan M.D., Bowden E.F., Chambers J.Q. Dynamic electrochemistry: methodology and application. *Anal. Chem*. 1994. **66**(12): 360–427. doi.org/10.1021/ac00084a015.

[7] Horn E.J., Rosen B.R., Baran P.S. Synthetic organic electrochemistry: an enabling and innately sustainable method. *ACS Cent. Scien*. 2016. **2**(5): 302–308. doi.org/10.1021/acscentsci.6b00091.

[8] Jiang Y., Xu K., Zeng C. Use of electrochemistry in the synthesis of heterocyclic structures. *Chem. Rev*. 2017. **118**(9): 4485–4540. doi.org/10.1021/acs.chemrev.7b00271.

[9] He J., Zhou X., Mei H. et al. Electrochemical reaction of indole-tethered alkynes enabling stereoselective synthesis of iodovinyl spiroindolenine-cyclopentanes. Chem. Commun. 2025. **61**(41): 7454–7457. DOI: 10.1039/D5CC01342A.

[10] Wang N., Xu J., Mei H. *et al*. Electrochemical Approaches for Preparation of Tailor-Made Amino Acids, *Chin. J. Org. Chem*. 2021. **41**: 3034–3049. DOI: 10.6023/cjoc202102043.

[11] Sequeira C.A., Santos D.M. Electrochemical routes for industrial synthesis. *J. Braz. Chem. Soc*. 2009. **20**: 387–406. doi.org/10.1590/S0103-50532009000300002.

[12] Li G.R., Xu H., Lu X.F. *et al*. Electrochemical synthesis of nanostructured materials for electrochemical energy conversion and storage. *Nanoscale*. 2013. **5**(10): 4056–4069. doi.org/10.1039/C3NR00607G.

[13] Schotten C., Nicholls T.P., Bourne R.A. *et al*. Making electrochemistry easily accessible to the synthetic chemist. *Green Chem*. 2020. **22**(11): 3358–3375. DOI: 10.1039/D0GC01247E.

[14] Sbei N., Listratova A.V., Titov A.A., Voskressensky LG. Recent advances in electrochemistry for the synthesis of *N*-heterocycles. *Synthesis*. 2019. **51**(12): 2455–2473. DOI: 10.1055/s-0037-1611797.

[15] Jing Q., Moeller K.D. From molecules to molecular surfaces. Exploiting the interplay between organic synthesis and electrochemistry. *Acc. Chem. Res*. 2019. **53**(1): 135–143. doi.org/10.1021/acs.accounts.9b00578.

[16] Devi S., Wadhwa D., Sindhu J. Electro-organic synthesis: an environmentally benign alternative for heterocycle synthesis. *Org. Biomol. Chem*. 2022. **20**(26): 5163–5229. doi.org/10.1039/D2OB00572G.

[17] Chen T.L., Kim H., Pan S.Y. *et al*. Implementation of green chemistry principles in circular economy system towards sustainable development goals: Challenges and perspectives. *Scien. Total Environ*. 2020. **716**: 136998. doi.org/10.1016/j.scitotenv.2020.136998.

[18] Liu J., Lu L., Wood D. New redox strategies in organic synthesis by means of electrochemistry and photochemistry. *ACS Cent. Scien*. 2020. **6**(8): 1317–1340. doi.org/10.1021/acscentsci.0c00549.

[19] Noël T., Cao Y., Laudadio G. The fundamentals behind the use of flow reactors in electrochemistry. *Acc. Chem. Res*. 2019. **52**(10): 2858–2869. doi.org/10.1021/acs.accounts.9b0041.

[20] Zhu C., Ang N.W., Meyer T.H. *et al*. Organic electrochemistry: molecular syntheses with potential. *ACS Cent. Scien*. 2021. **7**(3): 415–431. doi.org/10.1021/acscentsci.0c01532.

[21] Malapit C.A., Prater M.B., Cabrera-Pardo J.R. *et al*. Advances on the merger of electrochemistry and transition metal catalysis for organic synthesis. *Chem. Rev*. 2021. **122**(3): 3180–3218. doi.org/10.1021/acs.chemrev.1c00614.

[22] Han J., Konno H., Sato T., Soloshonok V.A., Izawa K. Tailor-made amino acids in the design of small-molecule blockbuster drugs. *Eur. J. Med. Chem.* 2021. **220**: 113448. doi: 10.1016/j.ejmech.2021.113448.

[23] Mei H., Han J., White S. *et al.* Tailor-made amino acids and fluorinated motifs as prominent traits in modern pharmaceuticals. *Chem.—Eur. J.* 2020. **26**(50): 11349–11390. doi: 10.1002/chem.202000617.

[24] Han J., Konno H., Sato T. *et al.* Peptidomimetics and Peptide-Based Blockbuster Drugs.

Curr. Org. Chem. 2021. **25**(14): 1627–1658.
doi: 10.2174/1385272825666210610155047.

[25] Liu J., Han J., Izawa K. *et al.* Cyclic tailor-made amino acids in the design of modern pharmaceuticals. *Eur. J. Med. Chem.* 2020. **208**: 112736.
doi: 10.1016/j.ejmech.2020.112736.

[26] Zhu Y, Han J, Wang J. *et al*. Modern approaches for asymmetric construction of carbon–fluorine quaternary stereogenic centers: synthetic challenges and pharmaceutical needs. *Chem. Rev*. 2018. **118**(7): 3887–3964.
doi.org/10.1021/acs.chemrev.7b00778.

[27] Zhu W., Wang J., Wang S. *et al*. Recent advances in the trifluoromethylation methodology and new CF_3-containing drugs. *J. Fluor. Chem*. 2014. **167**: 37–54.
doi.org/10.1016/j.jfluchem.2014.06.026.

[28] Du Y., Semghouli A., Wang Q. *et al*. FDA-approved drugs featuring macrocycles or medium-sized rings. *Arch. Pharm*. 2025. **358**(1): e2400890.
doi.org/10.1002/ardp.202400890.

[29] Wang Q., Han J., Sorochinsky A. *et al.* The Latest FDA-Approved Pharmaceuticals Containing Fragments of Tailor-Made Amino Acids and Fluorine. *Pharmaceuticals.* 2022. **15**(8): 999.
doi.org/10.3390/ ph150809991847558.

[30] Han J., Wzorek A. Dhawan G. *et al.* New drugs on the pharmaceutical market containing fluorine and residues of tailor-made amino acids. *Ukr. Chem. J.* 2024. **90**(9): 31–56.
doi: 10.33609/2708-129X.90.9.2024.31-56.

[31] Yin Z., Hu W., Zhang W. *et al.* Tailor-made amino acid-derived pharmaceuticals approved by the FDA in 2019. *Amino Acids.* 2020. **52**(9): 1227–1261.
doi: 10.1007/s00726-020-02887-4.

[32] Liu A., Han J., Nakano A. *et al.* New pharmaceuticals approved by FDA in 2020: Small-molecule drugs derived from amino acids and related compounds. *Chirality.* 2022. **34**(1): 86–103.
doi: 10.1002/chir.23376.

[33] Wang N., Mei H., Dhawan G. *et al.* New Approved Drugs Appearing in the Pharmaceutical Market in 2022, Featuring Fragments of Tailor-Made Amino Acids and Fluorine. *Molecules.* 2023. **28**(9): 3651.
doi: 10.3390/molecules28093651.

[34] Han J., Wzorek A., Dhawan G. *et al.* New drugs appearing on the market in 2023: molecules containing fluorine and fragments of tailor-made amino acids. *Ukr. Bioorg. Acta.* 2024. **19**(1): 3–20.
doi: 10.15407/bioorganica2024.01.003.

[35] Alicja Wzorek, Jianlin Han, Taizo Ono, Karel D. Klika, Daniel Baecker, Wei Zhang, Vadim A. Soloshonok. Synthesis of Tailor-Made Amino Acids Containing C(sp2)–F bonds. *Ukr. Chem. J.* 2025. **91**(8): 36–64.

[36] Alicja Wzorek, Jianlin Han, Taizo Ono, Karel D. Klika, Daniel Baecker, Wei Zhang, Vadim A. Soloshonok, Cutting-Edge Strategies in the Asymmetric Synthesis of α-Aminocyclopropyl Carboxylic Acids: Essential Scaffolds for Drug Discovery. *Ukr. Chem. J.* 2025. 91(10): 27–71.
doi: 10.33609/2708-129X.91.10.2025.27-71

[37] Han J., Remete A.M., Dobson L.S. *et al.* Next generation organofluorine containing blockbuster drugs. *J. Fluor. Chem.* 2020. **239**: 109639.
doi.org/10.1016/j.jfluchem.2020.109639.

[38] Mei H., Han J., Fustero S. *et al.* Fluorine-Containing Drugs Approved by the FDA in 2018. *Chem.—Eur. J.* 2019. **25**(51): 11797–11819.
doi: 10.1002/chem.201901840.

[39] Wang Q., Bian Y., Dhawan G. *et al.* FDA approved fluorine-containing drugs in 2023. *Chin. Chem. Lett.* 2024. **35**(11): 109780.
doi: 10.1016/j.cclet.2024.109780.

[40] Mei H., Remete A.M., Zou Y. *et al.* Fluorine-containing drugs approved by the FDA in 2019. *Chin. Chem. Lett.* 2020. **31**(9): 2401–2413.
doi: 10.1016/j.cclet.2020.03.050.

[41] Yu Y., Liu A., Dhawan G. *et al.* Fluorine-containing pharmaceuticals approved by the FDA in 2020: Synthesis and biological activity. *Chin. Chem. Lett.* 2021. **32**(11): 3342–3354. doi: 10.1016/j.cclet.2021.05.042.

[42] He J., Li Z., Dhawan G. *et al.* Fluorine-containing drugs approved by the FDA in 2021. *Chin. Chem. Lett.* 2023. **34**(1): 107578. doi: 10.1016/j.cclet.2022.06.001.

[43] Du Y., Bian Y., Baecker D. *et al.* Fluorine in the Pharmaceutical Industry: FDA-Approved Fluorine-Containing Drugs in 2024. *Chem.—Eur. J.* 2025. e202500662. doi.org/10.1002/chem.202500662.

[44] Jianlin Han, Alicja Wzorek, Taizo Ono, Karel D. Klika, Vadim A. Soloshonok. Modern pharmaceutical drugs featuring aliphatic fluorine-containing groups. *Ukr. Chem. J.* 2025. **91**(6): 15–54.

[45] Han J., Wzorek A., Dhawan G. *et al.* Chiral, fluorine-containing pharmaceuticals. *Ukr. Chem. J.* 2025. **91**(2): 55–90. doi.org/10.33609/2708-129X.91.2.2025.55-90.

[46] Ellis T.K., Hochla V.M., Soloshonok V.A. Efficient synthesis of 2-aminoindane-2-carboxylic acid via dialkylation of nucleophilic glycine equivalent. *J. Org. Chem.* 2003. **68**(12): 4973–4976. doi.org/10.1021/jo030065v.

[47] Wzorek A., Sorochinsky A.E., Klika K.D. *et al.* Asymmetric synthesis of chi-constrained glutamic acids and related compounds via Michael addition reactions. *Ukr. Chem. J.* 2024. **90**(8): 83–108. doi: 10.33609/2708-129X.90.8.2024.83-108.

[48] Han J., Liu H., Wang J. *et al.* Hamari's contribution to the asymmetric synthesis of tailor-made amino acids. *Ukr. Chem. J.* 2024. **90**(10): 88–134. doi: 10.33609/2708-129X.90.10.2024.88-134.

[49] Cai C., Soloshonok V.A., Hruby V.J. Michael Addition Reactions between Chiral Ni(II) Complex of Glycine and 3-(*trans*-Enoyl)-oxazolidin-2-ones. A Case of Electron Donor–Acceptor Attractive Interaction-Controlled Face Diastereoselectivity. *J. Org. Chem.* 2001. **66**(4): 1339–1350. doi: 10.1021/jo0014865.

[50] Soloshonok V.A., Kirilenko A.G., Fokina N.A. *et al.* Biocatalytic resolution of β-fluoroalkyl-β-amino acids. *Tetrahedron: Asymmetry*. 1994. **5**(6): 1119–1126. doi.org/10.1016/0957-4166(94)80063-4.

[51] Bravo P., Farina A., Kukhar V.P *et al.* Stereoselective additions of α-lithiated alkyl-*p*-tolylsulfoxides to *N*-PMP (fluoroalkyl) aldimines. An efficient approach to enantiomerically pure fluoro amino compounds. *J. Org. Chem.* 1997. **62**(11): 3424–3425. doi.org/10.1021/jo970004v.

[52] Turcheniuk K.V., Poliashko K.O., Kukhar V.P. *et al.* Efficient asymmetric synthesis of trifluoromethylated β-aminophosphonates and their incorporation into dipeptides. *Chem. Commun.* 2012. **48**(94): 11519–11521. DOI: 10.1039/c2cc36702e.

[53] Cherednichenko A.S., Rassukana Y.V. Recent advances in the asymmetric functionalization of *N*-(*tert*-butylsulfinyl) polyfluoroalkyl imines. *J. Org. Pharmaceut. Chem.* 2025. **23**(2): 3–22. doi.org/10.24959/ophcj.25.321224.

[54] Qiu W., Gu X., Soloshonok V.A. *et al.* Stereoselective synthesis of conformationally constrained reverse turn dipeptide mimetics. *Tetrahedron Lett.* 2001. **42**(2): 145–148. doi: 10.1016/S0040-4039(00)01864-5.

[55] Soloshonok V.A., Ono T. The effect of substituents on the feasibility of azomethine-azomethine isomerization: new synthetic opportunities for biomimetic transamination. *Tetrahedron*. 1996. **52**(47): 14701–14712. doi.org/10.1016/0040-4020(96)00920-9.

[56] Ellis T.K., Martin C.H., Tsai G.M. *et al.* Efficient synthesis of sterically constrained symmetrically α,α-disubstituted α-amino acids under operationally convenient conditions. *J.*

Org. Chem. 2003. **68**(16): 6208–6214. doi.org/10.1021/jo030075w.

[56] Soloshonok V.A., Cai C., Hruby V.J. Asymmetric Michael addition reactions of chiral Ni (II)-complex of glycine with (*N-trans*-enoyl) oxazolidines: improved reactivity and stereochemical outcome. *Tetrahedron: Asymmetry*. 1999. **10**(22): 4265–4269. doi.org/10.1016/S0957-4166(99)00483-8.

[57] Rizzo C., Amata S., Pibiri I. *et al.* FDA-approved fluorinated heterocyclic drugs from 2016 to 2022. *Int. J. Mol. Sci.* 2023. **24**(9): 7728. doi.org/10.3390/ijms24097728.

[58] He J., Wang C., Mei H. *et al.* Visible-light-promoted cyclization of 3-indolylallylamides enabling synthesis of tetrahydrocarbolinones. *Tetrahedron*. 2024. **150**: 133776. doi.org/10.1016/j.tet.2023.133776.

[59] Du Y., Mei H., Makarem A. *et al.* Copper-catalyzed multicomponent reaction of β-trifluoromethyl β-diazo esters enabling the synthesis of β-trifluoromethyl *N*,*N*-diacyl-β-amino esters. *Beilstein J. Org. Chem.* 2024. **20**(1): 212–219. doi.org/10.3762/bjoc.20.21.

[60] Javahershenas R., Mei H., Koley M. *et al.* Recent advances in the multicomponent synthesis of heterocycles using 5-aminotetrazole. *Synthesis.* 2024. **56**(16): 2445–2461. doi: 10.1055/s-0042-1751526.

[61] Abbas A.A., Farghaly T.A., Dawood K.M. Recent progress in therapeutic applications of fluorinated five-membered heterocycles and their benzo-fused systems. *RSC Adv.* 2024. **14**(46): 33864–33905. doi: 10.1039/D4RA05697C.

[62] Yamada T., Okada T., Sakaguchi K. *et al.* Efficient asymmetric synthesis of novel 4-substituted and configurationally stable analogues of thalidomide. *Org. Lett.* 2006. **8**(24): 5625–5628. doi: 10.1021/ol0623668.

[63] Takeda R., Kawamura A., Kawashima A. *et al.* Chemical dynamic kinetic resolution and *S*/*R* interconversion of unprotected α-amino acids. *Angew. Chem., Int. Ed.* 2014. **53**(45): 12214–12217. doi.org/10.1002/anie.201407944.

[64] Wang Y., Song X., Wang J. *et al.* Recent approaches for asymmetric synthesis of α-amino acids via homologation of Ni(II) complexes. *Amino Acids*. 2017. **49**(9): 1487–1520. doi: 10.1007/s00726-017-2458-6.

[65] Nian Y., Wang J., Zhou S. *et al.* Recyclable ligands for the non-enzymatic dynamic kinetic resolution of challenging α-amino acids. *Angew. Chem., Int. Ed.* 2015. **54**(44): 12918–12922. doi.org/10.1002/anie.201507273.

[66] Grygorenko O.O., Volochnyuk D.M., Vashchenko B.V. Emerging Building Blocks for Medicinal Chemistry: Recent Synthetic Advances. *Eur. J. Org. Chem*. 2021. (47): 6478–6510. doi.org/10.1002/ejoc.202100857.

[67] Leśniewska A., Przybylski P. Seven-membered *N*-heterocycles as approved drugs and promising leads in medicinal chemistry as well as the metal-free domino access to their scaffolds. *Eur. J. Med. Chem.* 2024. **275**: 116556. doi.org/10.1016/j.ejmech.2024.116556.

[68] Kumar N., Goel N. Heterocyclic compounds: importance in anticancer drug discovery. *Anticancer Agents Med. Chem*. 2022. **22**(19): 3196–3207. doi.org/10.2174/1871520622666220404082648.

[69] Rusu A., Moga I.M., Uncu L., Hancu G. The role of five-membered heterocycles in the molecular structure of antibacterial drugs used in therapy. *Pharmaceutics*. 2023. **15**(11): 2554. doi.org/10.3390/pharmaceutics15112554.

[70] Al-Bogami A.S., Saleh T.S., Moussa T.A. Green synthesis, antimicrobial activity and cytotoxicity of novel fused pyrimidine deri-

vatives possessing a trifluoromethyl moiety. *ChemistrySelect*. 2018. **3**(28): 8306–8311. doi.org/10.1002/slct.201801050.

[71] Soloshonok V.A., Mikami K., Yamazaki T., Welch J.T., Honek J.F. Eds. Current fluoroorganic chemistry: new synthetic directions, technologies, materials, and biological applications. ACS Symposium Series #949; Oxford University Press, 2007. doi: 10.1021/bk-2007-0949.

[72] Lyutenko N.V., Han J., Wzorek A. *et al.* Carbon nanotubes-catalyzed synthesis of fluorine-containing heterocycles. *Ukr. Chem. J.* 2024. **90**(6): 71–86. doi: 10.33609/2708-129X.90.6.2024.71-86.

[73] Jianlin Han, Alicja Wzorek, Taizo Ono, Karel D. Klika, Vadim A. Soloshonok, Mechanochemical Synthesis of Fluorine-Containing Heterocycles via Ball Milling. *Ukr. Chem. J*., 2025. **91**(7): 35–55.

[74] Yang Z., Zhang J., Hu L. *et al*. Electrochemical HI-mediated Intermolecular C–N Bond Formation to Synthesize Imidazoles from Aryl Ketones and Benzylamines. *J. Org. Chem*. 2020. **85**(9): 5952–5958. doi.org/10.1021/acs.joc.0c00316.

[75] Soloshonok V.A., Hayashi T., Ishikawa K., Nagashima N. Highly diastereoselective aldol reaction of fluoroalkyl aryl ketones with methyl isocyanoacetate catalyzed by silver (I)/triethylamine. *Tetrahedron Lett*. 1994. **35**(7): 1055–1058. doi.org/10.1016/S0040-4039(00)79964-3.

[76] Soloshonok V.A., Kacharov A.D., Avilov D.V. *et al*. Transition Metal/Base-Catalyzed Aldol Reactions of Isocyanoacetic Acid Derivatives with Prochiral Ketones, a Straightforward Approach to Stereochemically Defined β, β-Disubstituted-β-hydroxy-α-amino Acids. 1 Scope and Limitations. *J. Org. Chem*. 1997. **62**(11): 3470–3479. doi.org/10.1021/jo9623402.

[77] Elinson M.N., Dorofeeva E.O., Vereshchagin A.N. *et al*. Electrocatalytic stereoselective transformation of aldehydes and two molecules of pyrazolin-5-one into (*R**, *R**)-*bis*-(spiro-2, 4-dihydro-3 H-pyrazol-3-one) cyclopropanes. *Cat. Scien. Technol*. 2015. **5**(4): 2384–2387. doi.org/10.1039/C4CY01681E.

[78] Qian P., Jiang S., Fan H. *et al*. Electrochemically Enabled Cascade Cyclization Reaction of Aromatic Aldehydes and Pyrazol-5-amines: Synthesis of Bis-pyrazolo [3,4-b:4′,3′-e] pyridines. *J. Org. Chem*. 2022. **87**(14): 9242–9249. doi.org/10.1021/acs.joc.2c00988.

[79] Soloshonok V.A., Hayashi T. Gold(I)-catalyzed asymmetric aldol reaction of fluorinated benzaldehydes with α-isocyanoacetamide. *Tetrahedron: Asymmetry*. 1994. **5**(6): 1091–1094. doi: 10.1016/0957-4166(94)80059-6.

[80] Soloshonok V.A., Hayashi T. Gold(I)-catalyzed asymmetric aldol reaction of methyl isocyanoacetate with fluorinated benzaldehydes. *Tetrahedron Lett*. 1994. **35**(17): 2713–2716. doi: 10.1016/S0040-4039(00)77013-4.

[81] Mohammadi A.A., Makarem S., Ahdenov R., Notash N.A. Green pseudo-multicomponent synthesis of some new spirocyclopropane derivatives via electro-catalyzed reaction. *Mol. Diversity*. 2020. **24**: 763–770. doi.org/10.1007/s11030-019-09979-8.

[82] Zhang X., Zhao L., Liang Y.Y. et al. Electrochemical Synthesis of PhSe/CF_3-containing Dibenzazepines via Radical Cascade Cyclization of Alkynes. *Chem. Commun*. 2025. doi.org/10.1039/D5CC02355F.

[83] Qian X., Qing-Xiao T., Jian-Ji Z. Recent Progress on the Synthesis of Benzazepine Derivatives via Radical Cascade Cyclization Reactions. *Chin. J. Org. Chem*. 2022. **42**(12): 3979. DOI: 10.6023/cjoc202209025.

[84] Gao X., Wang P., Wang Q. *et al*. Electrochemical oxidative annulation of amines and aldehydes or ketones to synthesize polysubstituted pyrroles. *Green Chem*. 2019. **21**(18): 4941–4945.

DOI: 10.1039/C9GC02118C
[85] Kong W.J., Shen Z., Finger L.H, Ackermann L. Electrochemical access to aza-polycyclic aromatic hydrocarbons: Rhoda-electrocatalyzed domino alkyne annulations. *Angew. Chem. Int. Ed*. 2020. **59**(14): 5551–5556. doi.org/10.1002/anie.201914775.
[86] Zhang Y., Xu S., Zhu Y. *et al*. One-pot synthesis of 4-thiocyanato-1H-pyrazoles through electrochemical multicomponent thiocyanation under metal-and oxidant-free conditions. *Eur. J. Org. Chem*. 2023. **26**(2): e202201278. doi.org/10.1002/ejoc.202201278.
[87] Elinnson M.N., Ryzkova Y.E., Vereschagin A.N. *et al*. Electrochemically induced assembling of isatins, kojic acid, and malonic acid derivatives into substituted spiro [indole-3, 4′-pyran]-2 (1 H)-one scaffold and predicting potential protein targets. *J. Heterocyc. Chem*. 2022. **56**(2): 277–299. doi.org/10.11002/jhet.4579.
[88] Elinson M.N., Ryzkova Y.E., Ryzkov F.V. *et al*. Electrochemically Induced Facile and Efficient Multicomponent Approach to Medicinally Relevant 4-[4-oxo-4H-pyran-2-yl] (aryl)-methylisoxazol-5 (2H)-one Scaffold. *ChemistrySelect*. 2020. **5**(20): 5981–5986. doi.org/10.1002/slct.2002001592.
[89] Soloshonok V.A., Avilov D.V., Kukhar V.P. Highly diastereoselective asymmetric aldol reactions of chiral Ni (II)-complex of glycine with alkyl trifluoromethyl ketones. *Tetrahedron*: *Asymmetry*. 1996. **7**(6): 1547–1550. doi.org/10.1016/0957-4166(96)00177-2.
[90] Soloshonok V.A., Avilov D.V., Kukhar V.P. Asymmetric aldol reactions of trifluoromethyl ketones with a chiral Ni (II) complex of glycine: stereocontrolling effect of the trifluoromethyl group. *Tetrahedron*. 1996. **52**(38): 12433–12442. doi.org/10.1016/0040-4020(96)00741-7.
[91] Ryzkova YE, Elinson MN, Vereshchagin AN, Karpenko KA, Ryzhkov FV, Ushakov IE, Egorov MP. Multicomponent electrocatalytic selective approach to unsymmetrical spiro [Furo [3, 2-c] Pyran-2, 5′-Pyrimidine] scaffold under a column chromatography-free protocol at room temperature. Chemistry. 2022 Jun 19; 4(2): 61–529. doi.org/10.3390/chemistry4020044.
[92] Kumar D., Sharma S., Kalra S. *et al.* Medicinal perspective of indole derivatives: recent developments and structure-activity relationship studies. *Curr. Drug Targets*. 2020. **21**(9): 864–891. doi.org/10.2174/1389450121666200310111 5327.
[93] Mo X., Rao D.P., Kaur K. *et al.* Indole derivatives: a versatile scaffold in modern drug discovery–an updated review on their multifaceted therapeutic applications (2020–2024). *Molecules*. 2024. **29**(19): 4770. doi.org/10.3390/molecules29194770.
[94] Kaushik N.K., Kaushik N., Attri P. *et al.* Biomedical importance of indoles. *Molecules.* 2013. **18**(6): 6620–6662. doi.org/10.3390/molecules18066620.
[95] Kumar S., Ritika. A brief review of the biological potential of indole derivatives. *Future J. Pharm. Sci.* 2020. 1–9. doi.org/10.1186/s43094-020-00141-y.
[96] Xie C, Mei H, Wu L, Soloshonok VA, Han J, Pan Y. LDA-promoted asymmetric synthesis of β-trifluoromethyl-β-amino indanone derivatives with virtually complete stereochemical outcome. *RSC Adv*. 2014. **4**(9): 4763–4768. DOI: 10.1039/C3RA45773G.
[97] Taber D.F., Tirunahari P.K. Indole synthesis: a review and proposed classification. *Tetrahedron.* 2011. **67**(38): 7195–7210. doi.org/10.1016/j.tet.2011.06.040.
[98] Gribble G.W. Recent developments in indole ring synthesis–Methodology and applications. *Contemp. Org. Synth.* 1994. **1**(3): 145–172. doi: 10.1039/CO9940100145.
[99] Wu L., Xie C., Mei H. *et al.* Asymmetric

Friedel–Crafts Reactions of *N-tert*-Butylsulfinyl-3,3,3-trifluoroacetaldimines: General Access to Enantiomerically Pure Indoles Containing a 1-Amino-2,2,2-trifluoroethyl Group. *J. Org. Chem.* 2014. **79**(16): 7677–7681. doi.org/10.1021/jo5012009.

[100] Zhu Y., Mao Y., Mei H. *et al.* Palladium-Catalyzed Asymmetric Allylic Alkylations of Colby Pro-Enolates with MBH Carbonates: Enantioselective Access to Quaternary C–F Oxindoles. *Chem.—Eur. J.* 2018. **24**(36): 8994–8998. doi.org/10.1002/chem.201801670.

[101] Li T., Zhou S., Wang J. *et al.* Asymmetric synthesis of α-(1-oxoisoindolin-3-yl)glycine: synthetic and mechanistic challenges. *Chem. Commun.* 2015 **51**(9): 1624–1626; doi: 10.1039/C4CC05659K.

[102] Xie C., Zhang L., Sha W. *et al.* Detrifluoroacetylative in situ generation of free 3-fluoroindolin-2-one-derived tertiary enolates: design, synthesis, and assessment of reactivity toward asymmetric Mannich reactions. *Org. Lett.* 2016. **18**(13): 3270–3273. doi.org/10.1021/acs.orglett.6b01516.

[103] Zhang L., Zhang W., Mei H. *et al.* Catalytic asymmetric aldol addition reactions of 3-fluoro-indolinone derived enolates. *Org. Biomolec. Chem*. 2017. **15**(2): 311–315. doi.org/10.1039/C6OB02454H.

[104] Singh V.K., Dubey R., Upadhyay A. *et al.* Electrochemical approach for synthesis of 3-substituted indole derivatives. *Tetrahedron Lett*. 2017. **58**(45): 4227–4231. doi.org/10.1016/j.tetlet.2017.09.003.

[105] Soloshonok V.A., Kacharov A.D., Hayashi T. Gold (I)-catalyzed asymmetric aldol reactions of isocyanoacetic acid derivatives with fluoroaryl aldehydes. *Tetrahedron.* 1996. **52**(1): 245–254. doi.org/10.1016/0040-4020(95)00893-D.

[106] Ono T., Kukhar V.P., Soloshonok V.A. Biomimetic reductive amination of fluoro aldehydes and ketones via [1, 3]-proton shift reaction. 1 scope and limitations. *J. Org. Chem*. 1996. **61**(19): 6563–6569. doi.org/10.1021/jo960503g.

[107] Matin M.M., Matin P., Rahman M.R. *et al.* Triazoles and their derivatives: Chemistry, synthesis, and therapeutic applications. *Front. Molec. Bioscien*. 2022. **9**: 864286. doi.org/10.3389/fmolb.2022.864286.

[108] Mei H., Xiong Y., Xie C. *et al.* Concise and scalable asymmetric synthesis of 5-(1-amino-2,2,2-trifluoroethyl) thiazolo [3,2-b][1,2,4] triazoles. *Org. Biomolec. Chem.* 2014. **12**(13): 2108–2113. DOI: 10.1039/C3OB42348D.

[109] Zhao Z., He Y., Li M. *et al.* An electrochemical multicomponent [3+1+1] annulations to synthesize polysubstituted 1,2,4-triazoles. *Tetrahedron*. 2021. **87**: 132111. doi.org/10.1016/j.tet.2021.132111.

[110] Kabi A.K., Gujjarappa R., Singh V., Malakar C.C. Biological impacts of imidazoline derivatives. *Chem. Papers*. 2024. **78**(10): 5743–5752. doi.org/10.1007/s11696-024-03496-1.

[111] Mei H., Xie C., Wu L. *et al.* Asymmetric Mannich reactions of imidazo [2,1-b] thiazole-derived nucleophiles with (*SS*)-*N-tert*-butanesulfinyl (3,3,3)-trifluoroacetaldimine. *Org. Biomolec. Chem*. 2013. **11**(46): 8018–8021. DOI: 10.1039/c3ob41785a.

[112] Saney L., Panduwawala T., Li X. *et al.* Synthesis of fused tetramate-oxazolidine and-imidazolidine derivatives and their antibacterial activity. *Org. Biomolec. Chem*. 2023. **21**(23): 4801–4809. doi.org/10.1039/D3OB00594A.

[113] Soloshonok V.A., Ueki H., Jiang C. *et al.* A Convenient, Room-Temperature–Organic Base Protocol for Preparing Chiral 3-(Enoyl)-1,3-oxazolidin-2-ones. *Helv. Chim. Acta*. 2002. **85**(11): 3616–3623. doi.org/10.1002/1522-2675(200211)85:11<3616::AID-HLCA3616>3.0.CO;2-O.

[114] Claraz A., Djian A., Masson G. Electrochemical tandem trifluoromethylation of allylamines/formal (3+2)-cycloaddition for the rapid access to CF_3-containing imidazolines and oxazolidines. *Org. Chem. Front*. 2021. **8**(2): 288–296.
DOI: 10.1039/D0QO01307B.

[115] Lalezari I., Shafiee A., Yalpani M. Selenium-Nitrogen Heterocycles. *Adv. Heterocyc. Chem*. 1979. **24**: 109–150.
doi.org/10.1016/S0065-2725(08)60509-7.

[116] Soloshonok V.A., Nelson D.J. Alkene selenenylation: A comprehensive analysis of relative reactivities, stereochemistry and asymmetric induction, and their comparisons with sulfenylation. *Beilstein J. Org. Chem*. 2011. 7(1): 744–758.
doi.org/10.3762/bjoc.7.85.

[117] Wu Y., Chen J.Y., Ning J. *et al.* Electrochemical multicomponent synthesis of 4-selanylpyrazoles under catalyst-and chemical-oxidant-free conditions. *Green Chem*. 2021. **23**(11): 3950–3954.
DOI: 10.1039/d1gc00562f.

[118] Siyu M., Hongxia L., Zhilin W. *et al*. Electrocatalytic three-component synthesis of 4-bromopyrazoles from acetylacetone, hydrazine and diethyl bromomalonate. *Chin. J. Org. Chem*. 2022. **42**(12): 4292.
DOI: 10.6023/cjoc202211002.

[119] Ohkura H., Berbasov D.O., Soloshonok V.A. Chemo-and regioselectivity in the reactions between highly electrophilic fluorine containing dicarbonyl compounds and amines. Improved synthesis of the corresponding imines/enamines. *Tetrahedron.* 2003. **59**(10): 1647–1656.
doi.org/10.1016/S0040-4020(03)00138-8.

[120] Bravo P., Guidetti M., Viani F. *et al.* Chiral sulfoxide controlled asymmetric additions to C N double bond. An efficient approach to stereochemically defined α-fluoroalkyl amino compounds. *Tetrahedron.* 1998. **54**(42): 12789–12806.
doi: 10.1016/S0040-4020(98)00779-0.

[121] Shibata N., Nishimine T., Shibata N. *et al.* Organic base-catalyzed stereodivergent synthesis of (*R*)- and (*S*)-3-amino-4,4,4-trifluorobutanoic acids. *Chem. Commun.* 2012. **48**: 4124–4126.
doi:10.1039/C2CC30627A.

[122] Soloshonok V.A., Kirilenko A.G., Kukhar V.P., Resnati G. Transamination of fluorinated β-keto carboxylic esters. A biomimetic approach to β-polyfluoroalkyl-β-amino acids. *Tetrahedron Lett.* 1993. **34**(22): 3621–3624.
doi.org/10.1016/S0040-4039(00)73652-5.

[123] Makarem S., Fakhari A.R., Mohammadi A.A. Electro-organic synthesis of nanosized particles of 3-hydroxy-3-(1H-indol-3-yl) indolin-2-one derivatives. *Monat. Chem*. 2012. **143**: 1157–1160.
doi.org/10.1007/s00706-011-0693-1.

[124] He W.B., Zhao S.J., Chen J.Y. *et al*. External electrolyte-free electrochemical one-pot cascade synthesis of 4-thiocyanato-1H-pyrazoles. *Chin. Chem. Lett*. 2023. **34**(2): 107640.
doi.org/10.1016/j.cclet.2022.06.063.

[125] Torchinsky Y.M. Transamination: its discovery, biological and chemical aspects (1937–1987). *Trends Biochem. Scien*. 1987. **12**: 115–117.
doi.org/10.1016/0968-0004(87)90052-1.

[126] Wzorek A., Han J., Lyutenko N.V. *et al*. Discovery of biomimetic transamination as a general synthetic method for preparation of fluorine-containing amines and amino acids. *Ukr. Bioorg. Acta*. 2023. **18**(2): 3–15.
DOI: doi.org/10.15407/bioorganica2023.02.003.

[127] Fuchs M., Farnberger J.E., Kroutil W. The industrial age of biocatalytic transamination. *Eur. J. Org. Chem*. 2015. (32): 6965–6982.
doi.org/10.1002/ejoc.201500852.

[128] Xiao X., Zhao B. Vitamin B_6-based biomimetic asymmetric catalysis. *Acc. Chem. Res*. 2023. **56**(9): 1097–1117.
doi.org/10.1021/acs.accounts.3c00053.

[129] Chen J., Liu Y.E., Gong X. *et al*. Biomimetic chiral pyridoxal and pyridoxamine catalysts. *Chin. J. Chem*. 2019. **37**(2): 103–112 doi.org/10.1002/cjoc.201800478.

[130] Yasumoto M., Ueki H., Soloshonok V.A. Thermal 1,3-proton shift reaction and its application for operationally convenient and improved synthesis of α-(trifluoromethyl) benzylamine. *J. Fluor. Chem*. 2007. **128**(7): 736–739. doi.org/10.1016/j.jfluchem.2007.02.008.

[131] Soloshonok V.A., Kirilenko A.G., Kukhar V.P., Resnati G. A practical route to fluoroalkyl-and fluoroarylamines by base-catalyzed [1, 3]-proton shift reaction. *Tetrahedron Lett*. 1994. **35**(19): 3119–3122. doi.org/10.1016/S0040-4039(00)76845-6.

[132] Soloshonok V.A., Yasumoto M. Catalytic asymmetric synthesis of α-(trifluoromethyl) benzylamine via cinchonidine derived base-catalyzed biomimetic 1,3-proton shift reaction. *J. Fluor. Chem*. 2007. **128**(3): 170–173. doi.org/10.1016/j.jfluchem.2006.11.011.

[133] Soloshonok V.A., Ohkura H., Yasumoto M. Operationally convenient asymmetric synthesis of (*S*)- and (*R*)-3-amino-4,4,4-trifluorobutanoic acid: Part II. Enantioselective biomimetic transamination of 4,4,4-trifluoro-3-oxo-*N*-[(*R*)-1-phenylethyl)butanamide. *J. Fluor. Chem.* 2006. **127**(7): 930–935. doi: 10.1016/j.jfluchem.2006.04.004.

[134] Soloshonok V.A., Ohkura H., Uneyama K. Biomimetic reductive amination of perfluoroalkylcarboxylic acids to α,α-dihydroperfluoroalkylamines. *Tetrahedron Lett*. 2002. **43**(31): 5449–5452. doi.org/10.1016/S0040-4039(02)01104-8.

[135] Qian P., Zhou Z., Hu K. *et al*. Electrocatalytic three-component reaction: synthesis of cyanide-functionalization imidazo-fused *N*-heterocycles. *Org. Lett*. 2019. **21**(16): 6403–6407. doi.org/10.1021/acs.orglett.9b02317.

[136] Soloshonok V.A., Kukhar V.P. Biomimetic transamination of α-keto perfluorocarboxylic esters. An efficient preparative synthesis of β,β,β-trifluoroalanine. *Tetrahedron*. 1997. **53**(25): 8307–8314. doi.org/10.1016/S0040-4020(97)00517-6.

[137] Soloshonok V.A., Kirilenko A.G., Fokina N.A. *et al*. Chemo-enzymatic approach to the synthesis of each of the four isomers of α-alkyl-β-fluoroalkyl-substituted β-amino acids. *Tetrahedron: Asymmetry*. 1994. **5**(7): 1225–1228. doi.org/10.1016/0957-4166(94)80163-0.

[138] Soloshonok V.A, Kukhar V.P. Biomimetic base-catalyzed [1, 3]-proton shift reaction. A practical synthesis of β-fluoroalkyl-β-amino acids. *Tetrahedron*. 1996. **52**(20): 6953–6964. doi.org/10.1016/0040-4020(96)00300-6.

[139] Yang Z., Zhang J., Hu L. *et al*. Electrochemical HI-mediated Intermolecular C–N Bond Formation to Synthesize Imidazoles from Aryl Ketones and Benzylamines. *J. Org. Chem.* 2020. **85**(9): 5952–5958. doi.org/10.1021/acs.joc.0c00316.

[140] Soloshonok V.A., Kirilenko A.G., Galushko S.V., Kukhar V.P. Catalytic asymmetric synthesis of β-fluoroalkyl-β-amino acids via biomimetic [1,3]-proton shift reaction. *Tetrahedron Lett*. 1994. **35**(28): 5063–5064. doi.org/10.1016/S0040-4039(00)73320-X.

[141] Soloshonok V.A., Ono T., Soloshonok I.V. Enantioselective biomimetic transamination of β-keto carboxylic acid derivatives. an efficient asymmetric synthesis of β-(fluoroalkyl) β-amino acids. *J. Org. Chem*. 1997. **62**(22): 7538–7539. doi.org/10.1021/jo9710238.

[142] Soloshonok V.A., Soloshonok I.V., Kukhar V.P., Svedas V.K. Biomimetic transamination of α-alkyl β-keto carboxylic esters. Chemo-enzymatic approach to the stereochemically defined α-alkyl β-fluoroalkyl β-amino acids. *J. Org. Chem*. 1998. **63**(6): 1878–1884. doi.org/10.1021/jo971777m.

[143] Zhou K., Xia S., Liu Y., Chen Z. An electrochemical tandem Michael addition, azidation and intramolecular cyclization strategy for the synthesis of imidazole derivatives. *Org. Biomolec. Chem*. 2022. **20**(39): 7840–7844. doi.org/10.1039/D2OB01501C.

[144] Asghariganjeh M.R., Mohammadi A.A., Tahanpesar E. *et al*. Electro-organic synthesis of tetrahydroimidazo [1,2-a]pyridin-5(1H)-one via a multicomponent reaction. *Molec. Diversity.* 2021. **25**: 509–516. DOI: 10.1007/s11030-019-10029-6.

[145] You S., Ruan M., Lu C. *et al*. Paired electrolysis enabled annulation for the quinolyl-modification of bioactive molecules. *Chem. Scien*. 2022. **13**(8): 2310–2316. doi.org/10.1039/D1SC06757E.

[146] Jörres M., Aceña J.L., Soloshonok V.A., Bolm C. Asymmetric Carbon-Carbon Bond Formations under Solvent-Less Conditions in Ball Mills. *ChemCatChem.* 2015. **7**: 1265–1269. doi: 10.1002/cctc.201500102.

[147] Zou Y., Han J., Saghyan A.S. *et al.* Asymmetric Synthesis of Tailor-Made Amino Acids Using Chiral Ni(II) Complexes of Schiff Bases. An Update of the Recent Literature. *Molecules.* 2020. **25**(12): 2739. doi.org/10.3390/molecules25122739.

[148] Xie C., Wu L., Mei H. *et al.* Generalized access to fluorinated β-keto amino compounds through asymmetric additions of α,α-difluoroenolates to CF_3-sulfinylimine. *Org. Biomol. Chem.* 2014. **12**(39): 7836–7843. doi: 10.1039/C4OB01575D.

[149] Malviya B.K., Jassal A.K., Karnatak M. *et al*. Electro-Oxidative sp3 C–H Bond Functionalization and Annulation Cascade: Synthesis of Novel Heterocyclic Substituted Indolizines. *J. Org. Chem*. 2022. **87**(5): 2898–2911. doi.org/10.1021/acs.joc.1c02773.

[150] Yang N., Yuan G. A multicomponent electrosynthesis of 1, 5-disubstituted and 1-aryl 1, 2, 4-triazoles. *J. Org. Chem*. 2018. **83**(19): 11963–11969. doi.org/10.1021/acs.joc.8b01808.

Стаття надійшла 06.08.2025.

УДК 547.821.1:547.53.04 doi: 10.33609/2708-129X.91.11.2025.63-70

СИНТЕЗ 6-АЛКІЛЗАМІЩЕНИХ ПОХІДНИХ ПЕРХЛОРАТУ 7,8-ДИГІДРОКСИ-4-МЕТИЛ-2-ФЕНІЛБЕНЗО[b]ПІРИЛІЮ

Д. О. Барбалат, К. Д. Сазонов, К. В. Снігур, О. М. Гузенко, О. М. Жуковецька, Д. В. Снігур

Одеський національний університет імені І. І. Мечникова,
вул. Всеволода Змієнка, 2, Одеса 65082, Україна
e-mail: snigur@onu.edu.ua

Цю роботу присвячено розробленню способу одержання нових 6-заміщених похідних перхлорату 7,8-дигідрокси-4-метил-2-фенілбензо[b]пірилію, які можна використовувати як комплексоутворюючі реагенти для екстракційно-спектрофотометричного визначення іонів полівалентних металів, а також для зменшення тривалості та трудомісткості синтезу. Запропоновано підхід, який полягає в тому, що конденсацію еквімолярних кількостей 4-алкілпохідних пірогалолу та бензоїлацетону проводять при кип'ятінні протягом 30–60 хв за присутності перхлоратної кислоти, а утворені кристалічні продукти придатні для використання у спектрофотометричному аналізі та не потребують додаткового складного очищення, що призводить до зменшення трудомісткості та тривалості синтезу в 2–3 рази. Одержано сім нових 6-заміщених похідних перхлорату 7,8-дигідрокси-4-метил-2-фенілбензо[b]пірилію, які ідентифіковано методами ІЧ-, ЯМР- та мас-спектрометрії, а їхню чистоту та індивідуальність доведено методом високоефективної рідинної хроматографії.

Ключові слова: похідні 7,8-дигідроксибензо[b]пірилію, органічний синтез, органічні аналітичні реагенти, гетероциклічні ароматичні катіони, бензопірилієві барвники.

ВСТУП. Розроблення методик визначення цільових аналітів, зокрема іонів металів, у різних об'єктах навколишнього середовища, продуктах харчування та інших промислових зразках є одним із найважливіших завдань сучасної аналітичної хімії. Однак створення селективних, чутливих та експресних методів їхнього детектування прямими та комбінованими аналітичними методами залишається актуальним запитом. Вирішенню його сприяє розроблення нових органічних реагентів із покращеними хіміко-аналітичними характеристиками. Серед широкого кола сполук особливу увагу привертають похідні бензо[b]пірилію, зокрема ті, що містять дві віцинальні гідроксильні групи в бензольному фрагменті, оскільки вони здатні утворювати міцні та інтенсивно забарвлені комплекси з іонами полівалентних металів [1, 2], що

робить їх перспективними реагентами для розроблення селективних та чутливих прямих та комбінованих спектрофотометричних методик аналізу [3].

Широкому застосуванню зазначеного класу реагентів перешкоджають недоліки існуючих методів їхнього синтезу. Так, метод, описаний у праці [4], передбачає конденсацію ди- та тригідроксибензальдегідів із похідними метилстирилкетону в кислому середовищі протягом 8–12 годин. Незважаючи на простоту умов, недоліками способу є тривалість синтезу та необхідність очищення перекристалізацією, що призводить до втрат продукту. Подібні обмеження властиві й іншим підходам. Наприклад, у роботі [5] продемонстровано синтез аміно- та гідроксизаміщених похідних, однак і тут реакція триває від 8 до 48 годин, а виділення цільових сполук супроводжується низькими виходами та використанням препаративної хроматографії. Більш ранні методи, такі як спосіб, запропонований Н. Л. Оленович зі співавторами, також характеризують помірними виходами (30–50%) та аналогічною процедурою очищення [6]. Відомим є підхід, який запропоновано нами раніше [7]. Для синтезу похідних 6,7-дигідроксибензо[b]пірилію застосовано підвищену температуру (60–80°C), що дозволило скоротити час реакції.

Отже, завдання розроблення ефективного, швидкого та зручного методу синтезу похідних 7,8-дигідроксибензо[b]пірилію з високими виходами та аналітичною чистотою є своєчасним та актуальним. Цю роботу присвячено вдосконаленню способу отримання низки 6-алкілзаміщених перхлоратів 7,8-дигідрокси-4-метил-2-фенілбензо[b]пірилію.

ЕКСПЕРИМЕНТ ТА ОБГОВОРЕННЯ РЕЗУЛЬТАТІВ

Усі використані реактиви мали кваліфікації «для синтезу» з чистотою понад 98 %. Контроль реакцій проводили за допомогою тонкошарової хроматографії на платівках Silufol та Silufol UV-254. ЯМР-спектри знімали на приладі Bruker AVANCE DRX 500 МГц, спектри ЯМР 1Н реєстрували для 2% розчинів у ДМСО-d6 із ТМС як внутрішнього стандарту. Чистоту одержаних сполук та мас-спектри реєстрували за допомогою комбінованої системи ВЕРХ-МС – хроматограф Infinity 1260, Agilent та масспектрометр 6530 Accurate Mass Q-TOF, Agilent з іонізацією подвійним електроспреєм (DESI). ІЧ-спектри в діапазоні 4000–400 $см^{-1}$ реєстрували на спектрометрі FT-IR-8400S Shimadzu з приставкою порушеного повного внутрішнього відбиття (ППВВ) Specac Quartz.

Загальна методика синтезу 4-алкілзаміщенних пірогалолів

4-ацилпірогалоли. Розчин пірогалолу (100 ммоль) та відповідної кислоти (110 ммоль) у $BF_3 \cdot OEt_2$ (37 мл) нагрівали за 90–100 °С упродовж 4 годин, потім охолоджували, виливали у 10 % водний розчин ацетату натрію та перемішували упродовж 4 годин [8]. Цільові сполуки екстрагували етилацетатом. Органічний шар промивали насиченим розчином NaCl та сушили над безводним Na_2SO_4. Після видалення розчинника отримано цільові сполуки у вигляді твердих речовин, що мають забарвлення від світло-жовтого до жовтого. Виходи становили 30–40%.

4-алкілпірогалоли (1a-1g). $NaBH_4$ (80 ммоль) додали до розчину відповідного 4-ацилпірогалолу (10 ммоль) у 0,4 М

водному розчині NaOH (10 мл), і суміш нагрівали зі зворотнім холодильником упродовж 3 годин [9]. Після охолодження додали 5 М хлористоводневої кислоти для розкладання надлишку $NaBH_4$ на крижаній бані, допоки не припиняється виділення газу при додаванні нової порції HCl. Суміш екстрагували етилацетатом. Отримані продукти – від білих кристалічних до жовтих рідин, із виходами 70–80%.

Загальна методика синтезу 6-алкілзамі-щених похідних перхлорату 7,8-дигідрокси-4-метил-2-фенілбензо[b]пірилію

5,0 ммоль відповідного 4-алкілпірогалолу та 5,0 ммоль бензоїлацетону розчиняли в 7 мл оцтової кислоти за температури 60–80 °С при перемішуванні, додавали 1 мл 50% перхлоратної кислоти. Кип'ятили суміш зі зворотнім холодильником упродовж 30–60 хв. При охолодженні утворювався червоний кристалічний осад. Продукт відфільтровували, промивали оцтовою кислотою і диізопропіловим етером, сушили на повітрі.

6-Етил-7,8-дигідрокси-4-метил-2-фенілбензо[b]пірилію перхлорат (2a). Отримано оранжево-червоні кристали з виходом 50%, чистотою 99,5% (ВЕРХ-УФ). MS (m/z): $[M]^+$ розраховано для $C_{18}H_{17}O_3^+$ – 281,33; знайдено – 281,25. ІЧ (ППВВ), $см^{-1}$: 3219 (ν OH), 2980 (ν CH), 2971 (ν CH), 1622 (ν CO, HetAr), 1595 (ν CC, HetAr), 1545(ν ClO, ClO_4^-), 1438, 1431, 1391, 1312, 1283, 1254, 1194, 1163, 1117, 1082, 1046, 1028, 995 (CC, Ph), 955, 930, 876, 841, 779, 756, 698, 679, 621. ^{1}H ЯМР (400 MHz, ДМСО-d_6): δ 8,50 (с, 2H, Ar), 7,90–7,50 (м, 5H, Ph), 2,99 (с, 3H, CH_3-Ar), 2,74 (с, 2H, CH_2-Ar), 1,22 (с, 3H, CH_3).

6-Пропіл-7,8-дигідрокси-4-метил-2-фенілбензо[b]пірилію перхлорат (2b)

Отримано оранжево-червоні кристали з виходом 52%, чистотою 99,0% (ВЕРХ-УФ). MS (m/z): $[M]^+$ розраховано для $C_{19}H_{19}O_3^+$ – 295,35; знайдено – 295,33. ІЧ (ППВВ), $см^{-1}$: 3217 (ν OH), 2985 (ν CH), 2969 (ν CH), 1625 (ν CO, HetAr), 1592 (ν CC, HetAr), 1551 (ν ClO, ClO_4^-), 1431, 1391, 1312, 1283, 1249, 1194, 1111, 1076, 1040, 1034, 995 (CC, Ph), 954, 876, 841, 782, 754, 688, 673, 621. ^{1}H ЯМР (400 MHz, ДМСО-d_6): 10,84 (ш. с., 2H, Ar-OH), δ 8,54 (с, 2H, Ar), 7,90–7,50 (м, 5H, Ph), 2,98 (с, 3H, CH_3-Ar), 2,72 (с, 2H, CH_2-Ar), 1,40 (с, 2H, CH_2), 1,01 (с, 3H, CH_3).

6-Бутил-7,8-дигідрокси-4-метил-2-фенілбензо[b]пірилію перхлорат (2c). Отримано червоні кристали з виходом 42%, чистотою 99,2% (ВЕ РХ-УФ). MS (m/z): $[M]^+$ розраховано для $C_{20}H_{21}O_3^+$ – 309,38; знайдено – 309,27. ІЧ (ППВВ), $см^{-1}$: 3246 (ν OH), 2962 (ν CH), 2928 (ν CH), 1622 (ν CO, HetAr), 1597 (ν CC, HetAr), 1533 (ν ClO, ClO_4^-), 1476, 1427, 1398, 1317, 1283, 1248, 1188, 1163, 1111, 1018, 993 (CC, Ph), 957, 914, 878, 858, 785, 764, 746, 683, 648, 621. ^{1}H ЯМР (400 MHz, ДМСО-d_6) δ: 10,79 (ш.с., 2H, Ar-OH), 8,53 (с, 2H, Ar), 7,20–8,10 (м, 5H, Ph), 2,99 (с, 3H, CH_3-Ar), 2,71 (с, 2H, CH_2-Ar), 1,58 (с, 2H, CH_2), 1,34 (с, 2H, CH_2), 0,91 (с, 3H, CH_3).

6-Пентил-7,8-дигідрокси-4-метил-2-фенілбензо[b]пірилію перхлорат (2d)

Отримано червоні кристали з виходом 38%, чистотою 98,4% (ВЕРХ-УФ). MS (m/z): $[M]^+$ розраховано для $C_{21}H_{23}O_3^+$ – 323,41; знайдено – 323,38. ІЧ (ППВВ), $см^{-1}$: 3205 (ν OH), 2952 (ν CH), 2924 (ν CH), 1626 (ν CO, HetAr), 1593 (ν CC, HetAr), 1542 (ν ClO, ClO_4^-), 1474, 1432, 1399, 1280, 1258, 1188, 1119, 1019, 998 (CC, Ph), 975, 921, 878, 861, 784, 764, 742, 677, 621. ^{1}H ЯМР (400 MHz, ДМСО-d_6) δ: 10,78 (ш.с, 2H, OH), 8,52 (с, 2H, Ar), 7,80–7,70 (м, 5H, Ph), 3,00 (с, 3H, CH_3-Ar), 2,68 (с, 2H, CH_2-Ar), 1,59 (с, 2H, CH_2), 1,28 (с, 4H, CH_2), 0,86 (с, 3H, CH_3).

6-Гексил-7,8-дигідрокси-4-метил-2-фенілбензо[b]пірилію перхлорат (2e)

Отримано червоні кристали з виходом 38%, чистотою 99,0% (ВЕРХ-УФ). MS (m/z): $[M]^+$ розраховано для $C_{22}H_{25}O_3^+$ – 337,43; знайдено – 337,40. ІЧ (ППВВ), $см^{-1}$: 3117 (ν OH), 2955 (ν CH), 2924 (ν CH), 2857 (ν CH), 1620 (ν CO, HetAr), 1595 (ν CC, HetAr), 1549 (ν ClO, ClO_4^-), 1476, 1439, 1398, 1375, 1346, 1277, 1256, 1193, 1165, 1101, 1020, 999 (CC, Ph), 978, 924, 876, 866, 779, 760, 679, 621. ^{1}H ЯМР (400 MHz, ДМСО-d_6) δ: 10,75 (с, 2H, OH), 8,53 (с, 2H, Ar), 7,80–7,70 (м, 5H, Ph), 2,99 (с, 3H, CH_3-Ar), 2,70 (с, 2H, CH_2-Ar), 1,58 (с, 2H, CH_2), 1,27 (с, 6H, CH_2), 0,84 (с, 3H, CH_3).

6-Гептил-7,8-дигідрокси-4-метил-2-фенілбензо[b]пірилію перхлорат (2f)

Отримано червоні кристали з виходом 35%, чистотою 98,9% (ВЕРХ-УФ). MS (m/z): $[M]^+$ розраховано для $C_{22}H_{27}O_3^+$ – 351,46; знайдено – 351,47. ІЧ (ППВВ), $см^{-1}$: 3124 (ν OH), 2961 (ν CH), 2928 (ν CH), 2850 (ν CH), 1617 (ν CO, HetAr), 1596 (ν CC, HetAr), 1544 (ν ClO, ClO_4^-), 1476, 1428, 1390, 1373, 1345, 1283, 1250, 1191, 1167, 1143, 1120, 1051, 1025, 1003 (CC, Ph), 973, 966, 922, 870, 781, 678, 622. ^{1}H ЯМР (400 MHz, ДМСО-d_6) δ: 10,72 (с, 2H, OH), 8,52 (с, 2H, Ar), 7,80–7,70 (м, 5H, Ph), 2,99 (с, 3H, CH_3-Ar), 2,70 (с, 2H, CH_2-Ar), 1,58 (с, 2H, CH_2), 1,23 (с, 8H, CH_2), 0,81 (с, 3H, CH_3).

6-Октил-7,8-дигідрокси-4-метил-2-фенілбензо[b]пірилію перхлорат (2g). Отримано темно-червоні кристали з виходом 28%, чистотою 98,0% (ВЕРХ-УФ). MS (m/z): $[M]^+$ розраховано для $C_{24}H_{29}O_3^+$ – 365,48; знайдено – 365,45. ІЧ (ППВВ), $см^{-1}$: 3119 (ν OH), 2955 (ν CH), 2924 (ν CH), 2855 (ν CH), 1618 (ν CO, HetAr), 1595 (ν CC, HetAr), 1545 (ν ClO, ClO_4^-), 1472, 1419, 1397, 1375, 1346, 1279, 1248, 1192, 1167, 1125, 1088, 1051, 1030, 1020, 997 (CC, Ph), 968, 968, 932, 876, 779, 681, 621. ^{1}H ЯМР (400 MHz, ДМСО-d_6) δ: 10,69 (с, 2H, OH), 8,53 (с, 2H, Ar), 7,80–7,70 (м, 5H, Ph), 2,99 (с, 3H, CH_3-Ar), 2,69 (с, 2H, CH_2-Ar), 1,58 (с, 2H, CH_2), 1,21 (с, 10H, CH_2), 0,82 (с, 3H, CH_3).

Ключовим етапом у синтезі цільових похідних бензо[b]пірилію було отримання проміжних 4-алкілпірогалолів (**1a**-**1g**). Синтез проводили у дві стадії (схема 1). На першій стадії пірогалол зазнавав ацилювання за Фріделем – Крафтсом відповідною карбоновою кислотою (R'-COOH) з утворенням кетону. На другій стадії карбонільну групу відновлювали до метиленової (-CH_2-) за допомогою боргідриду натрію в лужному середовищі з подальшим обробленням кислотою. Дані щодо виходів та характеристик отриманих сполук наведено в Таблиці 1.

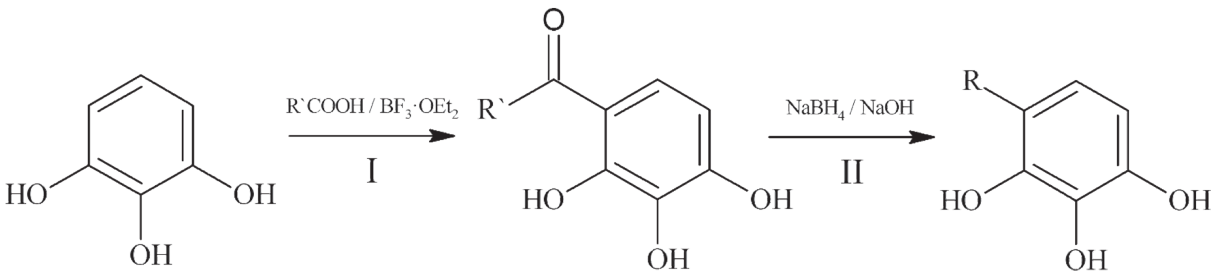

Схема 1. Синтез 4-алкілзаміщенних пірогалолів (1a–1g).
Scheme 1. Synthesis of 4-alkyl-substituted pyrogallols (1a–1g).

Табл. 1

Синтезовані 4-алкілпірогалоли

Table 1.

Synthesized 4-alkylpyrogallols.

№ сполуки	Алкільний замісник (R)	Вихід (%)
1a	$-C_2H_5$	80
1b	$-C_3H_7$	74
1c	$-C_4H_9$	70
1d	$-C_5H_{11}$	73
1e	$-C_6H_{13}$	76
1f	$-C_7H_{15}$	72
1g	$-C_8H_{17}$	76

Наступним етапом було перетворення одержаних алкілпірогалолів у цільові солі бензо[b]пірилію, які містять активні центри (функціонально-аналітичні групи) для подальшого комплексоутворення. Реакцією відповідних 4-алкілпірогалолів (таблиця 1) із бензоїлацетоном отримували похідні перхлорату 7,8-дигідрокси-4-метил-2-фенілбензо[b]пірилію **2a**–**2g** за схемою 2. Синтез проводили в середовищі оцтової кислоти з використанням перхлоратної кислоти як каталізатора та джерела протийонів, що призводило до утворення цільових сполук у вигляді стійких кристалічних осадів. Чистоту продуктів контролювала ТШХ, а їхню ідентифікацію здійснювали методами хроматомас-спектрометрії та ^{1}H ЯМР-спектроскопії. Усі синтезовані сполуки є голчастими кристалами від оранжево-червоного до темно-червоного кольору. Виходи отриманих сполук становили 25–65% та характеризувалися високою чистотою за даними ВЕРХ-УФ.

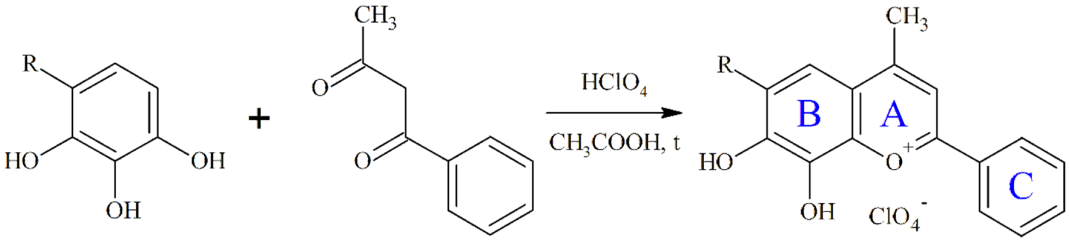

Схема 2. Синтез 6-алкілзаміщенних похідних перхлорату 7,8-дигідрокси-4-метил-2-фенілбензо[b]пірилію (2a–2g)

Scheme 2. Synthesis of 6-alkyl-substituted derivatives of 7,8-dihydroxy-4-methyl-2-phenylbenzo[b]pyrylium perchlorate (2a–2g).

У спектрах ЯМР 1H (розчинник ДМСО-d6) сполук **2c**–**2g** присутній широкий сигнал при 10,7 м. д., який належить гідроксильним групам, а у сполук **2a**–**2b** він відсутній внаслідок дисоціації та сольватації розчинником. Сигнали в області 8,7–7,5 м. д. належать атомам гідрогену ароматичних циклів. Синглет при 3,0 м. д. (3H) належить атомам гідрогену метильної групи, що з'єднана з циклом A. Сигнал при 2,7 м. д. (2H) відносять до метиленової групи алкільного радикалу (R), яка безпосередньо сполучена з кільцем B; сигнали в області 1,6–1,2 м. д. відносять до інших метиленових груп; сигнал при 1,22–0,84 м. д. метильної групи цього ж алкільного радикалу.

ВИСНОВКИ. Запропонований спосіб дозволяє одержувати 6-алкіл заміщені похідні 7,8-дигідрокси-4-метил-2-фенілбензо[b]пірилію перхлорати, які є перспективними комплексоутворюючими реагентами, використовуючи доступні вихідні реактиви. Використання перхлоратної кислоти дозволяє отримувати кристалічні та чисті продукти, які придатні для використання у спектрофотометричному аналізі, які не потребують додаткового складного очищення багатократним промиванням осадів та перекристалізацією, що призводить до зменшення трудомісткості та тривалості синтезу в 2–3 рази.

Роботу виконано в межах науково-дослідної теми «Розроблення та удосконалення комбінованих методів контролю якості фармацевтичних препаратів, продуктів харчування та об'єктів навколишнього середовища», державний реєстраційний номер: 0122U002302.

SYNTHESIS OF 6-ALKYL-SUBSTITUTED DERIVATIVES OF 7,8-DIHYDROXY-4-METHYL-2-PHENYLBENZO[b]PYRILIUM PERCHLORATE.

D.O. Barbalat, K.D. Sazonov, K.V. Snihur, O.M. Guzenko, O.M. Zhukovetska, D.V. Snigur

Odesa I.I. Mechnikov National University, Vsevoloda Zmiyenka str., Odesa 65082, Ukraine e-mail: snigur@onu.edu.ua

The development of new reagents based on benzopyrylium derivatives with enhanced chemical and analytical properties is of considerable interest, as their preparative synthesis is relatively straightforward and typically involves the condensation of triatomic phenols with β-dicarbonyl compounds. Benzopyrylium derivatives are highly reactive species capable of undergoing redox processes, forming complexes with multivalent metal ions, and participating in acid–base transformations in solution. It is particularly noteworthy that hydroxy-substituted benzopyrylium derivatives can convert into anhydro bases with a quinoid structure upon complex formation. This transformation results in a pronounced bathochromic shift of the absorption band and significantly enhances the contrast and detectability of analytical reactions. This work is devoted to the development of a method for obtaining new 6-substituted derivatives of 7,8-dihydroxy-4-methyl-2-phenylbenzo[b] pyrylium perchlorate, which can be used as complexing reagents for the extraction-spectrophotometric determination of polyvalent metal ions, as well as to reduce the duration and complexity of the synthesis. An approach is proposed, which consists in the condensation of equimolar amounts of 4-alkyl derivatives of pyrogallol and benzoylacetone at boiling for 30–60 min in the presence of perchloric acid, and the formed crystalline products are suitable for use in spectrophotometric analysis and do not require additional complex purification, which leads to a reduction in the complexity and duration of the synthesis by 2–3 times. Seven new 6-substituted derivatives of 7,8-dihydroxy-4-methyl-2-phenylbenzo[b] pyrylium perchlorate were obtained, which

were identified by IR, NMR, and mass spectrometry, and their purity and identity were proven by high-performance liquid chromatography.

Keywords: 7,8-dihydroxybenzo[b]pyrylium derivatives, organic synthesis, organic analytical reagents, heterocyclic aromatic cations, benzopyrylium dyes.

ЛІТЕРАТУРА

1. Чеботарьов О. М., Топоров С. В., Снігур Д. В., Барбалат Д. О. Похідні 6,7- та 7,8-дигідроксибензопірилію: синтез, властивості та аналітичне застосування (огляд). *Вісник Одеського національного університету. Хімія*. 2021. **26**(2). С. 73–88. https://doi.org/10.18524/2304-0947.2021.2(78).233829
2. Cruz L., Basílio N., Mateus N., De Freitas V., Pina F. Natural and Synthetic Flavylium-Based Dyes: the chemistry behind the color. *Chemical Reviews*. 2021. **122**(1). P. 1416–1481. https://doi.org/10.1021/acs.chemrev.1c00399
3. Walencik P.K., Choińska R., Gołębiewska E., Kalinowska M. Metal-Flavonoid Interactions – From simple complexes to advanced systems. *Molecules*. 2024. **29**(11). 2573 . https://doi.org/10.3390/molecules29112573
4. Calogero G., Citro I., Sebastianella G.C., Di Marco G., Diniz A.M., Parola A.J., Pina F. A Photoelectrochemical Study of Bioinspired 2-Styryl-1-Benzopyrylium Cations on TiO2 Nanoparticle Layer for Application in Dye-Sensitized Solar Cells. *Materials*. 2019. **12** (24). 4060 pp. https://doi.org/10.3390/ma12244060
5. Araújo P., Pereira A. R., de Freitas V., Mateus N., Fernandes I., Oliveira J. Synthesis, structural characterization and chromatic features of new 2-phenyl-1-benzopyrylium and 2-phenyl-styryl-1-benzopyrylium amino-based blue dyes. *Tetrahedron Letters*. 2021. **85**. 153487 pp. https://doi.org/10.1016/j.tetlet.2021.153487
6. Оленович Н. Л., Танцюра Г. Ф., Галанець З. Г., Гаврильченко А. І. Синтез і властивості деяких о-діоксихроменолів. *Укр. хім. журн.* 1977. **43**(8). С. 883–884.
7. Барбалат Д. О. Синтез і хіміко-аналітичні характеристики нових похідних 6,7-дигідроксибензопірилію та їх застосування в комбінованих спектрофотометричних методах аналізу : дис. на здоб. наук. ступеня д-ра філ. / Одеський національний університет імені І. І. Мечникова. Одеса, 2021. 148 с.
8. Wei G., Yu B. Isoflavone glycosides: synthesis and evaluation as A-Glucosidase inhibitors. *European Journal of Organic Chemistry*. 2008. **18**. P. 3156–3163. https://doi.org/10.1002/ejoc.200800239
9. Xiao Z.-P., Shi D.-H., Li H.-Q., Zhang L.-N., Xu C., Zhu H.-L. Polyphenols based on isoflavones as inhibitors of Helicobacter pylori urease. *Bioorganic & Medicinal Chemistry*. 2007. **15**(11). P. 3703–3710. https://doi.org/10.1016/j.bmc.2007.03.045

REFERENCES

1. Chebotaryov O.M., Toporov S.V., Snigur D.V., Barbalat D.O. 6,7- and 7,8-dihydroxybenzopyrylium derivatives: synthesis, properties and analytical applications (review). *Visn. Odes. nac. univ., Him*. 2021. **26**(2): 73–88. doi: 10.18524/2304-0947.2021.2(78).233829. *(in Ukrainian)*
2. Cruz L., Basílio N., Mateus N., De Freitas V., Pina F. Natural and Synthetic Flavylium-Based Dyes: the chemistry behind the color. *Chemical Reviews*. 2021. **121**(19): 1416–1481. doi: 10.1021/acs.chemrev.1c00399
3. Walencik P. K., Borys M., Kopeć W., Ekiert H. M. Metal–Flavonoid Interactions—From Simple Complexes to Advanced Systems. *Molecules*. 2022. **27**(9): 2573. doi: 10.3390/molecules27092573
4. Calogero G., Citro I., Sebastianella G.C., Di

Marco G., Diniz A.M., Parola A.J., Pina F. A Photoelectrochemical Study of Bioinspired 2-Styryl-1-Benzopyrylium Cations on TiO2 Nanoparticle Layer for Application in Dye-Sensitized Solar Cells. *Materials*. 2019. **12**(24): 4060.
doi: 10.3390/ma12244060

5. Araújo P., Pereira A. R., de Freitas V., Mateus N., Fernandes I., Oliveira J. Synthesis, structural characterization and chromatic features of new 2-phenyl-1-benzopyrylium and 2-phenyl-styryl-1-benzopyrylium amino-based blue dyes. *Tetrahedron Letters*. 2021. **85**: 153487.
doi: 10.1016/j.tetlet.2021.153487
6. Olenovich N.L., Tansyura G.F., Galanets Z.G., Gavrilchenko A.I. Synthesis and properties of some o-dioxychromenols. *Ukr. Chem. J.* 1977. **43**(8): 883–884. *(in Ukrainian)*
7. Barbalat D.O. Synthesis and chemical-analytical characteristics of new 6,7 dihydroxybenzopyrylium derivatives and their application in combined spectrophotometric methods of analysis : Thesis for obtaining a scientific degree of the Doctor of Philosophy in specialty 102 Chemistry, field of studies 10 Natural Science. – Odesa I.I. Mechnikov National University, Odesa. 2021. 148 p. *(in Ukrainian)*
8. Wei G., Yu B. Isoflavone glycosides: synthesis and evaluation as A-Glucosidase inhibitors. *European Journal of Organic Chemistry*. 2008. **18**: 3156–3163.
doi: 10.1002/ejoc.200800239
9. Xiao Z.-P., Shi D.-H., Li H.-Q., Zhang L.-N., Xu C., Zhu H.-L. Polyphenols based on isoflavones as inhibitors of Helicobacter pylori urease. *Bioorganic & Medicinal Chemistry*. 2007. **15**(11): 3703–3710.
doi: 10.1016/j.bmc.2007.03.045

Стаття надійшла 10.10.2025.